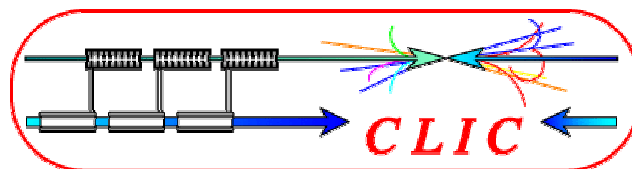


ORGANISATION EUROPEENNE POUR LA RECHERCHE NUCLEAIRE
CERN EUROPEAN ORGANIZATION FOR NUCLEAR RESEARCH



CLIC NOTE 553
January 2003

**AN ACTIVE PRE-ALIGNMENT SYSTEM
AND METROLOGY NETWORK FOR CLIC**

F. Becker, W. Coosemans, R. Pittin, I. Wilson

Geneva, Switzerland
28/01/2003

CLIC Note 553
January 2003

AN ACTIVE PRE-ALIGNMENT SYSTEM AND METROLOGY NETWORK FOR CLIC

F. Becker, W. Coosemans, R. Pitting, I. Wilson

Abstract

The pre-alignment tolerance on the transverse positions of the components of the CLIC linacs is typically ten microns over distances of 200 m. Such tight tolerances cannot be obtained by a static one-time alignment because normal seismic ground movement and cultural noise associated with human and industrial activity quickly creates significant errors. It is therefore foreseen to maintain the components in place using an active-alignment system which will be linked to a permanent metrology and geodetic network. This report describes the overall philosophy and implementation of such a system and proposes one possible solution for active-alignment which uses stepping-motors to move components and stretched-wires as reference lines. Special sensors have been developed to measure the position of the components with respect to the reference lines, and to measure local tilt and relative vertical position. An in-depth analysis has been made of the repercussions on the alignment system of perturbing effects due to the attraction of the moon and the sun, and of the presence of nearby geological masses. The active-alignment system was used to maintain the components of the 30 GHz Two-Beam Test Accelerator in position in the CLIC Test Facility CTF2 as a practical demonstration of successful operation in an accelerator environment. The hardware and control system that was built for this application are described together with the results obtained.

CONTENTS

1	Introduction.....	1
2	Getting an overview of the complete system by looking at the installation procedure: From geodesy to initial alignment	2
2.1	<i>The geodetic surface network</i>	2
2.2	<i>Underground surveys.....</i>	3
2.2.1	<i>Vertical drop procedure</i>	3
2.2.2	<i>Tunnel drilling and underground survey network</i>	3
2.3	<i>Metrology network and setting out the machine</i>	3
3	Choice of the way to establish the geometric reference network	4
4	Supporting and moving the accelerator components.....	4
4.1	<i>Accelerating cavities.....</i>	4
4.2	<i>Magnetic quadrupoles</i>	6
4.3	<i>Coupled movements</i>	7
4.4	<i>Connection with the tunnel floor.....</i>	7
4.5	<i>Micro-movers.....</i>	8
4.6	<i>First experimental test bench.....</i>	9
5	Sensors	10
5.1	<i>Introduction</i>	10
5.1.1	<i>Girders</i>	10
5.1.2	<i>Quadrupoles</i>	10
5.1.3	<i>Metrology network (details in chapter 6).....</i>	10
5.2	<i>Description of sensors.....</i>	10
5.2.1	<i>Tilt Measurement System (TMS).....</i>	10
5.2.2	<i>Hydrostatic Leveling System (HLS)</i>	11
5.2.3	<i>Wire Positioning System (WPS).....</i>	11
5.2.4	<i>Alignment System from NIKEF (RASNIK -CCD)</i>	13
5.3	<i>Experimental models set-ups</i>	13
6	Metrology network	16
6.1	<i>Specifications for the alignment of CLIC.....</i>	16
6.1.1	<i>Initial alignment of the accelerator.....</i>	16
6.1.2	<i>Controlling the displacements of the components.....</i>	16
6.2	<i>Geometric reference system.....</i>	16
6.2.1	<i>Stretched wires.....</i>	16
6.2.2	<i>Hydrostatic alignments.....</i>	20
6.2.3	<i>Optical alignments</i>	21
6.3	<i>Configuration of the metrology network.....</i>	21
6.3.1	<i>Positioning the alignment sensors</i>	22
6.3.2	<i>Calculation of the network and the positioning of the components.....</i>	23

6.4	<i>Study of perturbations of gravity and their consequences</i>	23
6.4.1	Repercussions of ground deformation on CLIC alignment	24
6.4.2	Effects which perturb the wire positioning systems (WPS).....	25
6.4.3	Effects which perturb the hydrostatic levelling systems (HLS).....	27
6.4.4	Effects which perturb the tilt monitoring systems (TMS)	36
6.4.5	Summary of the effects of gravity	36
6.5	<i>Determination of the optimum configuration for the network</i>	36
6.5.1	Simulation method	37
6.5.2	Development of computation software.....	37
6.5.3	Observational model	38
6.5.4	Networks tested.....	41
6.5.5	Optimum network.....	45
6.6	<i>Practical operation of the alignment system</i>	46
7	Practical demonstration of the active alignment system in CTF2	47
7.1	<i>CTF2 30GHz module layout</i>	47
7.2	<i>CTF2 Alignment control system</i>	48
7.3	<i>General Architecture of the system</i>	49
7.3.1	The Control Subsystem	49
7.3.2	Acquisition Subsystem	51
7.3.3	Drive Subsystem.....	52
7.4	<i>Results</i>	53
7.5	<i>Real Time Task</i>	55
7.5.1	Initialisation.....	55
7.5.2	Main Loop.....	55
7.5.3	30GHz Alignment System Console Application	55
7.6	<i>Remarks</i>	57
8	Conclusions	57
9	Acknowledgements	58
10	References	58
11	Annexes	59

LIST OF FIGURES

Fig. 1: CLIC Complex at 3 TeV.....	1
Fig. 2: CLIC module.....	1
Fig. 3: From geodesy to initial alignment.....	2
Fig. 4: Girder - supporting structure for accelerating cavities.....	5
Fig. 5 : Girder in CTF2.....	6
Fig. 6: Support structure for quadrupole.....	6
Fig. 7: Quadrupole in CTF2.....	7
Fig. 8: Concrete support.....	8
Fig. 9: First alignment test bench in TT2A.....	9
Fig. 10: Instrumentation in CTF2 (photo 1).....	12
Fig. 11: Instrumentation in CTF2 (photo 2).....	13
Fig. 12: Diagram of RASNIK-CCD system.....	13
Fig. 13: Second alignment test bench.....	14
Fig. 14: Distribution of the RASNIK components.....	14
Fig. 15: Schematic positioning of the RASNIK components in the girders.....	15
Fig. 16: The RASNIK system in the girders on the TT2A test bench.....	15
Fig. 17: Accelerator coordinate system.....	16
Fig. 18: Wire tensioning system.....	17
Fig. 19: Wire under gravity.....	17
Fig. 20: Curvature of gravitational field over 100 m.....	18
Fig. 21: Wire with ends at different heights.....	18
Fig. 22: Differences between a straight line and a hydrostatic alignment.....	20
Fig. 23: Start and end points of hydrostatic alignments.....	21
Fig. 24: Overlap of optical alignment systems.....	22
Fig. 25: Overlap of wire positioning systems.....	22
Fig. 26: Layout of the planned network.....	22
Fig. 27: Effect of a nearby mass anomaly.....	23
Fig. 28: Simplified tidal waveform propagated along the alignment of the CLIC.....	24
Fig. 29: Bending of the accelerator due to the periodic undulations of the earth tide.....	25
Fig. 30: Wire in a non-uniform gravitational field.....	26
Fig. 31: Wire in a curved gravity field.....	26
Fig. 32: Wire subjected to a longitudinal attraction.....	27
Fig. 33: Equipotential surface deformed by a topographic anomaly.....	28
Fig. 34: Heights above the ellipsoid and the geoid.....	28
Fig. 35: Geoid Profile along CLIC.....	29
Fig. 36: Calculation of the straightness defects.....	30
Fig. 37: Defects in the straightness of the profile in micrometers.....	30
Fig. 38: Set-up used for HLS trials.....	32
Fig. 39: Effect of tides on HLS readings.....	33
Fig. 40: Differences HLS 1 - HLS 2 : observed, and corrected for earth and water tide effects.....	34
Fig. 41: Accuracy of the corrections applied to HLS readings.....	35
Fig. 42: Distances from a point to a straight line.....	38
Fig. 43: Wire not parallel to the measuring surfaces.....	39
Fig. 44: Errors due to the inclination of the wire.....	39
Fig. 45: Angle of rotation of the sensor about the wire.....	40
Fig. 46: Distances between points on two straight lines.....	41
Fig. 47: Wire network: planimetry.....	42
Fig. 48: Wire alignment errors.....	42
Fig. 49: Wire network: altimetry.....	44
Fig. 50: CTF2 30 GHz modules.....	47
Fig. 51: Micro-movers and sensors in CTF2.....	48
Fig. 52: General architecture of the electronics in CTF2.....	49
Fig. 53: Flowchart of Control Subsystem.....	50
Fig. 54: AMCC Architecture.....	50
Fig. 55: Acquisition Subsystem.....	51
Fig. 56: Acquisition Card.....	52
Fig. 57: Drive Subsystem.....	52

Fig. 58: Driver Card	53
Fig. 59: Acquisition Tests	54
Fig. 60: Deviation of WPS on the Y axis	54
Fig. 61: Alignment system console program	56
Fig. 62: Offset windows and Cwin-Titer window.....	56

1 Introduction

The Compact Linear Collider (CLIC) Team at CERN is studying the technical feasibility of building a 3 TeV centre-of-mass e^{\pm} linear collider as a possible new experimental particle physics facility for the post-LHC era [1]. It is proposed to accelerate the beams using high frequency (30 GHz) normal-conducting structures operating at high accelerating fields (150 MV/m), this significantly reduces the length and, in consequence, the cost of the linac. The RF power to drive these structures is extracted by specially-designed decelerating structures from low-energy high-intensity electron beams that run parallel to the main linac. This novel use of a secondary beam to provide RF power for the acceleration of a primary beam is often referred to as Two-Beam-Acceleration or TBA. An overall layout of the 3 TeV CLIC collider is given in Fig. 1. The electron and positron main linacs are each 13.75 km long and are equipped with 21470 fifty cm long accelerating structures.

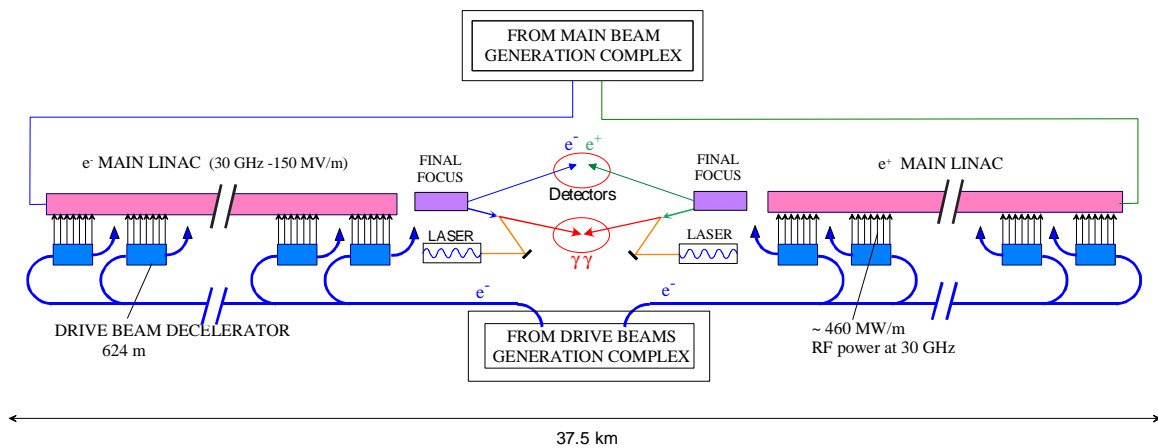


Fig. 1: CLIC Complex at 3 TeV

The peak RF power of 460 MW per metre length of each linac is generated by 22 drive beams. Each drive beam supplies power to a 625 m length of linac and is then sent to a dump. A beam delivery section at the end of each linac focuses the beams down to very small spot sizes (43 nm horizontally and 1 nm vertically) to create very intense beam/beam collisions at the interaction point.

The overall length of the complex is about 35 km. A typical 2.23 m long CLIC TBA module is shown in Fig. 2. The distance between the primary and secondary beams is about 60 cm. Magnetic quadrupoles keep the beams focused and on the correct trajectory. The excursions from the ideal trajectory is monitored by beam position monitors (BPMs). It is particularly important to limit transverse beam offsets in the accelerating structures because these offsets induce disruptive transverse wakefields which adversely affect the transverse emittance of the beam.

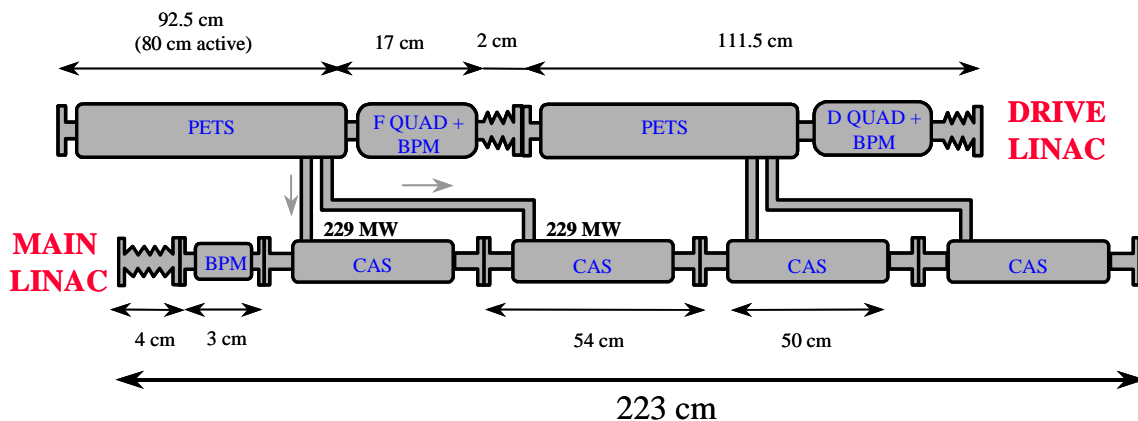


Fig. 2: CLIC module

This requires a tight alignment tolerance between the transverse positions of the structures and the BPMs. The longitudinal structure position is less important. It is foreseen to support four of these accelerating structures on a silicon-carbide girder. The alignment of the structures on the girders can be done very precisely (to within a few microns) in a laboratory or workshop environment before installation in the accelerator tunnel. Aligning the structures in the tunnel, is then a question of aligning the girders to some pre-determined accelerator reference axis. The magnetic centres of the quadrupoles must also be aligned along this same axis. This initial pre-alignment of components guarantees that when the first beams are injected into the linacs, they will not be too far off the design trajectory, and will produce signals in the BPMs that can be used in a second step to implement the more accurate beam-based alignment system.

The pre-alignment tolerance on transverse positions for the girders, quadrupoles and BPMs is presently $10\ \mu\text{m}$ over 200 m. Such tight tolerances cannot be obtained by a static one-time alignment because normal seismic ground movement and cultural noise associated with human and industrial activity, quickly creates significant errors. The components will therefore be equipped with an *active alignment system* which will form part of a *permanent metrology network*. The girders and quadrupoles will be moved by stepping motors.

2 Getting an overview of the complete system by looking at the installation procedure: From geodesy to initial alignment

The CLIC linacs will be installed in a tunnel dug underground at such a depth that the whole structure will be in geological formations (the molasse) which guarantee excellent stability for the machine. The tunnel will be connected to the surface by 13 shafts along its length, about 3.6 km apart and as close as possible to vertical from the tunnel. The connecting galleries between the bottoms of the shafts and the main tunnel will preferably be perpendicular to the latter. The geometric control points, also referred to in this chapter as pillars or reference points, are equipped with standard CERN reference sockets consisting of a spherical cup with a precision hole over which a sphere can be centred.

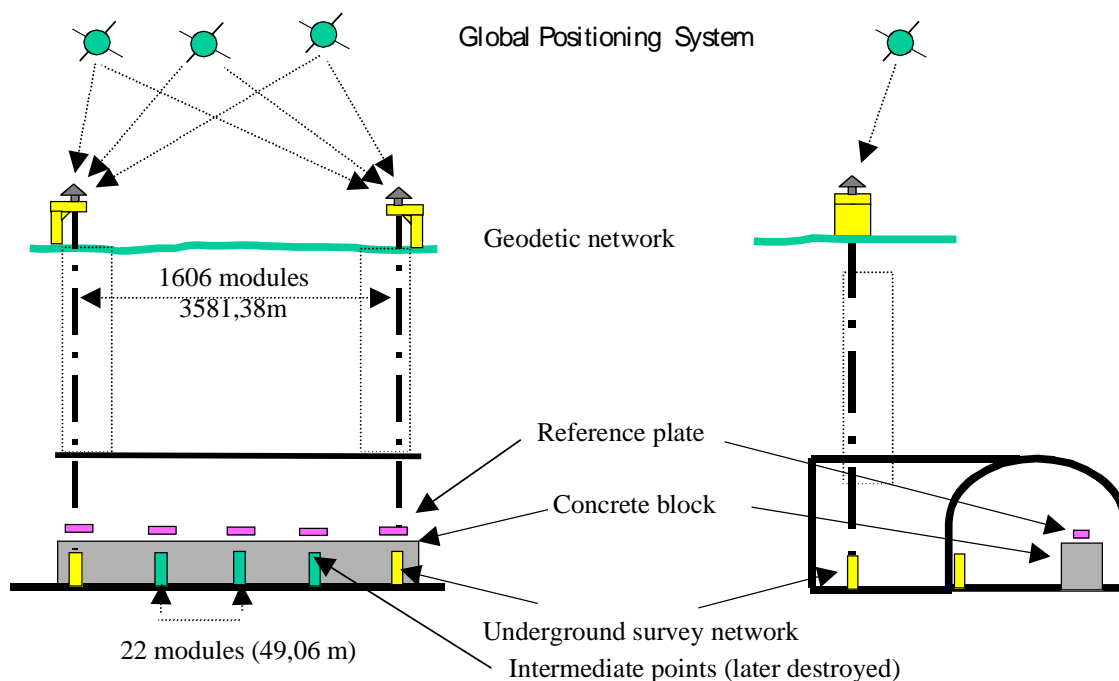


Fig. 3: From geodesy to initial alignment

2.1 The geodetic surface network

Having selected a site for the machine, the work begins with the establishment of a geodetic network on the surface. This will consist of survey pillars immediately next to each access pit for the underground construction, together with a number of pillars placed so as to create a well-conditioned control network. Observations for the network will be made by means of GPS, using differential techniques to guarantee an accuracy of about $\pm 1\ \text{mm}$ for the relative positions of the pillars (or reference points).

To determine the local deviations of the vertical, astronomical observations will be made using a zenith camera close to each pit.

2.2 Underground surveys

The techniques to be used are those developed for the tunnelling of LEP.

2.2.1 Vertical drop procedure

From the geodetic network, a secondary network is established, consisting of pillars to be used for the topographic surveys and measurements, especially for setting out the shafts.

Once the shafts have been sunk, reference pillars must be placed at the bottom of each, connected to the surface geodetic network.

To achieve this connection, at least three geometric reference points are fixed on brackets bolted to the curb-stone of each shaft, and are integrated into the geodetic network and thus known to the same accuracy as the geodetic pillars. These reference points are used to determine at least three reference pillars at the bottom of each shaft.

Depending on the size of the shafts and on whether there are any obstructions, these measurements are done by three dimensional triangulation and trilateration or by electronic plumb line and vertical distance measurement.

In view of the possibility that the recently built structure could move, it will be necessary to repeat the geodetic network and vertical drop measurements on a regular basis during the different phases of construction and probably also throughout the life of the machine. It is thus necessary to plan the installation of an automatic measurement system. Although a number of ideas of how to establish such a system are being considered, no detailed proposals have yet been formulated.

2.2.2 Tunnel drilling and underground survey network

The reference points at the bottom of the shafts are used to guide the drilling of the access gallery and then the drilling of the main tunnel. The survey technique used is classical traversing, involving the measurement of angles, distances and height differences. These observations are backed up by gyroscopic observations which supply true north. As the tunnel drilling advances, a reference pillar is placed on the tunnel wall every 49.06 m, thus forming the underground survey control network in conjunction with the pillars at the bottom of the shaft

When the tunnel reaches the next shaft, the traverse is closed onto the reference points for that shaft. In this way it is possible to improve the accuracy of the coordinates of the underground survey network. For this the observations of the geodetic network, the vertical drops and the underground network are repeated. For these measurements, in addition to the techniques indicated above, procedures more akin to metrology are used: stretched wire offset measurements and high precision distance measurements. In this way the underground network is fixed with an absolute accuracy of ± 5 mm in relation to the surface network, and a relative accuracy between three consecutive pillars of ± 1 mm.

2.3 Metrology network and setting out the machine

Starting from the underground survey network, the concrete blocks which will support the machine are put in place. It should be noted that for stability reasons these blocks form an integral part of the tunnel floor. The plates which will support the metrology network sensors are placed on the blocks at intervals of 49.06 m, and are aligned by means of the survey network. For this operation each support plate is fitted with two standard CERN reference sockets.

Once this has been done, the survey network pillars can be destroyed, with the exception of those at the bottom of each shaft and in the tunnel access galleries. The reference sockets on the plates become the geometric reference system for all subsequent operations.

From this new network the machine component support plates are set out, one plate per support girder articulation point and per quadrupole. These plates are equipped with reference sockets and fixations which allow the automatic location of all the components of the accelerator.

The components of the metrology network are then installed. This means fitting the sensors on the support plates, installing the alignment systems and the electronics in the radiation protected niches in the concrete base.

When installation is complete, the first network measurement is made, with the connection to the surface geodetic network. Two plates close to the access gallery are fitted with reference marks, thus enabling the geometric connection to the access gallery pillars. The geodetic network and vertical drop observations must then be repeated.

At the same time, for the reasons indicated in Chapter 6, gravimetric observations are made beneath all of the plates supporting the components of the metrology network.

After these measurements are made the positions of the support plates are computed and if necessary corrected. The girders and the quadrupoles can then be installed and connected to the metrology network. The pre-alignment of the machine components can then be carried out.

Before the accelerator is put into operation, a further connection of the metrology network to the geodetic network must be carried out.

After this final check the pre-alignment system is activated and it then maintains the components of the machine within the prescribed alignment tolerances.

3 Choice of the way to establish the geometric reference network

To achieve the CLIC alignment specifications a straight line in space must be established by means of a geometric reference network which is one or even two orders of magnitude more accurate than the networks presently being used for existing accelerators. Such a reference network can be set-up using either an optical alignment system or a mechanically established reference system.

Optical techniques come immediately to mind when faced with establishing a straight line in space, because in suitable conditions light is propagated in straight lines. The SLAC FFAC linac for example is aligned using a laser and Fresnel lens system and the physics groups preparing for the LHC experiments have developed different optical techniques for the geometric control of their detector elements. Such systems, with further development, could possibly be used to establish the required reference network for CLIC.

The difficulty with optical techniques is that, to obtain a high accuracy over long distances, it is essential to operate in a vacuum. In these conditions, the mechanical connection between the components to be checked and the reference network is not always direct, and ways have to be found to overcome the loss of accuracy which this entails. For CLIC, two parallel linacs have to be aligned. For each linac, connections to the reference network have to be made every 2.2m for the supports of the accelerating cavities, and to two points of each of the several hundred quadrupoles. Given the accuracy demanded for the initial positioning and the fact that the alignment must be dynamic, it was felt that the connection between the reference network and the points to be measured must be as direct as possible, and that it would be advantageous to investigate a mechanical technique.

The overlapping stretched wire technique, which is proposed in this report, is derived from a technique which has been widely used at CERN over a number of years. Since it is proposed to use the wires both for horizontal and vertical positioning, a vertical reference is required. This will be provided by a hydrostatic leveling network. Although the reference system proposed is essentially mechanically-based, use will also be made of an optical technique developed for the LHC experiments to align some points over short distances.

Although the solution proposed is simple to put in place and makes the connection between the linac components and the reference network more direct, in contrast to purely optical techniques it is directly dependent on knowledge of the geoid and of the phenomena which disturb it.

4 Supporting and moving the accelerator components

4.1 Accelerating cavities

To reduce the number of parts requiring alignment, several components are grouped together on one girder. Thus for the main linac four accelerating cavities and a beam position monitor (BPM) are typically placed together while two transfer cavities and a BPM are combined for the drive linac.

These components are supported on the girders by V-blocks which are aligned during manufacture to $\pm 3\mu\text{m}$. The maximum weight of components installed on a girder is about 40 kg. The girders are made of silicon carbide and the V-blocks of stainless steel. The dimensions of the girders and the properties of SiC are given in the following table.

Properties of SiC		Dimensions of girders	
density	2.56	length	2230 mm
coefficient of expansion	4.8×10^{-6}	section	120×60 mm
thermal conductivity	30 W/m [°] K	wall thickness	7.5 mm
specific heat	1050 J/kg	mass	6.7 kg/m
modulus of elasticity	21×10^3 kg/mm ²		

Table 1: Dimensions of girders and properties of SiC

It can be seen from the Table that the specific rigidity of a ceramic girder is three times greater than that of metallic girders (steel or aluminium). It is also three times less sensitive to deformations resulting from temperature gradients.

Before aligning the V-blocks, the support girders are loaded with their nominal weight to compensate for induced deflections. The resulting error in straightness of the axis generated by the two planes of the V-blocks is less than 3 μm. The difference between the coefficients of expansion of copper (the accelerating cavities themselves) and of silicon carbide could, if rigidly clamped, result in a bimetallic strip effect. To overcome this difficulty, the cavities are fixed firmly on one V-block and allowed to slide on the other. For a temperature difference (Δt) of 5°C and a distance of 200 mm, the relative movement is about 6μm.

Six axes have to be controlled to fix an element in space. In order to guarantee the continuous smooth transition between the positions of the girders, the ends of two adjacent girders rest on a common cradle. The cradle is connected to three micro-movers and to a micrometric stop through swivel-joint link rods (Fig. 4) (Fig. 5). The micro-movers and the micrometric stop are static. Two of the micro-movers control vertical movements, the third controls movements in the planes perpendicular to the longitudinal axis of the linac. The micrometric stop allows for a manual adjustment along the longitudinal axis; because this direction does not require a precise alignment this does not need to be motorised. The end of one girder is rigidly attached to the cradle while the end of the other is fixed to the same cradle through two link rods at an angle of approximately 45° degrees to the vertical. The system is designed in such a way that the movements of the micro-movers result only in rotations between the two girders about a virtual articulation point which is the intersection of the lines passing through the axes of the accelerating structures.

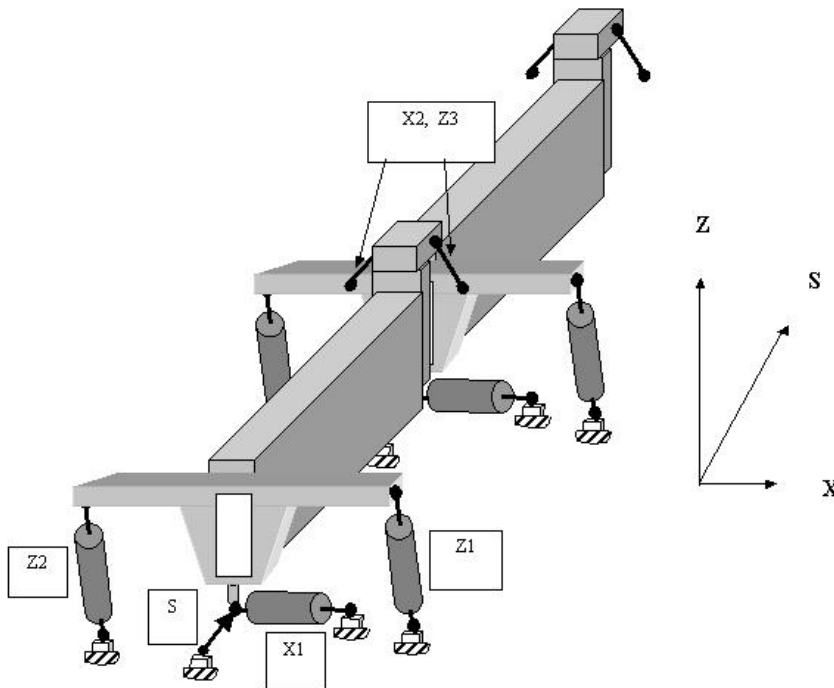


Fig. 4: Girder - supporting structure for accelerating cavities

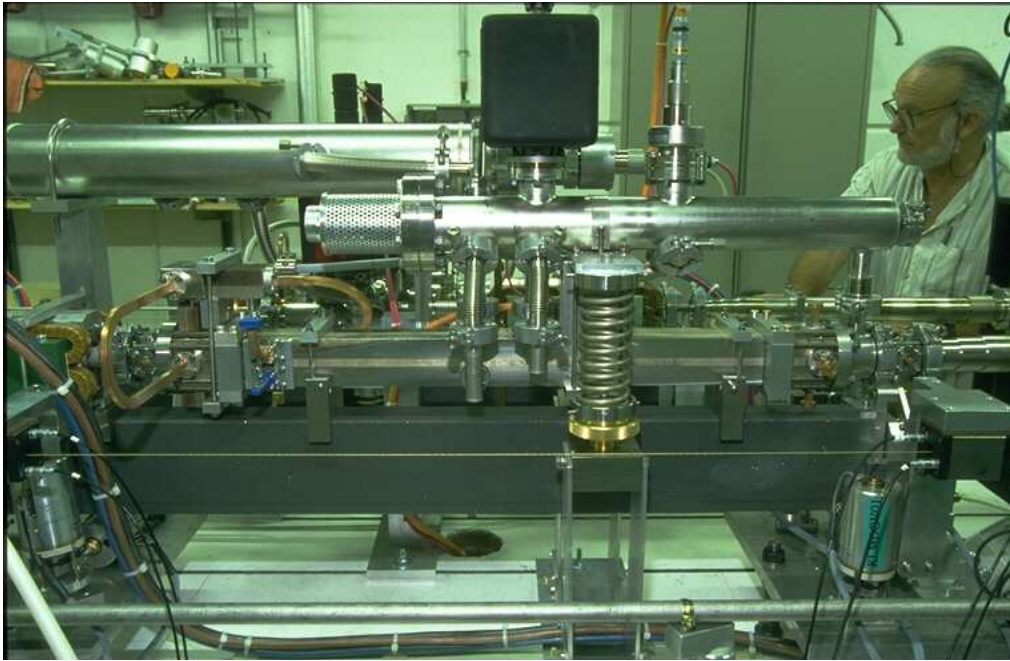


Fig. 5 : Girder in CTF2

4.2 Magnetic quadrupoles

Thanks to the system of link rods equipped with small diameter swivel joints, movements occur through rotations about a point, which are almost frictionless and do not introduce stresses in the structures. The assembly is so arranged that the micro-movers and swivels are always free of backlash. The weight of the cradle and the girders compresses the vertical micro-movers and the 45° link rods but extends the vertical link rods. These are offset from the thrust axes of the micro-movers and tilted so as to compress the horizontal micro-mover and its link rod, and to push the cradle against the micrometric stop.

These components are distributed along the length of the accelerator and they must be able to move independently of the girders. Wherever there is a quadrupole, there are of course no accelerating structures. They are supported by an L-shaped metal platform surrounding the girder. The horizontal part, equipped with three vertical micro-movers, supports the quadrupoles (Fig. 6), (Fig. 7). Two horizontal micro-movers for transverse horizontal displacements and a micrometric stop for longitudinal displacements are attached to the vertical part, which is parallel to the beam axis. Unlike the girders, in this case the micro-movers do not use link rods to transmit movements. They act as link rods themselves, being equipped with swivel joints at both ends.

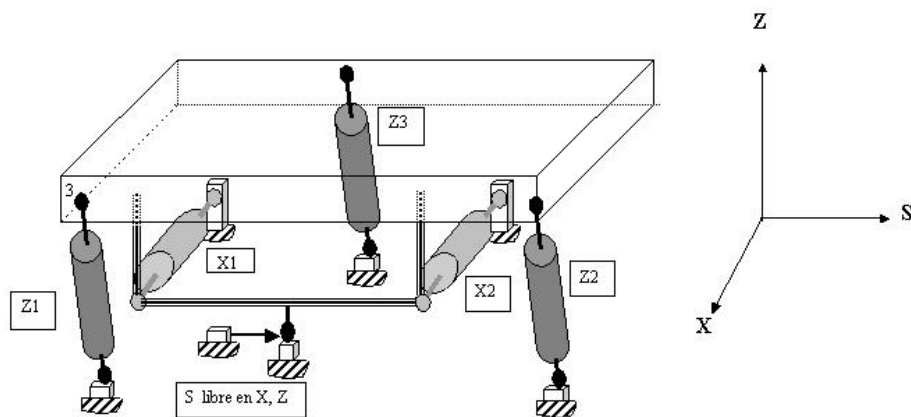


Fig. 6: Support structure for quadrupole

The vertical micro-movers are tilted slightly in two directions to apply pressure on the horizontal micro-movers, to eliminate backlash of the swivel joints and to press the vertical part of the support platform against the micrometric stop.

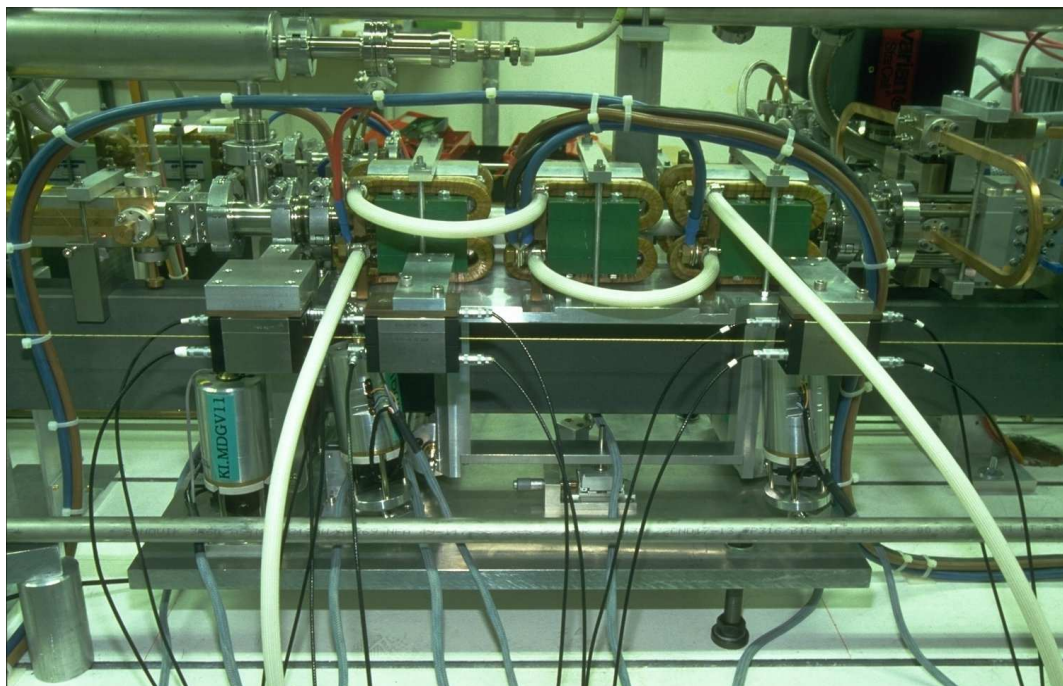


Fig. 7: Quadrupole in CTF2

4.3 Coupled movements

The mechanisms illustrated in Fig. 4 and Fig. 6 are associated with circular movements for which the non-linear equations were developed by Patrice Poirier in 1991 [2].

The disadvantage of the link rod system is that the movement of a micro-mover in one direction introduces a displacement in another direction. For a girder, this second-order effect is 0.07 mm for a 4 mm. displacement. Since the micro-movers are remotely controlled by software which manages the displacements, this coupled movement is therefore only a minor drawback.

4.4 Connection with the tunnel floor

All micro-movers acting upon the same cradle, girder support or quadrupole platform are attached to a metal plate which is in turn fixed to a concrete base by three threaded rods with nuts and lock nuts (Fig. 8). The concrete base is a continuous support integrated into the accelerator tunnel floor. For reasons related to accessibility and subsidiary equipment, the accelerator cannot be mounted on the floor itself. Compared to a metallic structure, the concrete support represents a more stable solution which minimizes the amplification of vibrations propagated through the floor. It also offers the possibility of providing recesses within it, in which the electronics can be protected from the harmful effects of radiation.

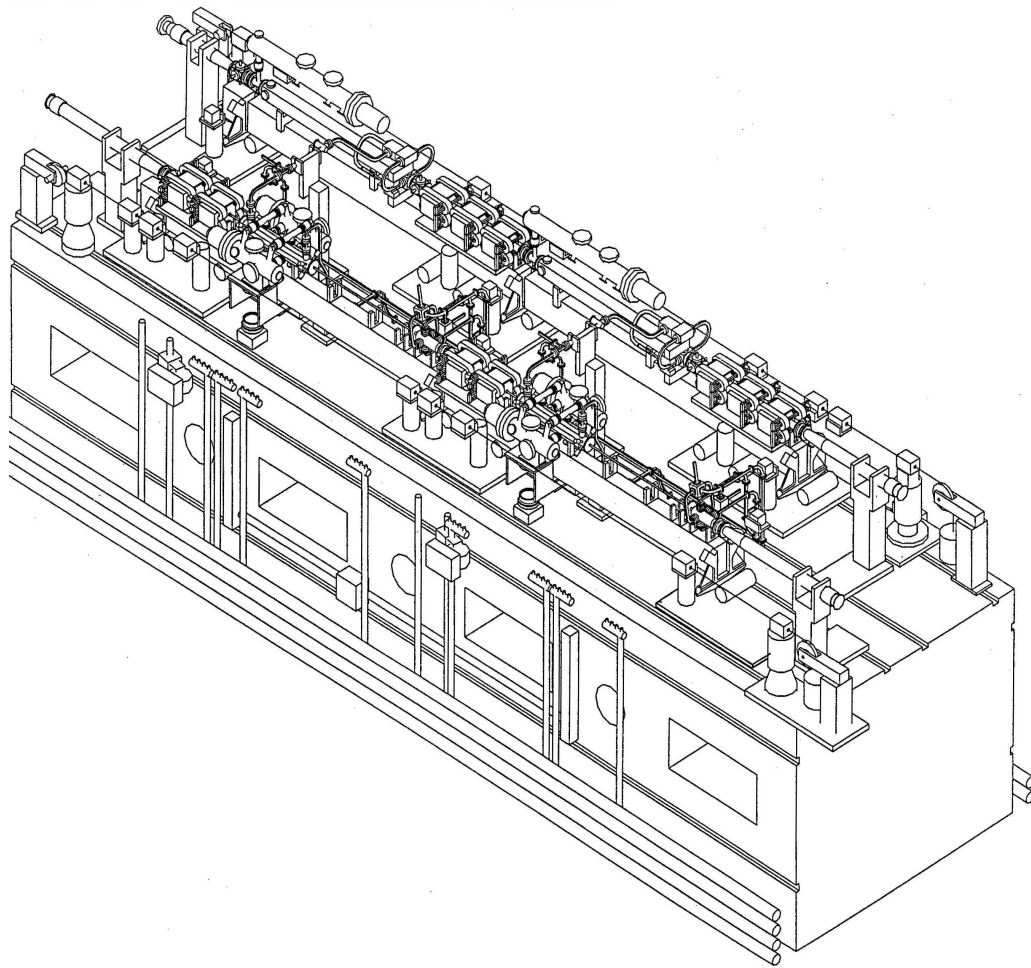


Fig. 8: Concrete support

4.5 Micro-movers

The micro-movers have been specially developed and manufactured to meet the specific CLIC requirements: precise displacement without hysteresis under loads of up to 40 kg, small overall dimensions and resistance to radiation. The active part of the micro-mover is identical for girders and quadrupoles, as indicated earlier, the only difference being in the system connecting the stationary part and the component to be moved. The device consists of a stepping motor, an all-metal reduction gearing with minimal backlash, and a high-precision micrometer screw. Three sensors manage the start and the end of each movement as well as the midway position. To meet the specifications correctly, a micro-mover must always work under compression. The micro-movers specifications are given in Table 2.

Range of movement	± 4 mm
Smallest step	$0.2 \mu\text{m}$
Co linearity	1/1000 of the distance
Maximum speed	0.83 mm/s
Maximum load	40 kg
Max. load along the thrust axis (quadrupoles)	30 kg
Max. load along an axis offset by 30 mm (girders)	1 kg
End of movement stop	closed at the end of the range
Midway stop repeatability	$\pm 2 \mu\text{m}$
Diameter	60 mm
Length	150 mm
Weight	1.5 kg

Table 2: Micro-movers specifications

For a continuous movement with displacements less than or equal to $\pm 5 \mu\text{m}$, at a frequency of 1 Hz, the expansion of the micro-mover due to heating from the motor is less than $2 \mu\text{m}$.

The control system is described in the chapter 7.

The motor responds to the following commands :

- relative displacement,
- absolute displacement,
- reading of position in relation to a position defined as the origin,
- status reading for the motor and the stops,
- automatic return to half-way stop position without passing through the end stops.

Using the micro-movers with an offset load (on the girders) is awkward and can lead to less good results. In the future it is therefore planned to use the same principle for girders as for quadrupoles, the micro-mover then being equipped with two end swivels and working as an expanding link rod.

4.6 First experimental test bench

The equipment describe in this chapter is the fruit of this experiment development program.

A first remote computer-controlled micro-movement test bench permitting controlled submicron displacements, was built in an unused underground accelerator tunnel TT2A to study the problems associated with the support and precise positioning in space of CLIC main linac components and to study the mechanics of coupling pairs of girders (Fig. 9: First alignment test bench in TT2A). This set-up consisting of two moveable girders and one fixed girder was used to demonstrate the feasibility of controlled sub-micron movement using commercially available components, details of this set-up and the results obtained are given in reference [3]. Piezo-electric movers with a stroke of $\pm 3 \mu\text{m}$ were mounted in series with some of the jacks to provide higher speed response.

The test facility is piloted remotely from an Olivetti PC and was programmed for automatic alignment with respect to independent transducers monitoring the position of the accelerating sections themselves. After deliberate misalignments (of 1 mm say) the system settled back to nominal positions within less than a micron.

The performance of this micro-movement test device can be summarized as follows :

- smallest step in any one direction = $0.2 \mu\text{m}$,
- hysteresis over $\pm 4 \text{ mm}$ = $3 \mu\text{m}$ (open loop),
- error over $\pm 4 \text{ mm}$ in closed loop = $0.2 \mu\text{m}$,
- frequency = 1 Hz.



Fig. 9: First alignment test bench in TT2A

5 Sensors

5.1 Introduction

In order to set up the initial alignment and to maintain the geometry of the elements within the required tolerances, the components are equipped with sensors which are referenced to the metrology network.

5.1.1 Girders

As seen in the previous chapter aligning the girders, which support the accelerating structures, implies the alignment of virtual points, each of which is the intersection of the lines passing through the axes of the accelerating structures. Each of these points is defined by the shape of the cradle, so the sensors are attached to the cradle itself. As the cradle is equipped with three micro-movers, three measurements with respect to the reference network are required: a vertical distance, a horizontal distance perpendicular to the beam, and the angle between the cradle and the horizontal in the direction perpendicular to the beam.

5.1.2 Quadrupoles

The support platform for the quadrupoles is equipped with five micro-movers. Therefore five measurements with respect to the reference network are required: two vertical distances, two horizontal distances perpendicular to the beam, and the angle between the support platform and the horizontal in the direction perpendicular to the beam.

Remark: The sensors are fixed on the girder cradles and on the quadrupole platforms during manufacture, with micrometric accuracy with respect to the mechanical axes of the elements to be aligned.

5.1.3 Metrology network (details in chapter 6)

For the metrology network, the reference systems are of four types:

- an absolute reference which is the local vertical,
- the free surface of a liquid which follows the shape of the geoid,
- a double line of stretched wires,
- two optical lines.

With the exception of the optical reference systems which are fixed directly onto the girders, the instrumentation is rigidly attached to platforms regularly spaced between the two linacs.

5.2 Description of sensors

There are four types of sensors:

- an inclinometer (tilt measurement system, TMS),
- a hydrostatic levelling system (HLS),
- a wire positioning system (WPS),
- an optical offset measurement system (RASNIK-CCD).

These sensors are resistant to radiation and can be used within the stray field of the magnetic elements.

5.2.1 Tilt Measurement System (TMS)

The reference frame for this instrument is the local vertical. Tilts are measured in relation to two orthogonal horizontal axes.

In the TMS, a mass is maintained in levitation by an electrostatic field. The displacements of the mass caused by the movements of the instrument are measured by capacitive sensors and the values obtained are converted into angular units.

From the outside, the instrument looks like a 40 mm cube; it does not include any electronic components. The control electronics are always positioned a few meters away from the instrument to protect them from radiation. Technical details of the TMS are given in Table 3.

Measuring range	± 0.010 radian
Pass-band	0 to 100 Hz
Resolution	10^{-7} radian
Repeatability	10^{-6} radian
Output signal for each measuring axis proportional to the measured angle	± 10 volts

Table 3: Technical details of the TMS

The bottom face of the instrument, parallel to the measuring axes, is machined and ensures an absolute accuracy of 10^{-4} radian with respect to the vertical. Due to the pass-band and the measuring technique, the instrument can be used as a low-frequency accelerometer. Eighteen of these instruments are in service in CTF2. In CLIC, girders, quadrupoles and support platforms for the metrology network would all be equipped with TMS.

5.2.2 Hydrostatic Leveling System (HLS)

The free surface of a “water network” provides the reference frame. The system works according to the principle of communicating vessels.

The network consists of vessels connected to each other by pipes. The pipe has a diameter of 60 mm and is partially filled with water, allowing water and air to circulate freely within it.

To eliminate the effects of differential variations of atmospheric pressure, the whole pipework system is only open to free air at one point.

The vessels are equipped with a temperature sensor. A sensor is fitted to each vessel through a watertight joint and measures capacitance in order to determine the distance to the free surface of the liquid.

To avoid salt deposition and the growth of flora and micro fauna, dematerialized water is used with a biocide additive. The vessels, the pipes and the casing of the sensor are made of stainless steel. As required, the electronics are included in the sensor or offset by a few meters. The unit consisting of a vessel and a sensor forms a cylinder, with a diameter of 100 mm and a height of 120 mm.

The technical details of the HLS are given in Table 4.

Measuring range	5 mm
Pass-band	linked to the shape of the network
Resolution	0.2 μm
Repeatability	1 μm
Absolute accuracy after linearisation	1 μm
Output signal proportional to distance	0-10 volts
Output signal proportional to temperature	0-10 volts

Table 4: Technical details of the HLS

HLSs have been used for checking the LOW-BETA sections of LEP (48 units). They will be used in LHC (100 units) for the same application. The CERN geodetic test bench for alignment systems is equipped with three of these instruments.

In CTF2, six HLSs monitor the stability of the concrete girder supporting the accelerator. For CLIC, it is foreseen to install HLSs on the platforms of the metrology network.

5.2.3 Wire Positioning System (WPS)

The WPS uses a capacitive measurement technique along two perpendicular axes, to measure the distance between its mechanical axis and a stretched wire which serves as a reference. On each measurement axis, the wire sits between two electrodes. The WPS (a parallelepiped of 4.5 x 4.5 x 70 mm), does not include any electronic components. The processing electronics are connected to the sensor by four triaxial cables.

The wire is made of carbon fibres and its geometry is maintained by a sheath of woven PEEKk (Polyetheretheretone) filaments. It is held in tension by a frictionless pulley system and a counterweight. Technical details of the WPS are given in Table 5.

Sensor	
Measuring range	± 5 mm
Pass-band	0 – 10 Hz
Resolution	0.1 μ m
Repeatability	1 μ m
Absolute accuracy after linearisation	1 μ m
Output signal for each measurement axis and proportional to the distance	0-10 volts
Wire	
Apparent diameter	0.30 mm
Linear weight	280 gr/km
Breaking strain	56 dN
Mass of the counterweight	between 15 and 20 kg
Accuracy of the tensioning system	10^{-5} N

Table 5: Technical details of the WPS

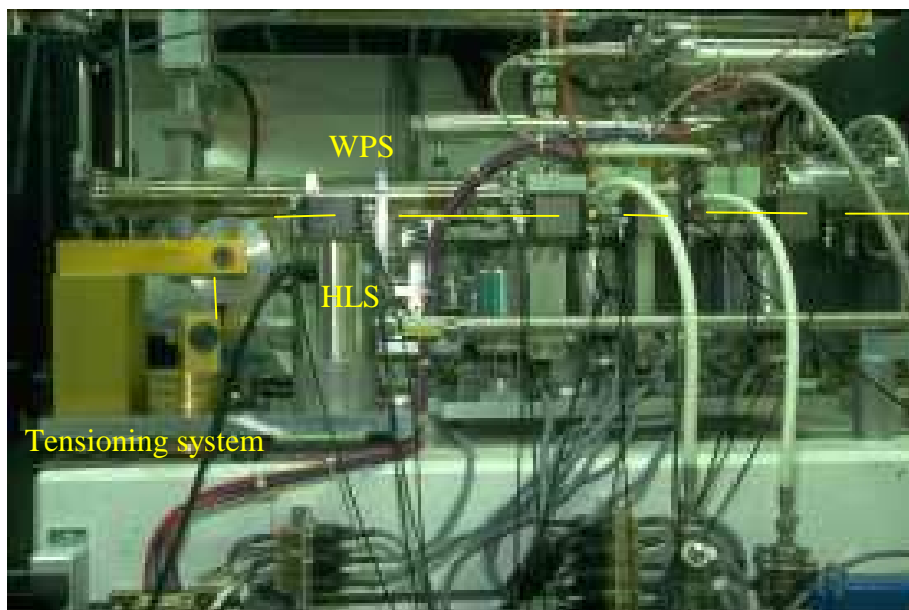


Fig. 10: Instrumentation in CTF2 (photo 1)

WPSs have been used to check the stability of the spectrometer elements installed in section 332 of LEP (18 sensors).

In CTF2, 34 sensors are installed on the girders and the quadrupoles. WPSs have also been used to monitor the movements of the LEP tunnel at points 5 and 1 during civil engineering work for the LHC (20 sensors). They will be used for checks on the LOW-BETA section of LHC (68 sensors).

The CERN geodetic test bench for alignment systems is equipped with four of these instruments.

For CLIC, it is foreseen to mount WPS on some of the girders, all of the quadrupoles and all support platforms of the metrology network.

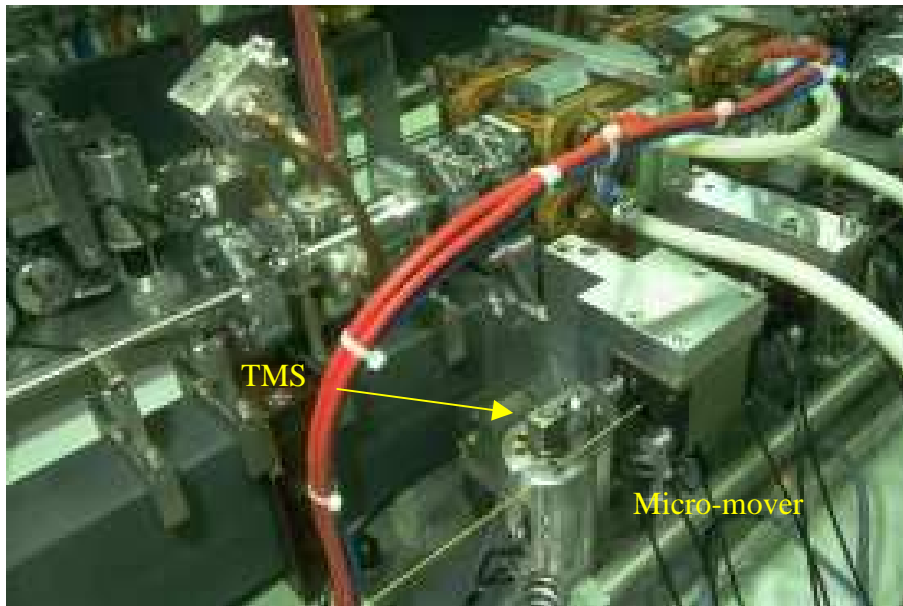


Fig. 11: Instrumentation in CTF2 (photo 2)

5.2.4 Alignment System from NIKEF (RASNIK -CCD)

The RASNIK-CCD system consists of two opto-electronic components and one optical element (Fig. 12).

Part of the image of a coded mask, illuminated by a network of infrared diodes through a diffusor, is projected into a digital camera by means of a lens. In this application, the camera and lens are considered to form the optical reference axis and the movements of the mask are measured with respect to this axis (Y). The camera is connected to a computer and the image is analysed and compared with the reference image to deduce the radial position (X, Z) of the mask with respect to the reference axis. The longitudinal movement (Y) can also be determined as well as the three angles of rotation about the X, Y and Z axes.

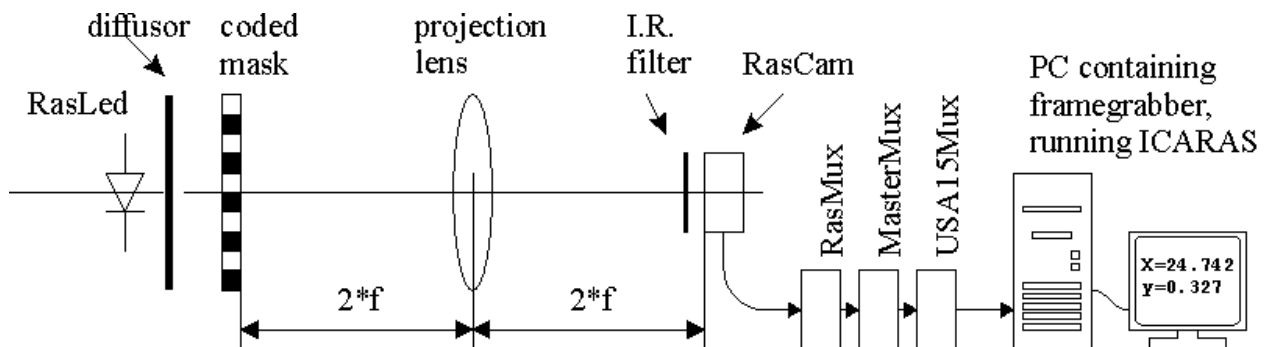


Fig. 12: Diagram of RASNIK-CCD system

The RASNIK-CCD system was developed by the electronics department of the Dutch National Institute for Nuclear Physics and High Energy Physics (NIKEF) [4]. Making use of the same principle but in a different form, it has been used extensively to control the position of the detector elements of the L3 experiment in LEP. It has also been used on the first CLIC alignment test bench. About 7000 RASNIK-CCD systems will be integrated into LHC.

For CLIC, it is foreseen to install the RASNIK-CCD system on all girder support cradles to ensure high accuracy of relative positioning of three consecutive girders.

5.3 Experimental models set-ups

A second test bench consisting of the same basic elements as the first but with six motorized girders is built to enable the new CLIC pre-alignment scheme to be studied (Fig. 13). In the test facility the structures to be aligned, dummy accelerating sections, are supported by V-blocks on 1.4m long silicon carbide girders. Movements of the set-up are monitored by linear and angular displacement transducers (0.1 μm and 10 μrad resolution respectively).

A stretched-wire running along the axis of the structures and passing through capacitive position transducers where the BPMs would normally be placed is used to simulate the beam. The set-up is piloted remotely from a small computer. After deliberate misalignments of 1 mm, the system which is programmed for automatic alignment with respect to any of the transducers, settles back to nominal positions within < 1 micron in 3 seconds.

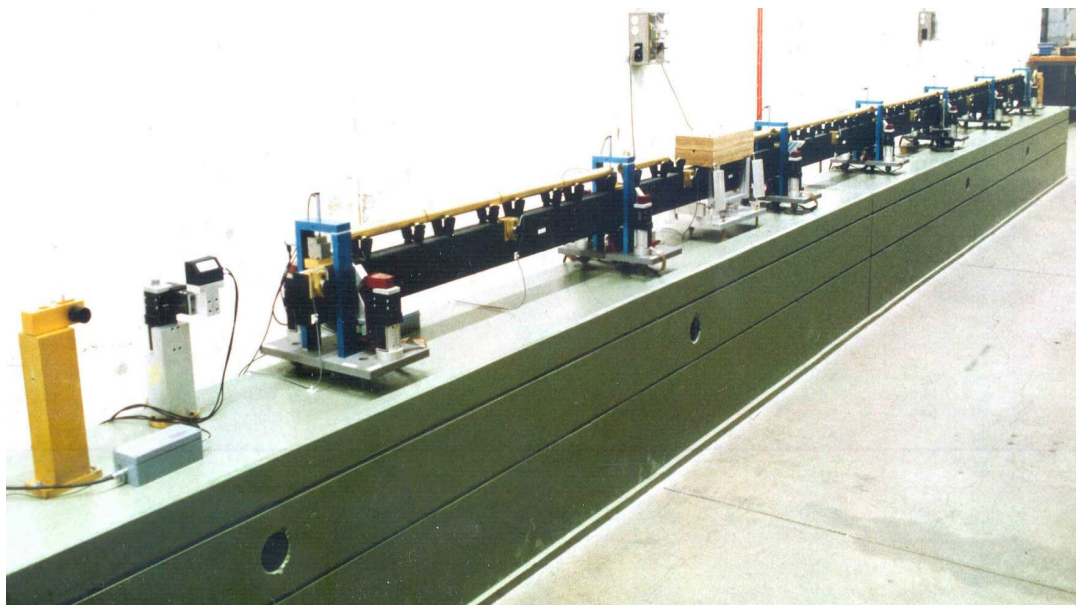


Fig. 13: Second alignment test bench

The set-up is being used to test Wire Positioning System (WPS) and optical system (RASNIK), used for pre-alignment before injection of the beam [5] [6].

For the second system the image of a square-shaped red light source is focused on a light-detecting four-quadrant cell by a thin lens. Displacements of the source, lens or four-quadrant cell out of the optical axis of the instrument produce an imbalance at the detector. This system has been incorporated, with overlapping and redundancy technique (Fig. 14 and Fig. 15), into the six hollow support girders of the test module (Fig. 16) and enables the relative positions of the far ends of two adjacent girders to be maintained in position with respect to the ideal straight line to < 2 μ m. This system is however unlikely to be used in CLIC because of fears of radiation damage; it will be replaced by a the new system RASNIK-CCD in a new configuration (Chap.6.3).

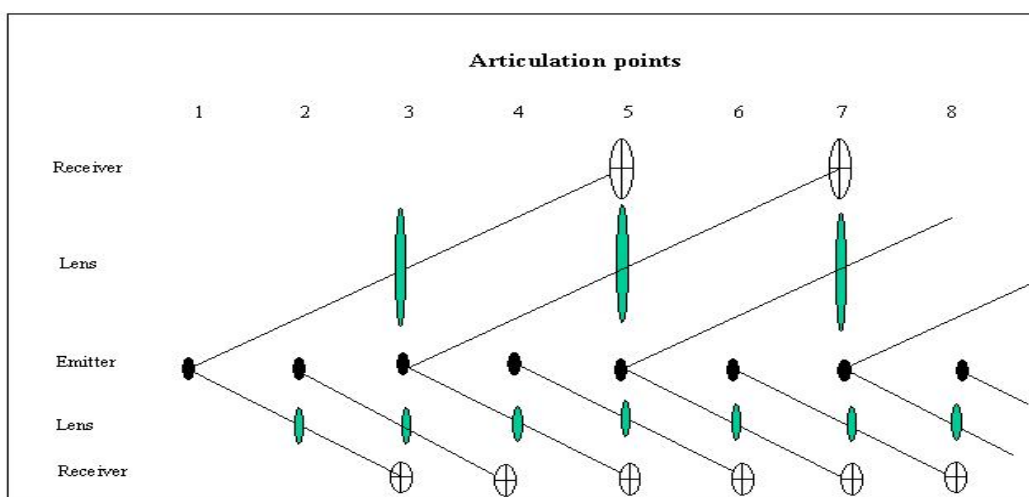


Fig. 14: Distribution of the RASNIK components

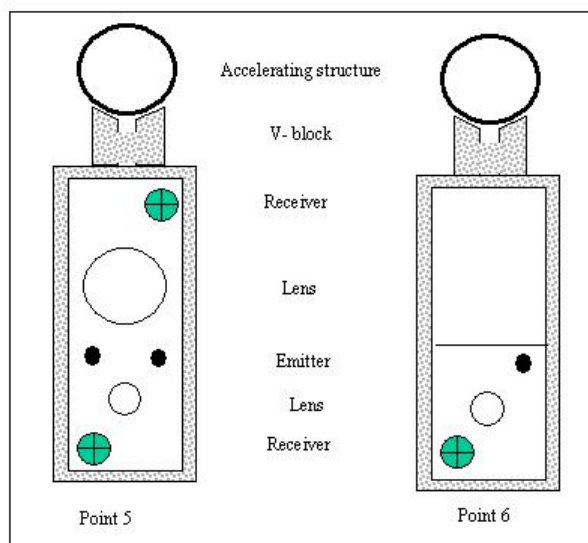


Fig. 15: Schematic positioning of the RASNIK components in the girders

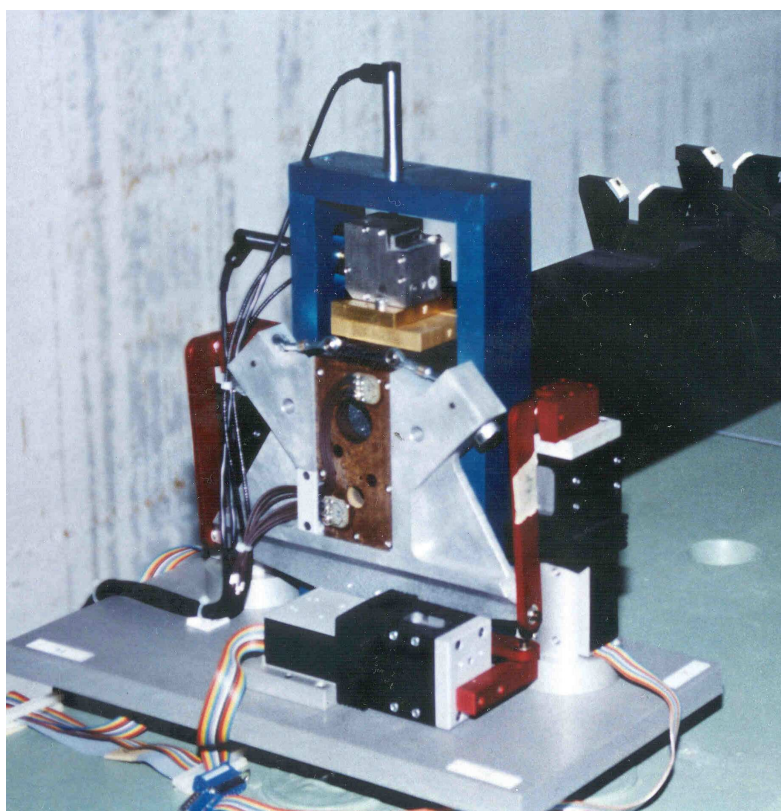


Fig. 16: The RASNIK system in the girders on the TT2A test bench

6 Metrology network

This chapter describes the metrology network. The metrology aspects of the CLIC alignment specification are first reviewed. Then the major features and general configuration of the geometric reference network are described. A section will cover an investigation of the effects of gravity. The final part of the chapter will give the results of the simulations which have been carried out to optimise the network.

6.1 Specifications for the alignment of CLIC

The metrology network must allow the rectilinear alignment of each of the two 14 km long linacs (linear accelerators) which form the complete accelerator. This alignment consists of the initial alignment before the injection of the beam, and the control of the displacements of certain components during operation of the accelerator with beam.

6.1.1 Initial alignment of the accelerator

The alignment of the CLIC linacs consists of two parts, an initial alignment to get a beam to pass through the beam position monitors (BPM's) installed at regular intervals along the length of the linacs, and then a beam-based alignment using these BPM's to keep the beam as close to the axis of the accelerator as possible. This initial alignment must be carried out with a relative accuracy of $\pm 10 \mu\text{m}$ along the X and Z axes over typical distances in the s direction of $\sim 200 \text{ m}$ (Fig. 17).

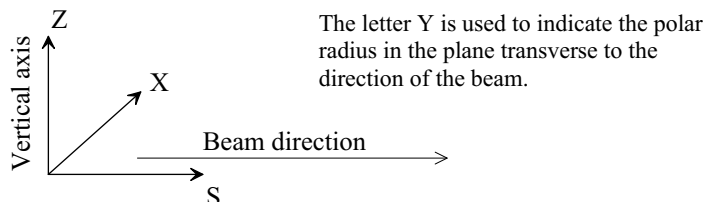


Fig. 17: Accelerator coordinate system

6.1.2 Controlling the displacements of the components

The beam-based alignment of the accelerator during the acceleration of the beam requires the displacement of the quadrupoles. These displacements are calculated from information on the position of the beam within the BPMs, and the corresponding instructions are then transmitted to micro-movers. The sensors of the alignment system will be used to quantify these displacements with sub-micron accuracy, by taking measurements relative to geometric reference points whose position will have been computed during the initial alignment phase.

6.2 Geometric reference system

To make effective use of the sensors described in the previous chapter, it is essential to have sufficiently precise knowledge of the geometric reference framework to which their measurements are referred.

The major features of the stretched wires and the hydrostatic and optical alignment systems are first discussed, pointing out the advantages and disadvantages of each system, and their usefulness in an alignment system such as that required for CLIC. Vertical alignment will be discussed in the section on the effects of the gravitational field.

6.2.1 Stretched wires

Essential features

The details of the wires currently used in the wire positioning system (WPS) are given in Chapter 5. The wires can be subjected to a tension of 20 kg without difficulty. This is one of the parameters on which the geometry of a wire depends and it is important that it be accurately known. A system as shown in Fig. 18 allows the transmission of the tension from a counterweight over a knife-edge pulley with a sensitivity of $\pm 10^{-5} \text{ N}$.

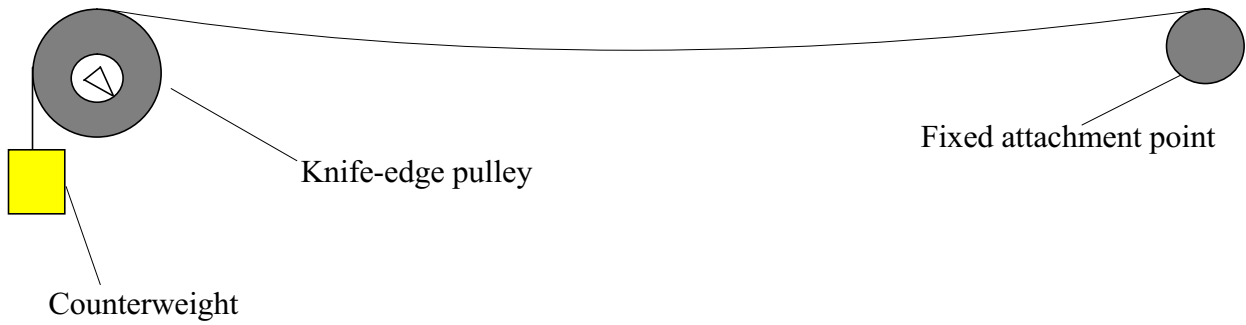


Fig. 18: Wire tensioning system

The frequencies of transverse and longitudinal vibration of a wire are given by the following equations:

$$F_t = \frac{1}{2rl} \cdot \sqrt{\frac{H}{\pi d}} \quad \text{Equation 1}$$

$$F_l = F_t \cdot \sqrt{\frac{l}{a}} \quad \text{Equation 2}$$

Where : r is the radius of the wire,
 l is the length of the wire,
 H is the tension applied to the wire,
 d is the density (mass per unit volume) of the wire,
 a is the elongation of the wire under the tension p .

A wire of length 100 m with the characteristics given in Chapter 5, subjected to a tension of 20 kg, has a transverse vibration frequency of about 4 Hz. This is an important parameter to consider when deciding on the data acquisition rate for a wire positioning system.

Equation in the vertical plane

Under the influence of gravity the wire forms a catenary in the vertical plane, whose equation and properties are described by Favre, 1953 [7] and Merrit, 1983 [8]. Referring to Fig. 19: Wire under gravity, the equation of the catenary is :

$$z = \frac{H}{q} \left(ch \left(\frac{qx}{H} - 1 \right) \right) \quad \text{Equation 3}$$

Where : H is the tension to the wire,
 Q is the weight per unit length of the wire.

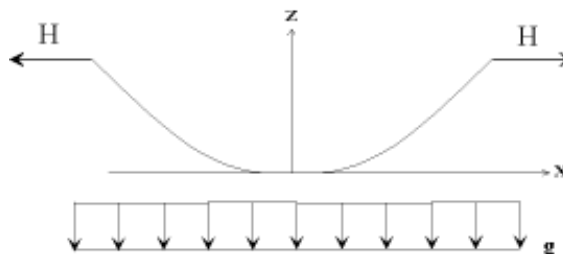


Fig. 19: Wire under gravity

It must be emphasised here that in reality the gravitational field is not uniform and rectilinear as shown in Fig. 19. Over a distance of 100 m, an equipotential surface departs from the straight line between two points on it by about 0.2 mm (Fig. 20). The effect of this phenomenon on the equation of the wire is examined in more detail in the section below.

Given the characteristics of the wire used for CLIC, Mainaud,1996 [9], shows that a very good approximation to Equation 3 is given by :

$$z = A(x) = \frac{qx^2}{2H} \quad \text{Equation 4}$$

For a wire of length 100 m, under a tension of 20 kg, with the characteristics mentioned previously, the sag is 1.8 cm.

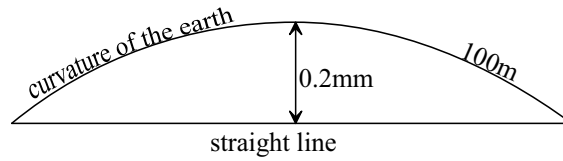


Fig. 20: Curvature of gravitational field over 100 m

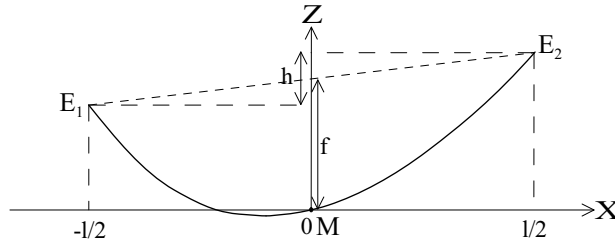


Fig. 21: Wire with ends at different heights

Equation 4 corresponds to the case where the ends of the wire are at the same height. In the general case where the heights are different, the equation (referring to Fig. 21) is as follows [Merrit, 1983] :

$$Z = \frac{4f}{l^2} \left(X + \frac{lh}{8f} \right)^2 - \frac{h^2}{16f} \quad \text{Equation 5}$$

Where : l is the horizontal distance between the ends of the wire

$$h = Z_{E_2} - Z_{E_1}$$

$$f = (Z_{E_2} + Z_{E_1})/2 - Z_M$$

The parameter f may be expressed as a function of the tension H and the weight per unit length q of the wire :

$$\frac{H}{q} = \frac{l^2}{8f} \quad \text{Equation 6}$$

Equation 5 then becomes :

$$Z = \frac{q}{2H} \left(S + \frac{Hh}{ql} \right)^2 - \frac{Hh^2}{2ql^2} \quad \text{Equation 7}$$

The wire's sensitivity in the vertical plane to the various parameters which affect the shape of its catenary are now examined. For these calculations, a wire of length 100m under a tension of 20 kg has been assumed.

Effect of the length of the wire

The wire is insensitive to variations in its length l , because this would need to change by 1.4 mm to alter the sag by 1 μm . In the present case l remains fixed and is known to the required accuracy.

Effect of the tension on the wire

The tension on the wire would need to vary by 1.1 g to change the sag by 1 μm . Thus this parameter has little effect on the wire, given that the tensioning system has a sensitivity of $\pm 10^{-5}$ N.

Effect of the mass per unit length of the wire

The catenary is very sensitive to the linear mass of the wire. In fact the sag changes by 1 μm for a variation of only $1.6 \cdot 10^{-5}$ g m $^{-1}$, it is very tricky to determine the linear mass of the wire with this degree of accuracy.

Effect of the accuracy of the measured height differences h and f .

The sensitivity of the determination of the catenary to the accuracy of these measurements is indicated in the table below. The uncertainty in the position of the wire increases with distance from the origin of coordinates with respect to which its equation is expressed, whether this origin is the midpoint or one of the ends of the wire.

Accuracy of a measurement of h or f	Maximum uncertainty in the form of the catenary
$\pm 3\mu\text{m}$	$\pm 3.4\mu\text{m}$
$\pm 4\mu\text{m}$	$\pm 4.5\mu\text{m}$
$\pm 5\mu\text{m}$	$\pm 5.7\mu\text{m}$

It emerges from this investigation of the parameters which determine the vertical curve of the wire that it is better to make use of equation 5, in which the linear mass of the wire does not appear.

Equation in the horizontal plane

When gravity and the tension are the only two forces acting on the wire, the projection of the wire on the horizontal plane is the straight line between its ends.

In the presence of transverse air currents, the wire can again form a catenary. Tests in the LEP tunnel revealed very slight lateral winds which were difficult to measure, being turbulent and thus tending to cause the wire to oscillate. Their effect may be eliminated by adjusting the time interval (data rate) for offset measurements. Alternatively, and more simply, as is proposed, the wires could be enclosed within a tube to shelter them from air movements.

In the horizontal plane the wire provides a geometric reference frame directly. For the vertical plane it is important to determine the height differences h and f as accurately as possible.

Advantages of stretched wires

The advantages of using stretched wires to provide the geometric reference framework are as follows :

- offsets can be measured with micron precision (see previous chapter), the wires are unaffected by radiation,
- a large number of sensors can be used simultaneously on the same reference line,
- in relation to the accuracy of measurements, long distances can be covered,
- planimetric position is very well defined, only the positions of the two end points need to be known,
- vertical position is very well defined provided that the two height differences are measured with sufficient accuracy.

Disadvantages of stretched wires

The major disadvantage of stretched wires lies in their use as a vertical reference frame. The two height differences which enable the vertical curve to be computed must be measured, and cartesian coordinates must be calculated, with the highest possible accuracy.

Use of stretched wires in the CLIC alignment system

Stretched wires provide a very good two dimensional geometric reference frame covering a long distance with relatively few unknowns involved. They are thus suitable for providing the high order metrology network for the initial alignment of the accelerator.

In addition, offset measurement systems can be fitted to the components to be moved during the acceleration of the beam. Thus, once the network of wires has been determined, the movements can easily be controlled by direct measurements of offsets from the wire.

The wire thus constitutes a very valuable geometric reference system provided that there is a separate high-precision vertical reference system. This leads to the discussion of the hydrostatic levelling system (HLS).

6.2.2 Hydrostatic alignments

Essential details

The hydrostatic alignments to which measurements by the HLSs are referred lie on an equipotential surface in the earth's gravity field. As a first approximation it is assumed that this forms a spherical surface whose radius is that of the earth.

It is desired to use these alignments as the vertical reference frame for the positioning of components of the accelerator along a straight line. The different paths followed by a water surface at rest and by a straight line are shown in Fig. 22. The difference in height to the end of the straight line is far too great to be able to consider using only a single hydrostatic alignment over the whole length of a linac.

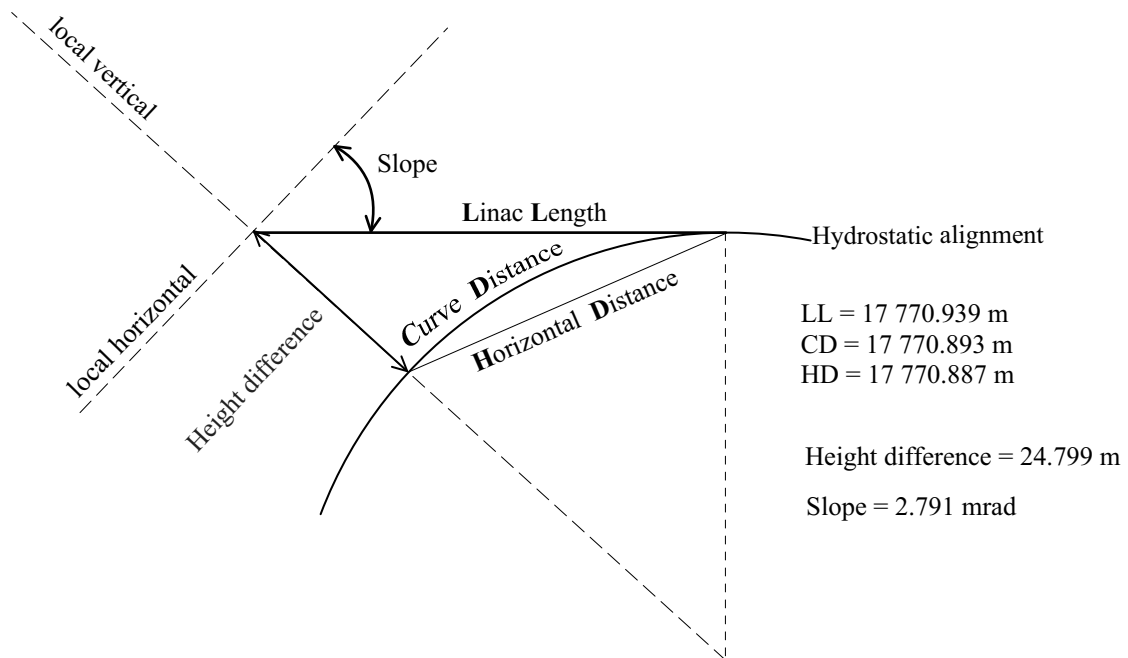


Fig. 22: Differences between a straight line and a hydrostatic alignment

In order to restrict the vertical offsets separating the HLSs from the linac to reasonable values, several hydrostatic lines will be required. A set-up like that shown in Fig. 23 allows the relative positions of successive lines to be determined and thus ensures the continuity of the geometric reference system.

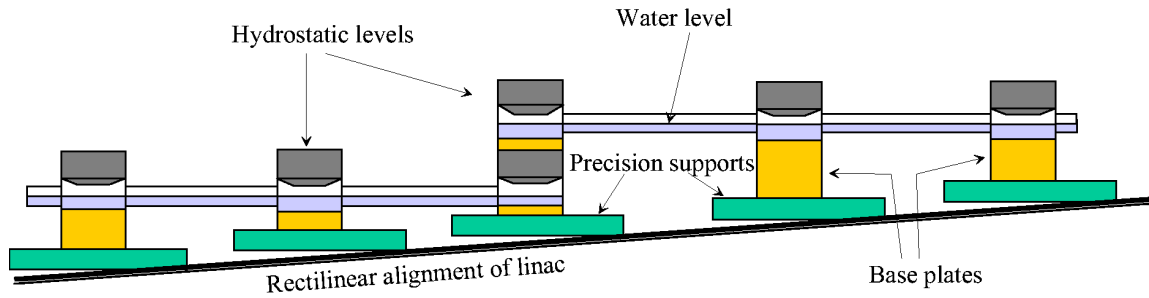


Fig. 23: Start and end points of hydrostatic alignments

Advantages of hydrostatic alignments

In the present case the use of hydrostatic alignments as the geometric reference frame has two advantages :

- they can provide height measurements to micron precision (see chapter 4), they are unaffected by radiation,
- the long and continuous reference system which they provide allows height differences to be determined very accurately by reference to a water level over much greater ranges than optical levelling.

Disadvantages of hydrostatic alignments

The major disadvantage of using hydrostatic alignments for vertical referencing is that water levels follow equipotential surfaces of the earth's gravitational field. It is difficult to determine the geometry of such surfaces in relation to a reference frame so as to allow a straight line to be established. This problem will be rediscussed in the section devoted to gravitational anomalies.

Use of hydrostatic levelling lines in the CLIC alignment system

The hydrostatic levelling lines provide the geometric reference frame for the measurement of the two height differences required to determine the catenary of the stretched wires. They are also employed for the measurement of the differences in height used directly in the establishment of the reference network.

These may include, for example, height differences between successive stretched wires or even between those which are further apart, depending on the available knowledge of the geometry of the equipotential surface.

6.2.3 Optical alignments

The laws of propagation of light rays through a thin lens will not be repeated here. As has already been seen, gravity complicates the use of both wires and hydrostatic systems. The advantage of using light rays to provide geometric reference frameworks is their insensitivity to gravity. With a system such as that described in chapter 5, this enables measurements of vertical offsets to be as accurate as those of horizontal offsets. Furthermore, the optical systems foreseen to be used can also measure tilts and have a significant cost advantage over the wire sensors.

The disadvantage of optical systems is that the length over which they may be used with sufficient accuracy is limited by the medium through which the light is propagated. In the case of air, even small temperature gradients can cause significant deflections. It would be necessary to operate in a vacuum to overcome these limitations, but this would lead to other constraints.

6.3 Configuration of the metrology network

The purpose of this section is to introduce the basic configuration of the metrology network which is foreseen for CLIC. The possible variations on this network, and the selection of the optimum configuration will be discussed in the section dealing with the simulations which have been carried out.

The configuration of sensors and their associated geometric reference frames are first described, and then the method of computing the network is explained.

6.3.1 Positioning the alignment sensors

The layout of the planned network is shown in Fig.26. It has been shown that the initial alignment consists of aligning the articulation points of the girders on which the accelerating cavities are mounted. Each articulation point is equipped with a RASNIK-CCD transmitter, lens and sensor side by side, as shown in Fig. 24.

This allows the measurement of the misalignment of each articulation point with respect to the straight line joining the two adjacent articulation points. At regular intervals of approximately 49 m (22 modules), the articulation points are connected to a network of stretched wires by a combination of two offset and tilt monitor measurements. This network consists of two lines of wires about 98 m long, parallel to the linacs and overlapping by half their length (Fig. 25) [10]. The fixing and tensioning systems for these wires are mounted on platforms fixed on the concrete block.

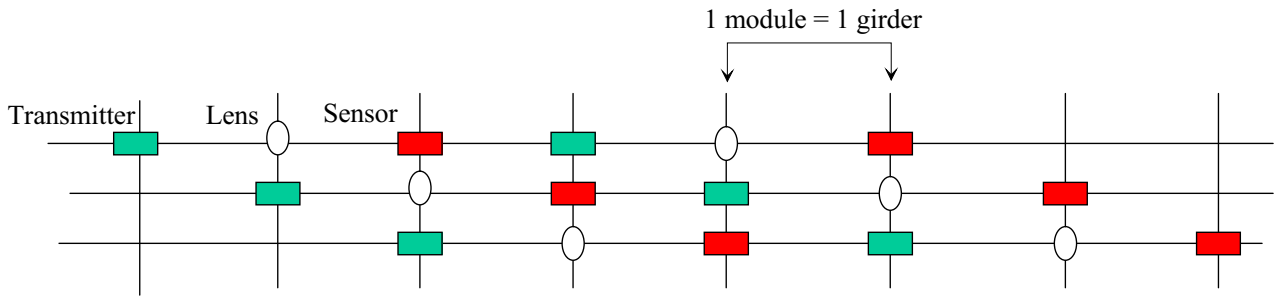


Fig. 24: Overlap of optical alignment systems

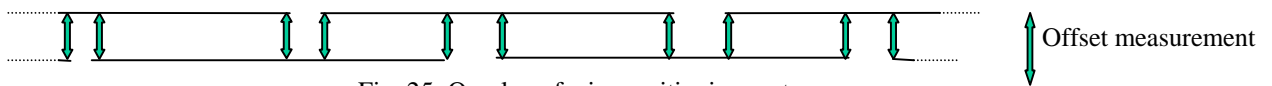


Fig. 25: Overlap of wire positioning systems

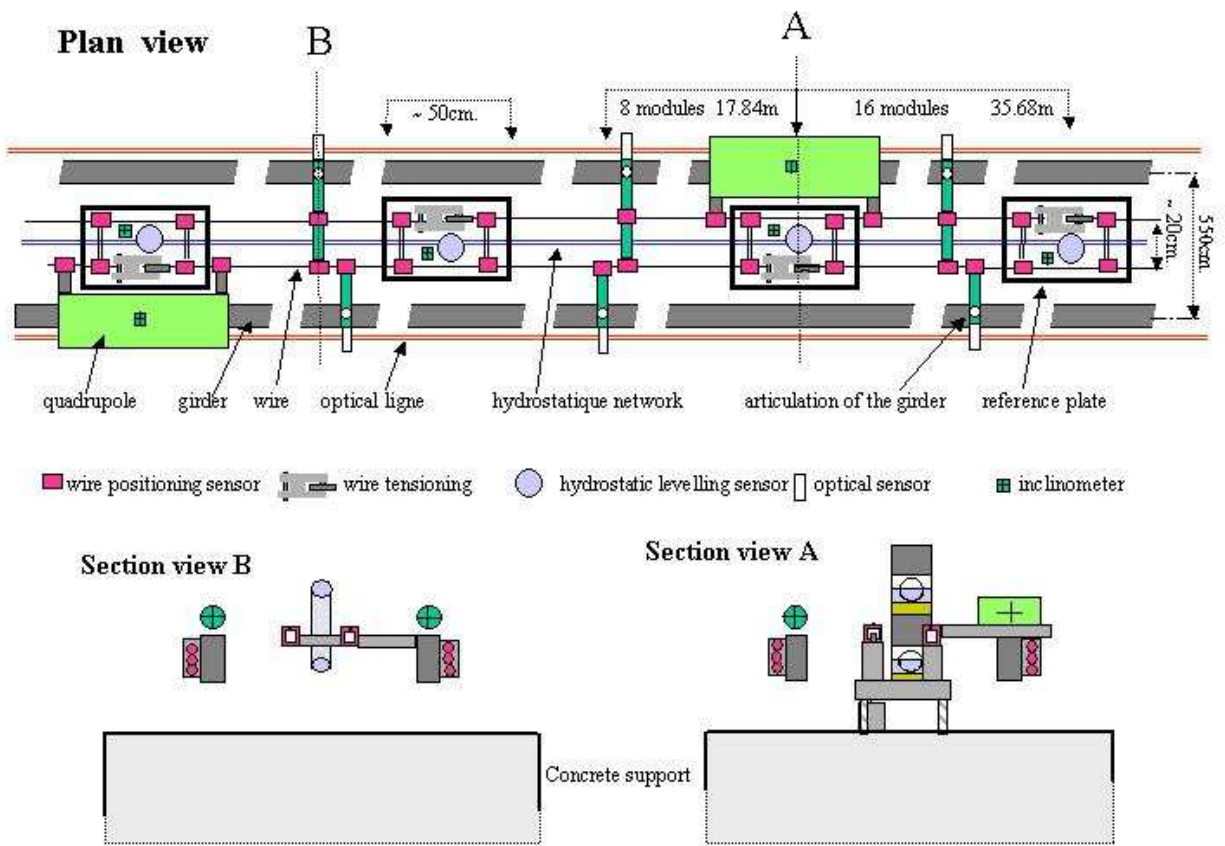


Fig. 26: Layout of the planned network

The platforms act as supports for pairs of wire positioning systems measuring the transverse and vertical offsets between two wire ends in one line and the overlapping wire of the parallel line. These measurements serve to fix the wire network. Between two consecutive platforms, in terms of connections between wires and girders, the offsets between wires are measured using other pairs of WPSs combined with tilt monitors. This type of measurement leads to improvements in the redundancy in the computation of the wires.

These platforms also serve as supports for the sensors for the hydrostatic levelling network. Their inclination is measured using a two-axis tilt monitor. Thus the height information from the HLS can be used for the vertical measurements for the four WPSs on the platform. The hydrostatic levels are used for the measurement of the two height differences needed to determine the form of the catenary of each wire, as well as for the height difference measurement between neighbouring wires. Meanwhile the magnetic quadrupoles, which are independent of the girders, are equipped with offset measurement systems and tilt monitors with which they are positioned in relation to the wires.

6.3.2 Calculation of the network and the positioning of the components

The major part of the establishment of the network lies in the computation of the positions of the stretched wires, which can be considered as the primary metrology network.

Once these positions are known it is possible to determine the positions of the articulation points of the girders to which the wires are connected. The secondary network can then be computed, this consists of the overlapping optical offset measurement systems and is placed between pairs of points connected to the primary network. The computation of this secondary network is at the same time the computation of the positions of the girder articulation points.

Finally the positions of the quadrupoles are derived from measurements of the TMSs, and the WPSs which are fitted to each quadrupole.

6.4 Study of perturbations of gravity and their consequences

In order to derive any benefit from the high accuracy achieved by our sensor measurements relative to the geometric reference systems introduced in 6.2, it is essential that these should themselves be defined with micrometric accuracy in a reference frame which allows us to establish a straight line such as that of the CLIC linac.

As these reference frames are for the most part sensitive to gravity, it is not possible in this situation to consider the earth's gravity field as uniform and spherical, nor even everywhere perpendicular to an ellipsoidal model of the earth.

In this section the disturbing effects which cause the gravity field to depart from a regular ellipsoidal form, and the extent to which this affects the components of the CLIC alignment system are discussed. Two phenomena disturb the gravity field, the distribution of mass in the neighbourhood and the attraction of the moon and the sun.

The distribution of mass in the neighbourhood

Topographic relief and differences in density of the body of the earth can be considered as anomalies which result in a gravity field which is different from that of a homogenous ellipsoid. Thus for example the mountains in the neighbourhood of CERN exercise on any mass m an attraction dg which must be combined with the attraction γ , normal to the ellipsoid, to obtain the true attraction g (Fig. 27).

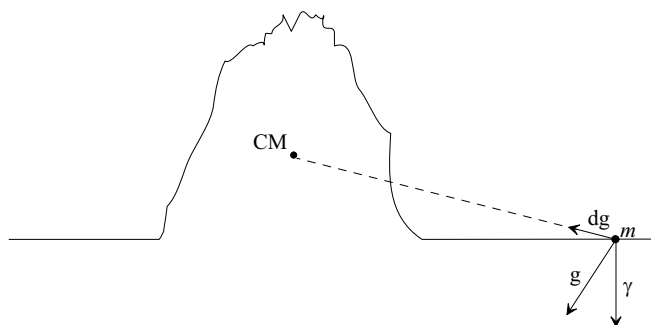


Fig. 27: Effect of a nearby mass anomaly

A study of the gravity field in the neighbourhood of CERN is given in Bell, 1985 [11]. The results of a simulation using a model of the masses covering an area of 70×50 km indicate a maximum deviation of the vertical of 15" (sexagesimal seconds) relative to the ellipsoid of the CERN system, at the level of the topographic surface, oriented perpendicular to the line of the Jura mountains (the upward vertical is deflected by 7" to the south and 13" to the east). We will use this maximum value in the following section in order to analyse the effects of masses in the neighbourhood.

Attraction of the moon and the sun

Acting as perturbing masses, the moon and the sun modify the terrestrial gravitational field. Their peculiarity is that their effect at a given point varies continuously with their varying positions in relation to the earth. The acceleration due to gravity \bar{g} thus changes continuously both in direction and in intensity. The intensity varies within a range of $\pm 2.4 \times 10^{-6} \text{m.s}^{-2}$, while the direction can vary by $\pm 0''05$ (Melchior, 1973, chap. 1.5) [12].

Elsewhere, marine tides are another more conspicuous consequence of lunar and solar attraction. It is in part because of its response to the continuous variations in gravitational potential that the free surface of the oceans is in constant motion. If the terrestrial globe is considered as an elastic fluid, this also deforms continuously under the influence of the moon and the sun. This is the "earth tide" phenomenon, studied by Melchior, 1966 [13] and Jobert and Coulomb, 1973 [14].

The perturbing effects described above are liable to have consequences for the geometry of the ground surface and hence also the geometry of the accelerator itself, as well as for the use of wire positioning systems, hydrostatic levels and inclinometers.

6.4.1 Repercussions of ground deformation on CLIC alignment

The ground surface deforms continuously under the influence of the moon and the sun. Since earth tides are a periodic phenomenon, the accelerator, rigidly fixed within the ground, could be subjected to deflexions which are incompatible with its proper operation (Fig. 28)). These deformations would then have to be corrected by the alignment system.

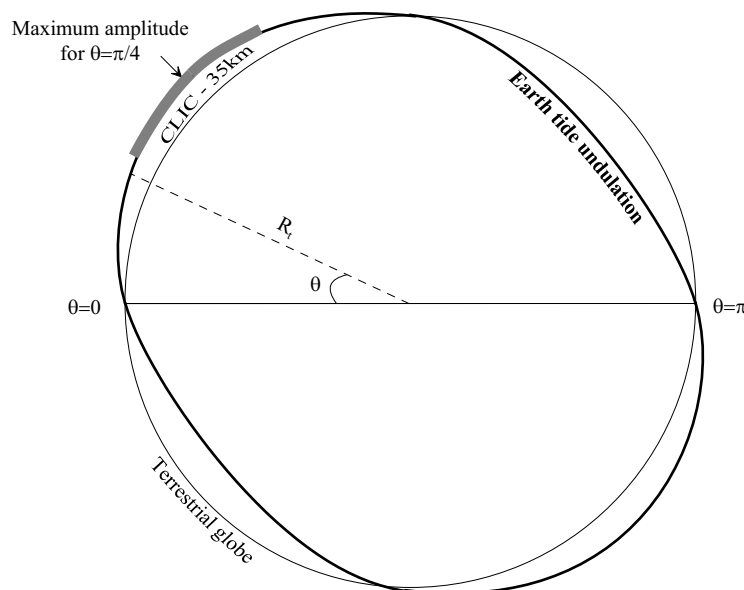


Fig. 28: Simplified tidal waveform propagated along the alignment of the CLIC

A preliminary approximate computation allows us to analyse the possible deformations due to earth tides over the range of 35 km. According to Melchior, 1973, the maximum amplitude of this wave is about ± 40 cm and it can be broken down into elementary sinusoidal components. The elementary components with the largest amplitudes have periods of about 12 hours. Consider the most unfavourable situation, with a sinusoidal wave of amplitude 40 cm and a period of 12 h, propagated along the alignment of CLIC. This situation is illustrated in Fig. 29 which shows the plane section through the centre of the earth which contains the accelerator.

The 35 km line has a maximum curvature when its mid-point is at the peak of this oscillation, as shown in Fig. 28. The deflexion due to the earth tide can thus be estimated by simple differences of ordinates on this sine wave.

From an approximate computation, the value of the deflection over 35 km is 6.0 μm and thus remains far smaller than the accuracy of $\pm 10 \mu\text{m}$ over 200 m which has to be maintained. The deformations of CLIC due to ground movements engendered by the attraction of the moon and the sun are therefore negligible.

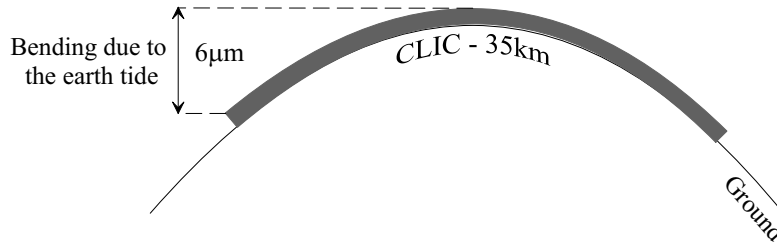


Fig. 29: Bending of the accelerator due to the periodic undulations of the earth tide

6.4.2 Effects which perturb the wire positioning systems (WPS)

For the correct use of the WPS, it is essential to have precise knowledge of the geometry of the stretched wires. This geometry depends on the tension applied to the wire and its weight per unit length (which is assumed to be constant), and on the gravitational field.

Equations 3 and 4 which model the shape of the wire in a gravitational field which is uniform and vertical with respect to the chosen frame of reference have already been presented in 6.2.1.

As the tension applied to the wire is provided by a counterweight, the ratio q/H of the linear weight to the applied tension remains constant when the vertical component of \vec{g} varies uniformly. From the above equations it can thus already be deduced that in the vertical plane the wire does not deform as a result of uniform variations of the acceleration due to gravity. However other types of perturbation are liable to alter the geometry of the wire, these are discussed as follows.

Non-uniformity of the gravity field

Equations 3 and 4 were established on the basis that \vec{g} is the same everywhere. However in reality this is not strictly true and it is necessary to evaluate the variations in the intensity of the gravity field which bring about the following three phenomena:

(a) Variations with latitude

On the terrestrial ellipsoid, the normal attraction $\vec{\gamma}$ (see Fig. 27) increases with the latitude φ and diminishes with the altitude h in accordance with the relationship (8) given below (R is the radius of curvature of the earth's surface, which is approximately 6378.7 km in the region of CERN), defined by the International Union of Geodesy and Geophysics *IUGG*³ [Vanicek and Krakiwsky, 1982, p.79] [15]:

$$\gamma = 9.7803185 \cdot \left(1 + 0.005278895 \sin^2 \varphi + 0.000023462 \sin^4 \varphi \right) \cdot \left(1 - \frac{2h}{R} \right) \quad \text{Equation 8}$$

The difference between the normal attraction at the ends of a 100m wire will be greatest if the wire is oriented north-south. Around CERN this maximum difference will be in accordance with $\Delta g_\varphi \cong 8 \cdot 10^{-7} \text{ m} \cdot \text{s}^{-2}$.

(b) Nearby masses

The deviation of the vertical due to nearby masses is not constant and diminishes as one gets further away from the Jura [Bell, 1985] [11]. Taking the extreme case with the deviation at its maximum of 15'' at one end of a wire and zero at the other, the effect on g would be $\Delta g_m \cong 2.6 \cdot 10^{-8} \text{ m} \cdot \text{s}^{-2}$.

(c) Luni-solar attraction

Since the positions of the moon and the sun in relation to the two ends of a wire are different, a different alteration in the intensity of \vec{g} will result at each end (see 6.4.1). According to calculations, for the region of CERN, the maximum resulting discrepancy in g is $\Delta g_{ls} \cong 3 \cdot 10^{-11} m \cdot s^{-2}$.

Thus the effects of nearby masses and of lunar and solar attraction on the variations in the intensity of the gravitational field are negligible compared with those resulting from variations in latitude. As a consequent only the latter have been taken into account in analysing the consequences of non-uniformity of the gravitational field for the geometry of a wire. It has been assumed that \vec{g} would vary linearly from one end of a wire to the other.

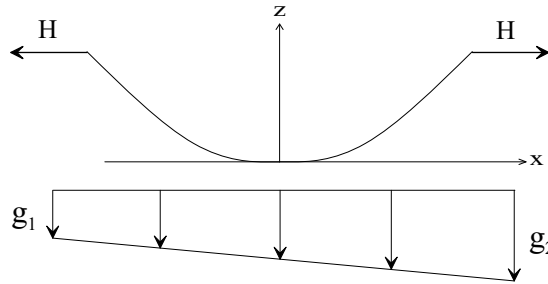


Fig. 30: Wire in a non-uniform gravitational field

It can be calculated that, with the origin of coordinates at the lowest point of the wire, the differences between the catenaries of two wires, of which one is immersed in a uniform gravity field (Fig. 19) and the other is in one which is non-uniform, can reach the non-negligible value of $9 \mu m$. It should be possible to confirm this theoretical result by experiment. If it transpires that the wire is indeed deformed because of the difference in latitudes between its ends and that the assumed model is sufficiently close to reality, it would be possible to correct for this effect when wires are used for the vertical alignment.

Curvature of the gravitational field

It has been shown in 6.2.1 that the curvature of the earth, which to a first approximation is also that of the gravity field, represents about $200 \mu m$ over $100 m$ (Fig. 20). The effect of this on the shape of the wire has been calculated the field of force shown in Fig. 31.

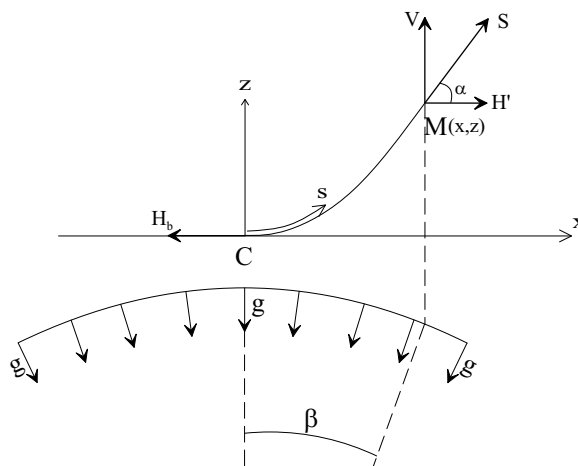


Fig. 31: Wire in a curved gravity field

The calculation shows that, with the origin of coordinates at the lowest point of the wire, the differences between the catenaries of the two wires, of which one is immersed in a uniform gravity field (Fig. 19) and the other is in a curved field (Fig. 31), remain substantially less than $1 \mu m$. *The effects of the curvature of the gravity field on the wires of the WPS may therefore be neglected.*

Nearby masses

Assume first that along a 100 m wire the deviation of the vertical due to nearby masses is constant.

It has already been shown that in this case the wire is not deformed in the vertical plane. However it could be deformed transversely or longitudinally depending on the orientation of the horizontal component of \vec{g} .

(a) Transverse deformation

If it is assumed that the horizontal component of \vec{g} is oriented perpendicularly to the wire, the horizontal projection of the system of forces is analogous to that of Fig. 19. A numerical computation was made to calculate the deformation for a maximum deviation of the vertical of 15" perpendicular to the wire. The results indicate that for a 100 m stretched wire the transverse deformation is slightly greater than 1 μm . If CLIC has to be built in a site where such deviations are encountered, it would be necessary to determine these and apply the necessary corrections when a wire is used for horizontal alignment.

(b) Longitudinal deformation

The case where \vec{g} has a horizontal component parallel to the wire has also been considered (Fig. 32), and the deformations of the wire due to this longitudinal attraction have been evaluated.

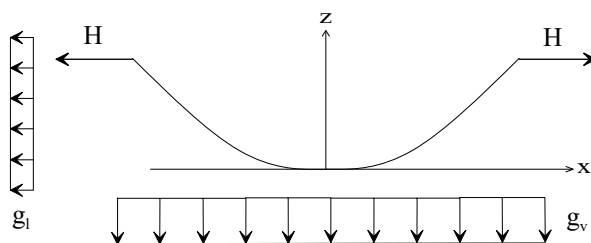


Fig. 32: Wire subjected to a longitudinal attraction

With the origin of coordinates at the lowest point of the equilibrium curve of the wire, the differences between the parabola (Fig. 19) and the curve obtained by applying the maximum longitudinal attraction (Fig. 32) remain substantially less than 1 μm . It also transpires that the values taken on either side of the lowest point are sufficiently symmetrical to consider that this point is not displaced longitudinally.

The longitudinal effect of nearby masses on the geometry of a CLIC WPS wire is thus negligible.

Effects of attraction by the moon and the sun

As with nearby masses, the moon and the sun lead to a deviation of the vertical. According to Melchior, 1966 [13], p.20 this deviation never exceeds 0.05" which is well under the value of 15" which has been assumed above in studying the effects of nearby masses on the wires, which were seen to be negligible. The deviation of the vertical due to luni-solar effects can therefore also be neglected. Moreover it has also been shown that the non-uniformity of the gravity field caused by the attraction of the moon and the sun is negligible.

Thus the effect of the attraction of the moon and the sun on the geometry of the CLIC WPS wires is negligible.

6.4.3 Effects which perturb the hydrostatic levelling systems (HLS)

The water at rest in the network of pipes connecting the HLS vessels is intended to provide a reference surface for the vertical alignment of CLIC. This obviously only makes sense if the geometry of the reference surface itself, which is an equipotential of the gravitational field, is known to the required degree of accuracy. The deformation of such equipotentials by nearby masses is constant, while the deformations induced by the attraction of the moon and the sun are variable with time. The repercussions of these two phenomena for the use of the HLS will now be examined

Effect of nearby masses

In the presence of a topographic anomaly the equipotential surfaces of the gravity field are deformed, as shown in Fig. 33. Among results given by Bell 1985 are the differences between the equipotential surfaces and the ellipsoid model of the earth used for geodetic computations at CERN. Although almost zero at the Meyrin site, these differences can exceed 20 cm towards the Jura.

The heights of a point above the ellipsoid and the geoid can thus be significantly different. However the primary interest is the height differences between pairs of points. If the height differences with respect to each of the two surfaces were sufficiently similar for each point, the undulations of the equipotential surface could be ignored and the raw height differences obtained with the HLS could be considered to refer to the ellipsoid.

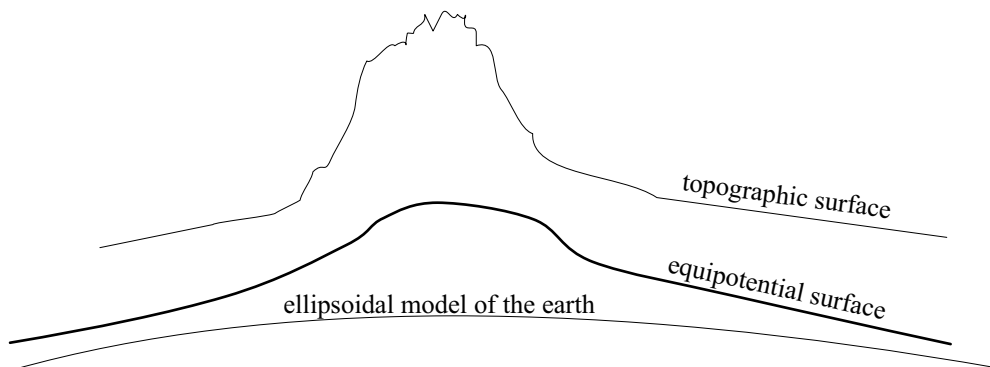


Fig. 33: Equipotential surface deformed by a topographic anomaly

To investigate this potential problem, the following procedure and subsequent calculation was made for the LEP site:

- Selection of two sets of points (100 m grid) defined in geocentric coordinates and contained in the plane of the LEP accelerator; the first set relates to an area where there is only slight ground relief, while the second set is at the foot of the Jura;
- With coordinate transformation programs and making use of the correct geoid and ellipsoid for CERN, computation of the heights of the points in relation to each of the reference surfaces (Fig. 34);
- Calculation and comparison of the two types of height difference between pairs of points 100 m apart.

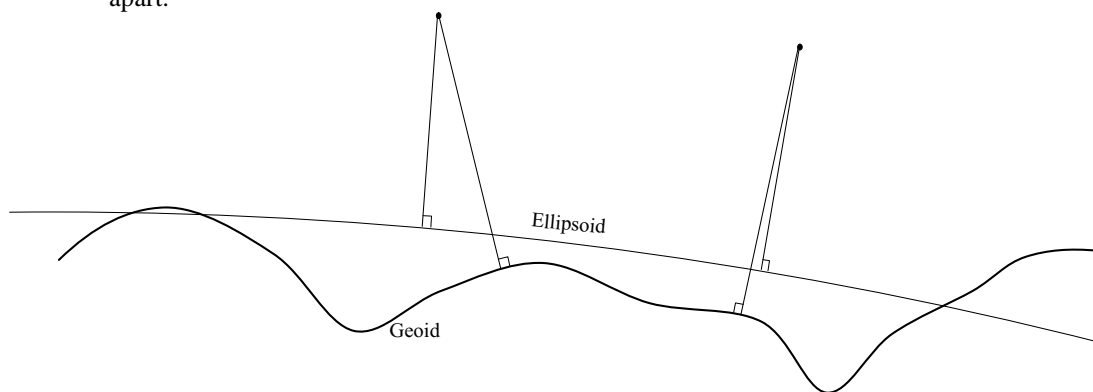


Fig. 34: Heights above the ellipsoid and the geoid

The results of this computation are given in Table 6. These results show us that it will not be possible to disregard the undulations of the hydrostatic surfaces with respect to the ellipsoid. **Knowledge of the geometry of the equipotential surfaces due to gravity is thus essential for the use of the HLS for the alignment.** The required accuracy (a few micrometres in height differences between points about a hundred meters apart) is very unusual in gravimetry. Steps have been taken to find out the best accuracy available from current methods for this type of determination.

	<i>Flat ground on the surface</i>	<i>Accideted ground on the surface</i>
Number of pairs of points	110	110
Mean difference (μm)	153	366
Mean difference (μm)	246	458
Minimum difference (μm)	60	273

Table 6: Differences between height differences referred to the ellipsoid and the geoid

Undulations of an equipotential surface with respect to a reference ellipsoid

A 40 km geoid profile of a possible CLIC installation site has been calculated. This profile (Fig. 35) is based on the geoid model CHGEO98 established by the Federal Topography Office in Bern.

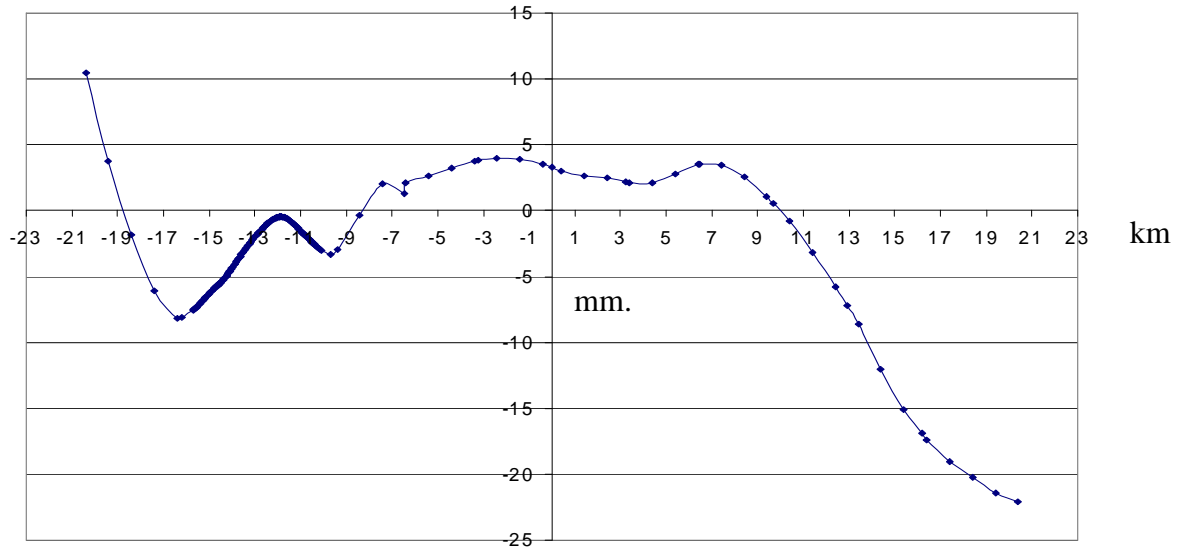


Fig. 35: Geoid Profile along CLIC

The geoid is a particular equipotential surface, and we can therefore reasonably suppose that the profile in Fig. 35 may be considered to be that of the water in the HLS tubes.

It is important to realise that one can interpret this profile as that of an accelerator in a Cartesian reference frame if we started from the principle that hydrostatic lines follow a trajectory parallel to an ellipsoid surface, and that this hypothesis forms the basis for the determination of the corrections to be made in order to return to a straight line.

As one can see, the profile includes a section where the density of points is higher, where there are points every 20 or 40 m, and two other sections where there is only a point every kilometre.

We have used this increased density of points to evaluate the geoidal undulations, which give a good indication of the straightness that an accelerator would have if one supposed that the hydrostatic lines had a perfectly elliptical curve.

For each 200 m segment included in the denser section (Fig. 36), the maximum offset of the geoid profile has been calculated with respect to a straight line passing through the point at each end of the segment. These defects are relatively large, even though they are less than the $\pm 10 \mu\text{m}$ threshold over 200 m. In fact, these would be the defects in the CLIC if it could be perfectly aligned with respect to an ellipsoidal surface. It should be said however that the measurements and the mechanical links of the metrological network will also introduce their own errors.

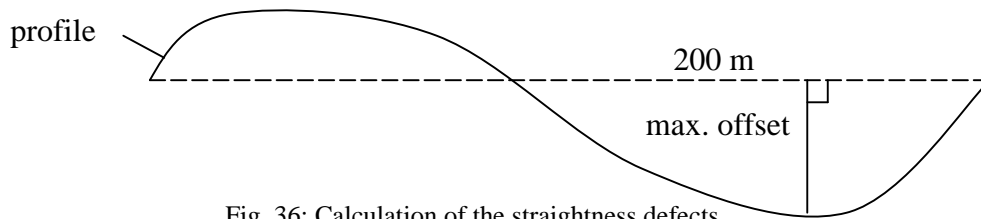


Fig. 36: Calculation of the straightness defects

The results of these calculations are presented in Fig. 37. The rms of the straightness defects over 200 m is $\pm 8.4 \mu\text{m}$.

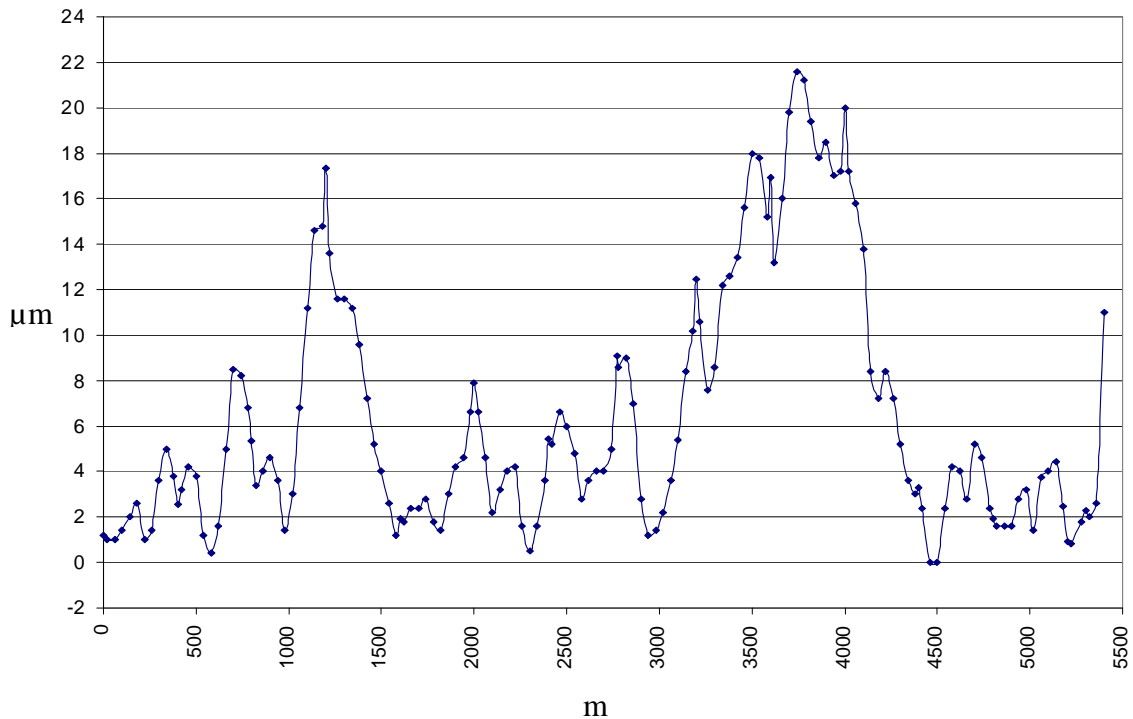


Fig. 37: Defects in the straightness of the profile in micrometers

The approximations made in neglecting the fact that the hydrostatic lines do not have an elliptic curvature are therefore too large, even more so since the calculations that have been made are based upon a geoid model likely to show differences with respect to the real situation.

Knowledge of the equipotential surfaces of the gravity field is consequently indispensable for the use of HLSs for this alignment.

The required precision (several microns in the height differences between two points a hundred metres or so apart) is very unusual in gravimetry, and the CERN survey group has undertaken steps to understand the best precision achievable with current techniques for this type of determination.

Effects of the attraction of the moon and the sun

The HLS are affected by both oceanic and earth tides because the water in the pipes and the ground to which the whole system is fixed are being continuously deformed under the influence of the moon and the sun and are thus modifying the values recorded by the sensors.

It has been shown that earth tides do not affect the straightness of the alignment of the accelerator, but merely vary the inclination of the whole system. Tidal effects on the HLS must thus be corrected and not interpreted as alignment errors.

The theoretical values of the tides which result from the attraction of the moon and the sun, will now be examined and compared with the readings which have been taken on a hydrostatic line at CERN.

Theory of tides

Tides result from the fact that water surfaces at rest, together with the earth considered as an elastic fluid, deform in response to the continuously changing gravitational field. This change results primarily from the continuously varying positions of the moon and the sun relative to the earth.

According to Melchior, 1966, p.15 [13], the disturbing attraction of the moon or the sun is derived from the potential W_2 as follows:

$$W_2 = \frac{GM_e (M_c/M_e)}{2} \cdot \frac{a^2}{r^3} \cdot (3 \cos^2 z - 1) \quad \text{Equation 9}$$

G : Newton's gravitational constant

M_e, M_c : masses of the earth and of a given celestial body

a : distance from a given point to the centre of the earth

r : distance from the celestial body to the earth

z : zenith angle of the celestial body at the point

G, M_e and M_c/M_e are known, a can be calculated from the coordinates of the point in question using geodetic formulae, and z and r may be calculated using astronomical ephemerides.

From Equation 9 it can be deduced that the resultant deformation ξ of the gravitational equipotential surfaces, given by Melchior, 1966, p.16 is as follows:

$$\xi = W_2/g \quad \text{Equation 10}$$

Knowing that :

$$g = \frac{GM_e}{a^2} \quad \text{Equation 11}$$

It can be shown that :

$$\xi = \frac{m_l \cdot a^4}{2r_l^3} (3 \cos^2 z_l - 1) + \frac{m_s \cdot a^4}{2r_s^3} (3 \cos^2 z_s - 1) \quad \text{Equation 12}$$

m_l, m_s : ratio of the masses of the moon and the sun to that of the earth

z_l, z_s : zenith angles of the moon and the sun at the point

r_l, r_s : distances from the moon and the sun to the earth

The computation leads to values of ξ which can reach several tens of centimetres in absolute terms. The variations in the height of a liquid at rest (which is known to conform to an equipotential surface) do not reach these values because the liquid changes its potential rather than following the same equipotential with its movements. On the other hand one can observe variations in the differences of level of a liquid which illustrate the changing deformations of equipotential surfaces and of the ground.

The difference between the readings of two HLS vessels thus combines the tidal effects on the water in the pipes and on the ground which supports the whole system. These tilt effects must be corrected. In fact, if this is not done, the height differences obtained from the HLS could be interpreted as departures from rectilinearity in the accelerator components, whereas it has been shown in 6.4.1 that the tidal flexing of the accelerator is negligible.

Love's numbers

Love's numbers [Melchior, 1966, part 2, chap.1] [13] are used to formalise the expression of different aspects of earth tides. These will be useful for the interpretation of HLS data. The application of Love's numbers is very straightforward and each type of elastic deformation due to tidal effects can be represented by a combination of these numbers. They are linked by rather complex differential equations to the distribution of densities and of module of rigidity within the earth, but can be considered as functions solely of the distance from the point in question to the centre of the earth.

On the earth's surface and for the phenomena of interest, the two Love numbers which will be used are known as h and k .

h represents the ratio of the height of the earth tide to the height of the corresponding tide of an ocean at rest.

The effects of the density variation which accompanies the deformation and displacement of masses due to the attraction of the sun and the moon can be modelled by means of an additional potential. k represents the ratio of this additional potential caused by the deformation itself to the disturbing potential W_2 .

Thus the total disturbing potential is $(1+k)W_2$, and the tide observed on an ocean at rest would have a height of $(1+k) \cdot W_2/g$. However, if this tide is observed by means of a reference mark attached to the earth's surface, the mark is itself displaced because of the earth tide by a height of $h \cdot W_2/g$ in relation to the surface of the earth (considered as spherical). The observed deformation ξ_0 will thus be :

$$\xi_0 = (1+k-h) \cdot \frac{W_2}{g} \quad \text{Equation 13}$$

The values usually accepted for h and k are as follows [Jobert and Coulomb, 1973] [14]:

$$(1+k) = 1.3 \quad \text{and} \quad h = 0.6 \quad \text{hence} \quad \boxed{(1+k-h) = 0.7}$$

This implies that the tide observed on an ocean at rest by means of a reference mark attached to the earth's surface would be 70% of that which would be observed if the earth were infinitely rigid ($h=k=0$).

Knowing these values it is then possible to calculate the corrections to be applied to readings taken on the HLS.

Correction of HLS readings for tidal effects

A hydrostatic line about 70 m long has been installed in a part of CERN which is stable and free of vibration. HLS vessels were placed at each end in order to read the distance separating their reference surfaces from the plane of a free water surface (Fig. 38). Recordings of the sensor values were taken at the desired frequency. Knowing the geodetic coordinates of the two HLS, the values of the tides have been calculated in order to correct the differences between the readings $l_{HLS2} - l_{HLS1}$.

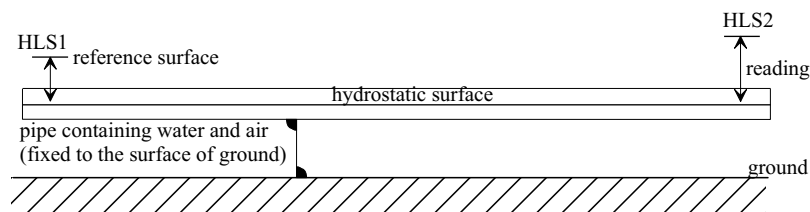


Fig. 38: Set-up used for HLS trials

The HLS are used to determine height differences by means of differences between the readings taken on each. With neither an earth nor a water tide, this difference would give us the height difference between the points directly, relative to a gravitational equipotential whose geometry would be invariant with time. But in reality the difference between the readings also includes the differences between the amplitudes of the water and earth tides as shown in Fig. 39.

In Fig 39(a), the water tide alone is considered, and it is assumed that the attraction of the moon and the sun is greater at HLS2 than at HLS1. At HLS2 the water will thus be attracted more strongly towards the reference surface of the HLS vessel than at HLS1, and, if the tide is ignored, HLS2 would appear to be too low compared with HLS1. The error in the height difference $l_{HLS1} - l_{HLS2}$ would be $(1+k)(W_{22}/g - W_{21}/g)$

W_{22} and W_{21} denote the tidal potentials at points HLS2 and HLS1 respectively, see equation 9.

In fig 39(b), the earth tide alone is considered, and it is again assumed that the attraction of the moon and the sun is greater at HLS 2 than at HLS1. As the HLS vessels are rigidly attached to the ground which is raised more at HLS2 than at HLS1, the reference surface will move further away from the water surface at HLS2 than at HLS1, and if the tide is ignored, HLS2 would appear to be too high compared with HLS1. The error in the height difference $l_{HLS1} - l_{HLS2}$ in this case would be $-h(W_{22}/g - W_{21}/g)$ note the opposite sign from case (a).

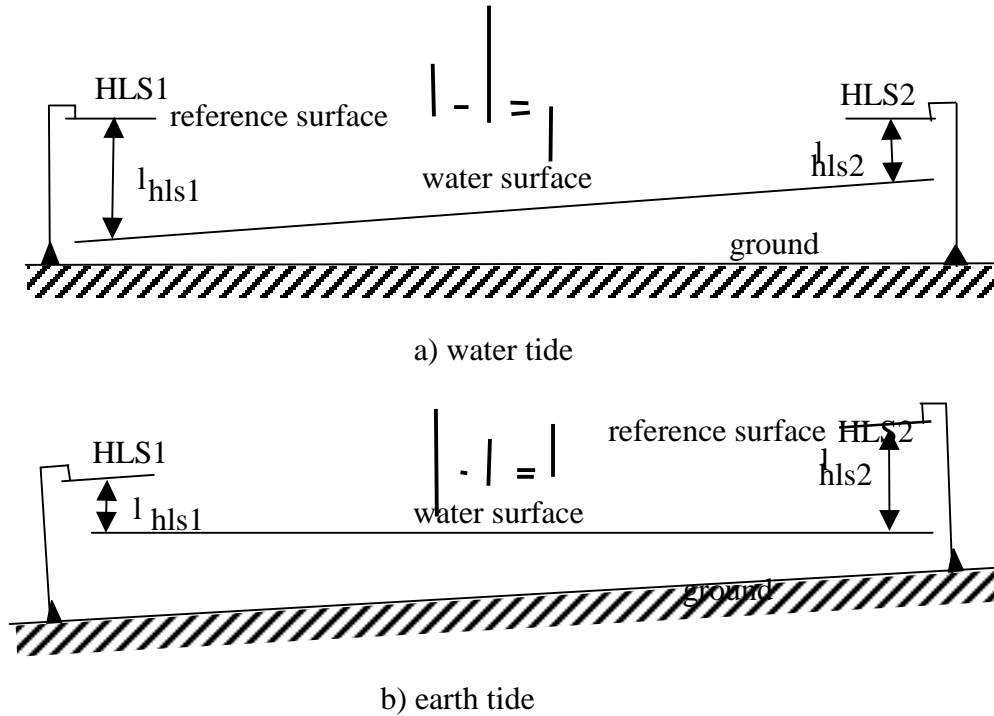


Fig. 39: Effect of tides on HLS readings

It can be seen that the earth and water tides, although always of the same sign, have opposite effects on HLS readings. It is this which explains why h is subtracted from $1+k$ in the determination of the amplitude of tides observed by means of a reference mark attached to the ground as in the present case. If the HLS readings at points 1 and 2 are denoted by l_{HLS1} and l_{HLS2} , the corrected height difference Δ_2^1 is obtained from :

$$\Delta_2^1 = (l_{HLS1} - l_{HLS2}) - (1 + k - h)(W_{22}/g - W_{21}/g) \quad \text{Equation 14}$$

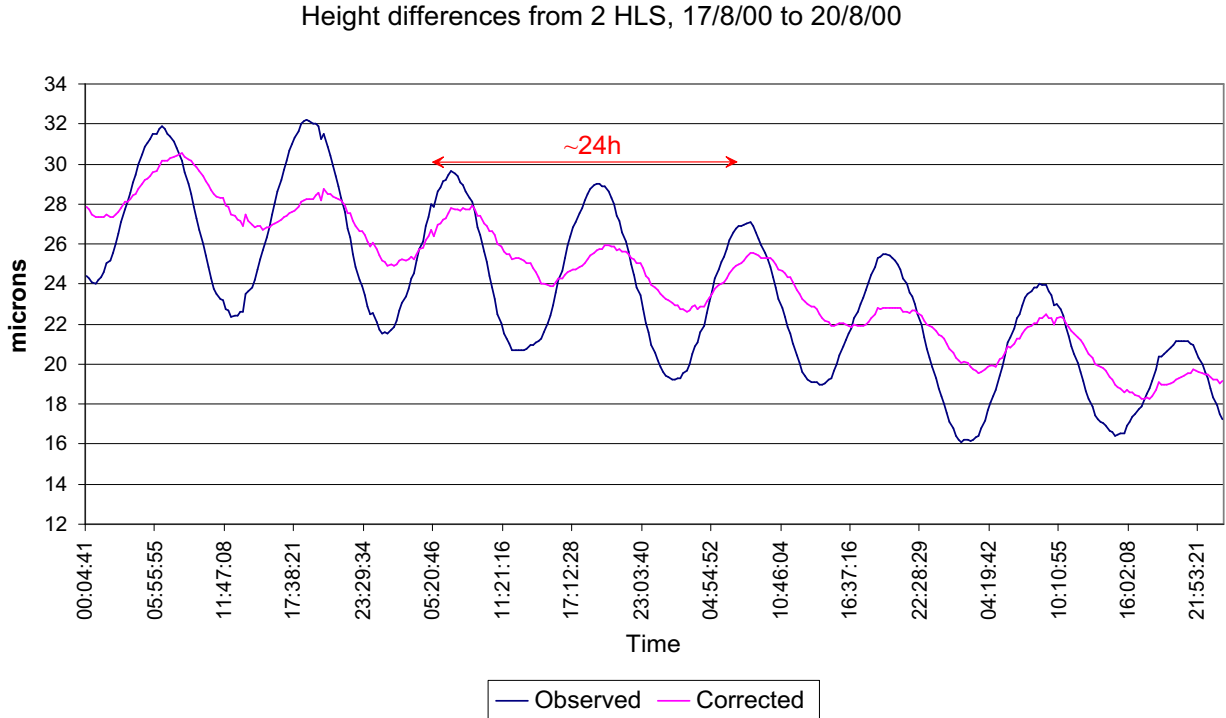


Fig. 40: Differences HLS 1 - HLS 2 : observed, and corrected for earth and water tide effects.

Fig. 40 illustrates the results which have been obtained. The test which will be now described covered a period of four days (a total of 393 readings taken at quarter hour intervals).

It can be seen that the difference HLS1 -HLS2, corrected for the tidal effects, shows both a more general diminishing movement together with residual semi-diurnal undulations with amplitudes of over 2 μm . The reduction appears to express a more general movement of the ground. The residual movements can be attributed in part to the accuracy of the data used in equation 12 (see below), but also relate to other phenomena which have yet to be addressed and which could involve alignment errors. These might include periodic ground movements other than tidal effects (such as thermal or diurnal effects) or local water heating.

An important question is whether this corrected signal is a good representation of the variations of height in relation to a straight line which rocks under the effect of tides, or whether the correction applied needs to be improved. Equation (6.10) is in fact very general, and by analysing in situ readings covering a period of one to three months it is possible to define tidal parameters for a particular site [Ducarme, 2001] [16]. This is a solution which will certainly be used for CLIC. In fact the HLS will be among the first equipment to be installed, and enough time will therefore be available to collect the data needed to establish a local tidal model.

The next section examines whether the parameters used to compute the corrections are known with sufficient accuracy.

Accuracy of corrections

It is necessary to evaluate the accuracy of the corrections calculated using expressions 12 and 13. Table 7 shows the accuracies of the parameters used in the test illustrated in Fig. 38. The accuracies shown for z_l et z_s are in fact averages calculated over a period of a year. For a given celestial body z is obtained as follows:

$$z = \sin \varphi \cdot \sin \delta + \cos \varphi \cdot \cos \delta \cdot \cos(\theta - \alpha) \quad \text{Equation 15}$$

- Where :
- φ is the latitude of the point in question $\sigma_{\varphi} \cong \pm 5 \text{ m}$ (for our test)
 - δ is the angle between the body in question and the plane of the equator
 $\sigma_{\delta_l} = \pm 0.03''$ for the moon et $\sigma_{\delta_s} = \pm 0.3''$ for the sun
 - θ is the sidereal time at the point in question $\sigma_{\theta} = \pm 1.2 \cdot 10^{-7} \text{ h}$
 - α is an angle between the body in question and the prime meridian
 $\sigma_{\alpha_l} = \pm 0.03''$ for the moon and $\sigma_{\alpha_s} = \pm 0.3''$ for the sun

Love's numbers are known with sufficient accuracy to consider them to be exact (they are now known to six places of decimals but one significant figure is sufficient for the present). The a-priori accuracy of the corrections applied, for a period of a year have been calculated. Fig. 41 illustrates the results obtained.

Parameter	Type	Accuracy
m_l	Physical constant	$\pm 1.10^{-9}$
m_s	Physical constant	$\pm 1.10^{-2}$
z_l	Ephemerides and geodesy	± 0.14 "
z_s	Ephemerides and geodesy	± 0.32 "
r_l	Ephemerides	± 4 m
r_s	Ephemerides	± 15 km
α	Geodesy	± 5 m

Table 7: Accuracies of parameters used to compute tidal corrections

It can be seen that the a priori accuracy of the corrections which has been applied are always better than $\pm 1 \mu\text{m}$. This result is entirely satisfactory at present but it can be further improved if necessary. In fact the points which were used for the trial were only fixed to ± 5 m in relation to the centre of the earth, while current geodetic methods easily allow an accuracy of better than ± 1 m to be achieved. As a guide, with the latter value, the accuracy of corrections to be applied to HLS readings would be of the order of $\pm 0.3\mu\text{m}$.

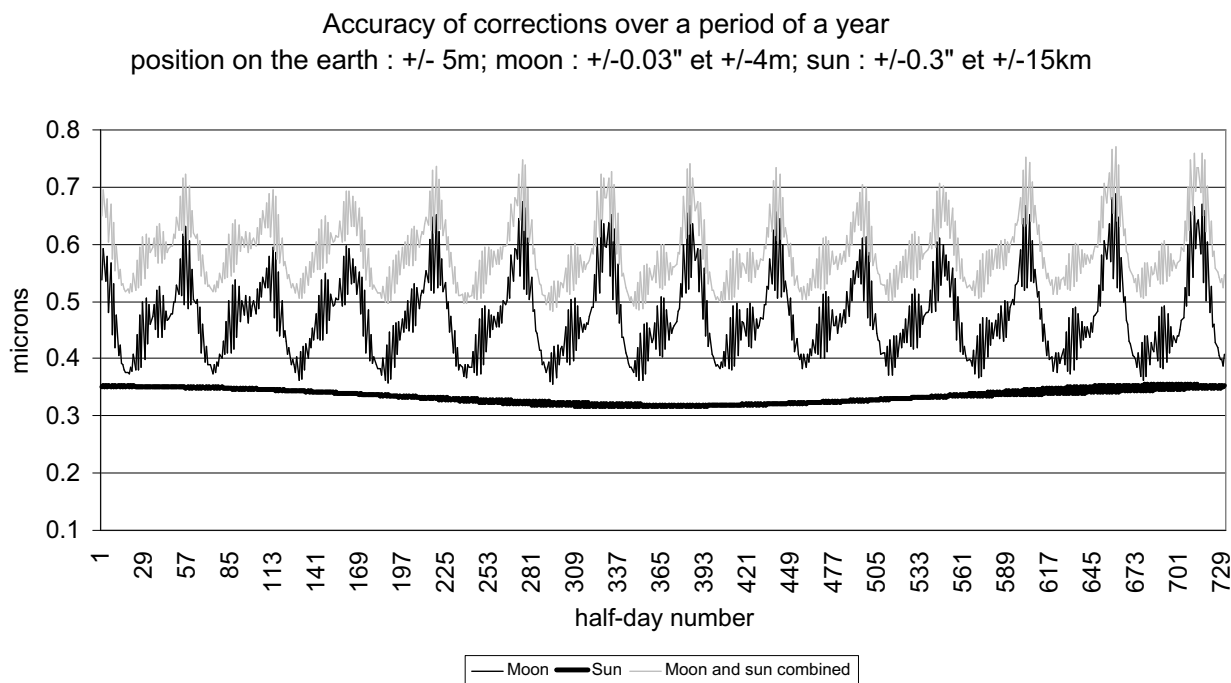


Fig. 41: Accuracy of the corrections applied to HLS readings

6.4.4 Effects which perturb the tilt monitoring systems (TMS)

The angles given by the tilt measurement systems relate to the local vertical. If there is a deviation of the vertical it may be necessary to apply corrections to inclinometer readings so as to reduce the computations to a frame of reference which allows the alignment of CLIC to be controlled. The next section examines the extent to which the deviation of the vertical affects the information obtained from the TMS and what corrections it is possible to apply.

Effect of the attraction of the moon and the sun

According to Melchior, 1966 [13], the deviation of the vertical due to the attraction of the moon and the sun never exceeds $0''05$, or $2.4 \cdot 10^{-7}$ radians since the accuracy of the TMS is currently only 10^{-6} radians, the deviation is imperceptible.

Thus the effect of the attraction of the moon and the sun on the use of the TMS is negligible with the current equipment.

Effect of nearby masses

Fig. 26 shows the effect of nearby masses on the direction of the local vertical. The results given in Bell 1985 [11] indicate deviations of the order of a sexagesimal second ($4.8 \mu\text{rad}$) at the CERN site, with a maximum of $15''$. These values are large enough to significantly affect the information supplied by the TMS and their effect must be corrected in order to achieve the reliability to $1 \mu\text{rad}$ which is expected from the sensor.

As for the HLS, a sufficiently accurate model of the local geoid is thus required, from which the deviations of the vertical can be deduced.

6.4.5 Summary of the effects of gravity

The consequences of the perturbations of the gravity field on the alignment of CLIC have been investigated.

The non-uniformity of the gravitational field and the deviation of the vertical are liable to deform the wires of the WPS significantly, but these two effects can easily be corrected.

In the CLIC configuration, in order to use the HLS, it will be necessary to take into account the effects of nearby masses as well as the attraction of the sun and moon (tidal effects).

The anomalies caused by the distribution of nearby masses demand a very accurate definition of the gravitational equipotential surfaces; a further study must be undertaken to determine whether current techniques are capable of achieving the level of accuracy required. If this does not prove to be the case, the use of the HLS for CLIC will be seriously compromised. It will then be necessary to develop an alternative solution which is capable of providing an adequate vertical reference system.

The tidal effects of the moon and the sun, which have been corrected during trial tests can be determined to the required accuracy.

The use of inclinometers is subject to the same restrictions as the hydrostatic levels in terms of knowledge of the equipotential surfaces and thus of deviations of the vertical.

6.5 Determination of the optimum configuration for the network

An important part of this study consists of the optimisation of the metrology network introduced in 6.3, by carrying out computer simulations to determine the alignment accuracy obtainable from the different possible variants of the network.

The method of simulation used is first described. Then brief details of the computation software which had to be developed will be given. The models used for each type of observation will be described and the different variants of the network which were tested will be presented. In conclusion the configuration which is believed to be the best will be outlined.

6.5.1 Simulation method

The principle of the simulations is to assign simulated values to the network observations. These can then be computed as if the network had really been observed, and the effects of perturbations which might affect the geometry can be estimated. In this first investigation into the network, such perturbations will be limited to normally distributed random errors of measurement.

In the method of simulation used at CERN [Mayoud, 1987] [17], the provisional values of the unknowns are considered as ideal. They are used in the program to compute the exact value of each observation. A random number generator then adds a random error to this ideal value, taking account of the a priori standard deviation of the measurement. Repeating this operation several times generates a collection of hypothetical observed networks.

The statistics derived from the results of this collection of network observations then give a very good indication of the suitability of the network being modelled to meet its predetermined objectives.

6.5.2 Development of computation software

A project of the size of CLIC demands a powerful least squares adjustment tool which allows the analysis of the propagation of errors and thus to the optimisation of the network. The general adjustment software (Logiciel Général de Compensation - LGC) developed and used by the CERN metrology group meets this need, but in its current version it has a major shortcoming for the CLIC study in that it does not allow the processing of two-dimensional observations of offsets from a wire or of distances between wires. This software, whose source code represents about 10 000 lines of Fortran, has undergone numerous updates although its maintenance has now become very hazardous.

This explains why new software was developed. This was done as a team effort, because the metrology group, in parallel with the CLIC study, also underlined the need to develop a more advanced tool and allotted resources for this.

Without going into the details of its development, the guiding principles are given as follows.

Guiding principles of the development

A research project of this nature is continuously evolving. For example, new sensors or new types of observation which are not under consideration at present may quite possibly be incorporated into a proposal for a future alignment system. It is thus very important that the computation software should be extremely flexible in terms of updates and must allow the speedy addition of new functionality without endangering that which is already in place.

In addition it is inevitable, and it is in any case desirable, that software on this scale will be developed by a team. The model adopted must also be modular so as to allow team members to work separately on specific parts of the program and then to combine them without mishap.

For these reasons it was decided to operate in C++. This programming language is object oriented [Budd, 1992] [18] and thus meets the requirements which have just been outlined. Moreover it is very powerful and numerous libraries of mathematical subroutines are available.

In practice the choice of an object-oriented design and of C++ has proved to be very beneficial. Development is truly modular and the connection between old and new modules is very easy.

The mechanisms of inheritance and polymorphism provide a great deal of flexibility with several important aspects of the software. Thus, while at present only networks expressed in cartesian coordinates can be computed, the model already allows the use of other reference systems, and the team is confident that moving over to computations on the ellipsoid will not present any problem.

In terms of taking new types of measurement into account, the operations required are few, and more-over the developer can make rapid progress in comparison to what is already in place. Three days' work are sufficient for a person who is familiar with the model to include a new type of observation in the software. It is important to note that this timescale remains constant however many types of measurement are already included, whereas with laborious programming in C or Fortran it tends to increase, sometimes by a substantial margin.

6.5.3 Observational model

For this first study it was sufficient to express all the observations and carry out all of the computations in a local cartesian coordinate system. The observation equations for every type of observation in the network are given, as well as the remarks applicable to each, in the section which follows.

Orthogonal distances from a point to a straight line

In Fig.39 the horizontal and vertical distances from a point to a straight line are expressed as follows:

$$E_h = \frac{(S_B - S_A)(X_M - X_A) - (X_B - X_A)(S_M - S_A)}{\sqrt{(S_B - S_A)^2 + (X_B - X_A)^2}} \quad \text{Equation 16}$$

$$E_v = \frac{(S_B - S_A)(Z_M - Z_A) - (Z_B - Z_A)(S_M - S_A)}{\sqrt{(S_B - S_A)^2 + (Z_B - Z_A)^2}} \quad \text{Equation 17}$$

These equation are used to model WPS and RASNIK-CCD observations.

(a) WPS observation model

In the WPS, the offsets are measured from the mechanical centre of the sensor, perpendicular to its measuring surfaces. The true situation is not as shown in Fig. 42 for two reasons. The first results from the fact that the wire is not a straight line. The catenary of the wire must therefore be determined (see 6.2.1) and corrections must be made so that the distances used in the computation relate to the straight line joining the ends of the wire. The second reason is due to the orientations of the sensor and the wire. The wire is not necessarily parallel to each of the planes defined by the two measuring surfaces of the sensor, and it is necessary to know the altitude of the latter in the coordinate system being used. One may begin by calculating the error introduced if the inclination of the wire to the sensor is ignored (Fig. 43) and hence if the offsets measured are not perpendicular to the wire.

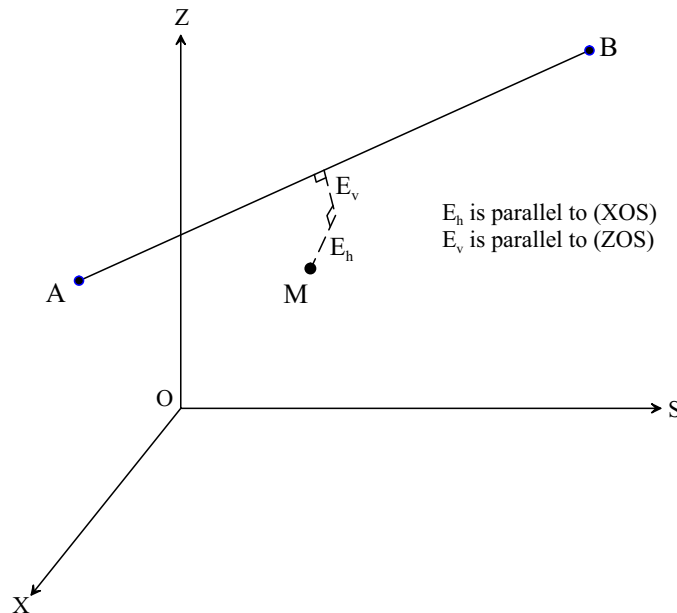


Fig. 42: Distances from a point to a straight line

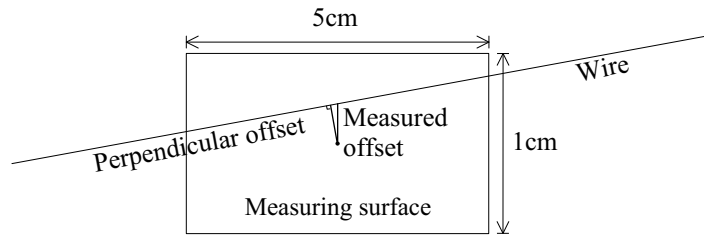


Fig. 43: Wire not parallel to the measuring surfaces

The graph in Fig. 44 shows this error as a function of the distance measured for various inclinations of the wire to the measuring surfaces. If errors of less than $\pm 1 \mu\text{m}$ are considered to be negligible, it can be seen that the inclination of the wire can be ignored if it falls within the central part of the sensor beam and if its inclination remains moderate (50 mrad representing 1 mm over 5 cm). This is possible if the components of the metrology network (sensors and support plates) are positioned with sufficient care.

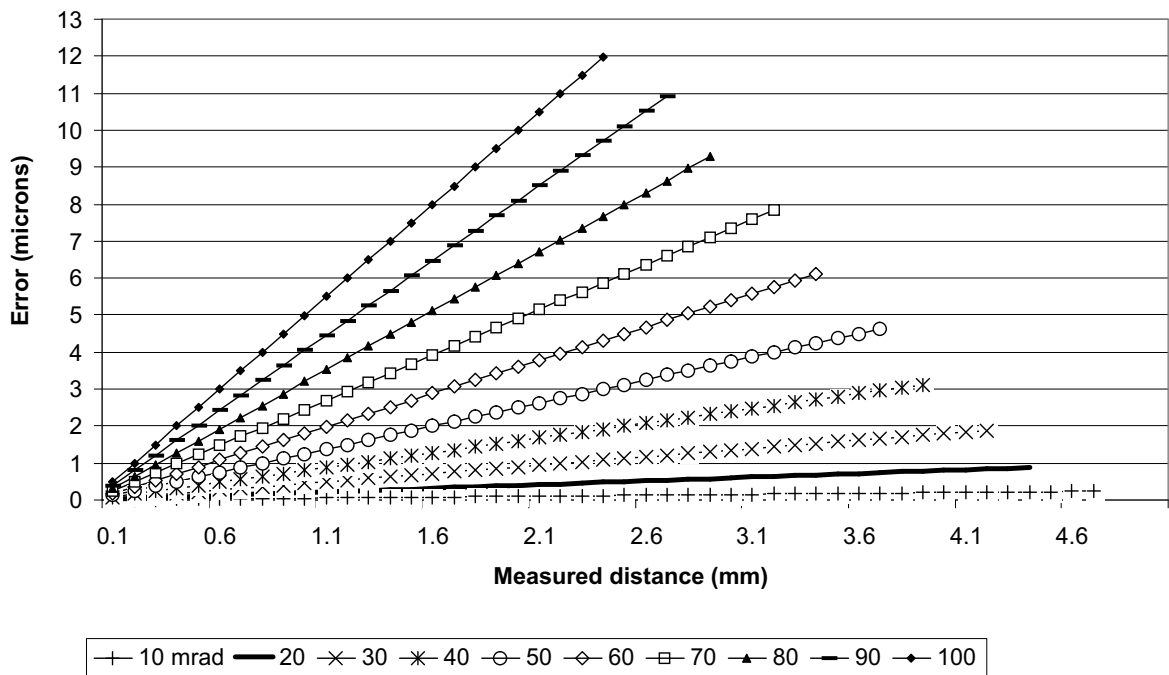


Fig. 44: Errors due to the inclination of the wire

If it is assumed that the wire and the measuring surfaces of the sensor are parallel, it remains only to determine the angle of the rotation of the sensor around the wire (Fig. 45) in order to express the measured distances in the required coordinate system. This angle cannot be measured directly, but knowledge of the orientation of the sensor in relation to its support platform as well as the inclinometer attached to the latter allows the inclination of the sensor to the local vertical to be determined. As the deviation of the vertical is known, it is then possible to express the measured distances in the local coordinate system.

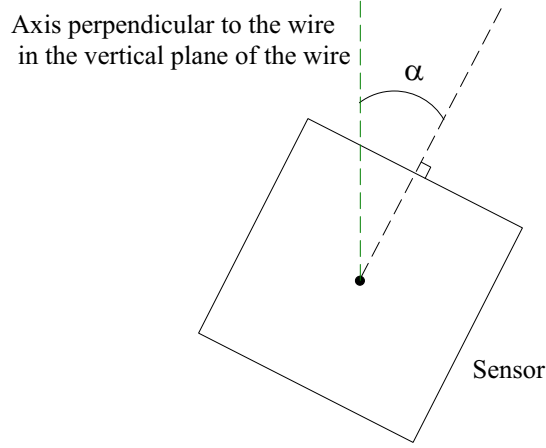


Fig. 45: Angle of rotation of the sensor about the wire

(b) RASNIK-CCD observation model

It has been shown in chapter 4 that the RASNIK-CCD sensors measure three distances and three rotations about the axis of the system, which is a straight line. In combining this information with the tilt measurements made at each girder articulation point (where the RASNIK-CCD sensors are placed), it is possible to express the measured offsets in the local coordinate system using equations 16 & 17.

Orthogonal distances between points on two straight lines

In the reference frame of Fig. 46, the horizontal and vertical distances between two points on two straight lines are as follows:

$$E_h = \left(\left[\left(S_A + \frac{l_1(S_B - S_A)}{AB} \right) - \left(S_C + \frac{l_2(S_D - S_C)}{CD} \right) \right]^2 + \left[\left(X_A + \frac{l_1(X_B - X_A)}{AB} \right) - \left(X_C + \frac{l_2(X_D - X_C)}{CD} \right) \right]^2 \right)^{\frac{1}{2}}$$

Equation 18

Ev =

$$\left(\left[\left(S_A + \frac{l_1(S_B - S_A)}{AB} \right) - \left(S_C + \frac{l_2(S_D - S_C)}{CD} \right) \right]^2 + \left[\left(Z_A + \frac{l_1(Z_B - Z_A)}{AB} \right) - \left(Z_C + \frac{l_2(Z_D - Z_C)}{CD} \right) \right]^2 \right)^{\frac{1}{2}}$$

Equation 19

With :

$$AB = \sqrt{(S_B - S_A)^2 + (X_B - X_A)^2 + (Z_B - Z_A)^2}$$

$$CD = \sqrt{(S_D - S_C)^2 + (X_D - X_C)^2 + (Z_D - Z_C)^2}$$

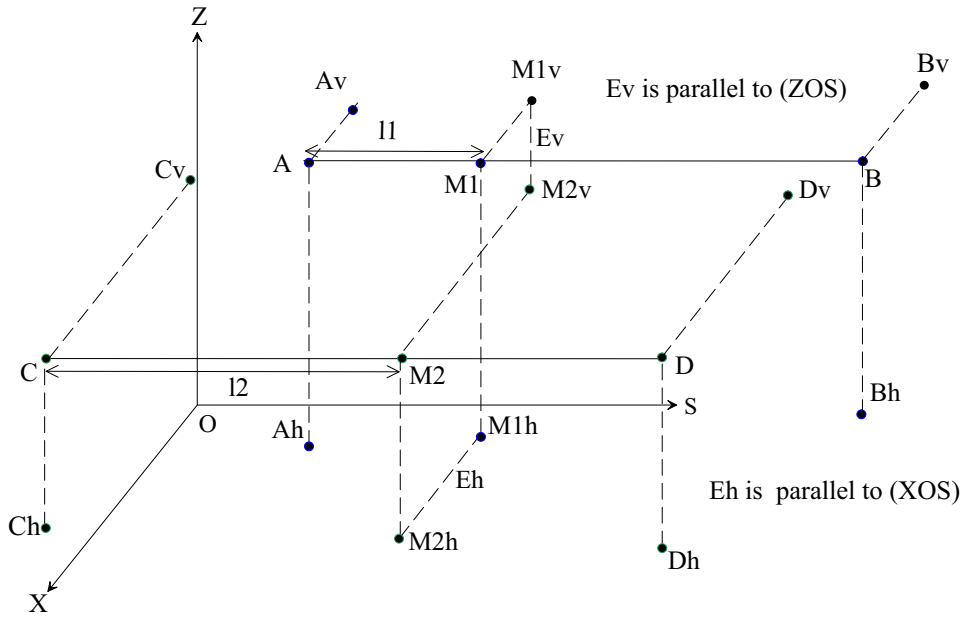


Fig. 46: Distances between points on two straight lines

These equations are used to model the observations of distances between wires, whose goal is to assist the determination of the positions of the ends of the wires. This explains why the offsets are not expressed in terms of the coordinates of points M1 and M2 (Fig. 46) on the wires.

Model for distances between wires

This type of measurement is made using two rigidly-connected WPSs (Fig. 26), combined with a Tilt Measurement System (TMS).

As with the WPSs it is first necessary to determine the catenary of the wires in order to reduce the measured offsets to offsets relative to the straight lines.

Uncertainties exist in E_h and E_v caused by the orientation of the sensors in relation to the wires and also to the horizontal. This uncertainty results in uncertainty in s_1 and s_2

The computations show that in the case of two parallel 100 m wires 20 cm apart, the uncertainty in the measured offsets does not exceed $\pm 1 \mu\text{m}$ provided that s_1 and s_2 are known to $\pm 5 \text{ mm}$. Accurate positioning of the components of the metrology network will minimize the inclination of the sensors with respect to the wires. As the TMS, together with knowledge of the deviation of the vertical, gives the inclination relative to the latter, it should be easy to achieve this accuracy of $\pm 5 \text{ mm}$ in s_1 and s_2

Using equations 18 & 19 to express the measured offsets in the local coordinate system, the parameters s_1 and s_2 can be considered to be known.

Vertical distances

It has been assumed for this computation that the height differences measured with the HLS can be expressed in the local coordinate system (see 6.4). The equation used for the vertical distance between two points A and B is thus very simple:

$$\Delta Z_A^B = Z_B - Z_A \quad \text{Equation 20}$$

6.5.4 Networks tested

The typical configuration of the networks tested is shown in Fig. 26. The computations of planimetry and height were separated because that offered a considerable saving in computation time. Moreover, the wires and the girders are oriented along an axis parallel to the beam, as the positions of the unknown points in the S direction are of less importance they were always considered to be fixed. The unknowns to be calculated are thus the X and Z coordinates.

For each network tested, the results for the absolute and relative positions of the components to be aligned will be presented, together with information on the residuals of the observations. For each data value d shown graphically, the following curves for the n simulations carried out have been drawn:

- root mean square (rms) value: $\sqrt{\frac{\sum_{i=1}^n d_i^2}{n}}$
- arithmetic mean: $\frac{\sum_{i=1}^n |d_i|}{n}$
- maximum: $\max\{|d_i|\}$
- minimum: $\min\{|d_i|\}$

Wire network: planimetry

(a) Characteristics of the computed network

This computation only determines the planimetric positions of the ends of the wires, along the whole length (about 14 000 m) of one of the CLIC linacs. The first and last points of each line are taken as known. All other points are variable in X only. The wire network is connected to three known points of the underground survey network, equally spaced along the length of the linac, with an accuracy of ± 5 mm.

Each wire has a length of about 100 m, and the accuracy attributed to the two types of offset measured is $\pm 5 \mu\text{m}$ (Fig. 47). This network represents 932 observations which allow the determination of 614 unknowns.

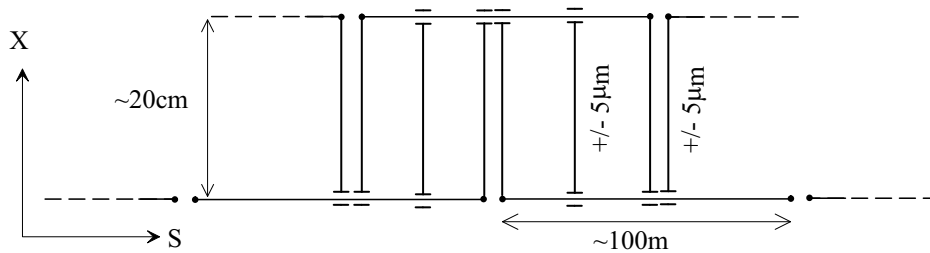


Fig. 47: Wire network: planimetry

(b) Results

The graph in Annex 1a represents the offsets of the platforms, and therefore of the ends of the wires, with respect to their ideal positions, in terms of the abscissa S of these ends. The rms value of these offsets reaches ± 1.3 mm.

The graph in Annex 1b, the most important, represents the alignment errors of the ends of the wires over a distance Ld of about 200 m (Fig. 48), in terms of the abscissa S of these wire ends.

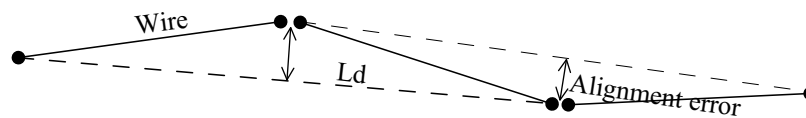


Fig. 48: Wire alignment errors

It can be seen that this configuration enables the primary metrology network to achieve the desired relative alignment accuracy of $\pm 10 \mu\text{m}$ over 200 m.

The graphs in Annexes 1c and 2d show the residuals for the two types of offsets observed. The rms error of the residuals of the observations between a wire end and the overlapping wire is about $\pm 2 \mu\text{m}$, while that of the residuals of the observations between parallel wires is of the order of $\pm 4 \mu\text{m}$. As the a priori accuracy of these observations is the same, this shows that the first type of offset has a more important role in determining the positions of the points than does the second. This can be explained geometrically since, unlike the second case, the first type of offset can be considered as a direct observation from the end of the wire concerned.

Combined computation of wires and girders: planimetry

(a) Characteristics of the computed network

This computation simultaneously determines the planimetric position of the ends of the wires and the articulation points of one of the lines of girders, over a length of about 2 km. A shorter length has been chosen because the alignment errors, of most interest, are independent of the length of the linac. That avoided a computation covering 14 km which would have greatly increased the demands on memory and computing time.

The first and last points of each line of wires are considered to be known, all other points representing variables in X only. The articulation points of the girders are each positioned in relation to the others by means of the network of overlapping RASNIK-CCD observations (Fig. 24). The network of optical observations is combined with the network of wires by using the WPS measurements between the girder articulation points and the adjacent wires. These connecting measurements are regularly spaced every 22 articulations. The a priori accuracy of the measurements of the offset from a wire is $\pm 5 \mu\text{m}$, while that of the RASNIK-CCD observations is $\pm 2 \mu\text{m}$. This network consists of 1065 observations for 983 unknowns.

(b) Results

The graph in Annex 2a represents the displacements of the ends of the wires from their ideal positions, in terms of the abscissa S of these ends. The rms value of these displacements can reach $\pm 0.15 \text{ mm}$. This result, which is better than that for the previous network, was predictable because the known points are only 2 km apart. On the other hand this improvement owes nothing to the incorporation of RASNIK-CCD measurements, since computation of the wire network alone over a distance of 2 km gives exactly the same results. The smaller displacements from the ideal position are thus due only to the shorter length under consideration.

The graph in Annex 2b represents the alignment errors of the ends of the wires over a length of about 200 m in terms of the abscissa S of these ends. As with the previous network, the rms value of these misalignments is about $\pm 10 \mu\text{m}$. From this it can be deduced that the combination of RASNIK-CCD and WPS observations does not improve the relative alignment of the wires.

The graph in Annex 2c represents the displacements of the articulation points of the girders from their ideal positions, in terms of the abscissa S of these articulation points. The general effect is the same as for the position of the wires because of the connection to them. The systematic increase in the displacements between pairs of connection points (49.06 m) should also be noted.

The graph in Annex 2d represents the misalignments of girder articulation points over a length of about 200 m. A cyclic variation related to the connections to the wires is found. The rms value of these misalignments is around $\pm 40 \mu\text{m}$, which is much too high a value. This result was improved by means of more frequent connections between the articulation points and the wires. The errors of alignment which result from such a network, with connections every four or five articulations, are shown in Annex 2e. This configuration gets much closer to the $\pm 10 \mu\text{m}$ required, and represents a good compromise between the number of connections (and hence of WPS sensors) and the accuracy obtained.

The graph in Annex 2f represents the residuals of WPS observations between ends of wires and the overlapping wires, with a connection every four or five modules. Their rms error is about $\pm 2.4 \mu\text{m}$. The residuals of WPS observations for connections between girders and wires, shown in Annex 2g, are smaller: their rms error is about $\pm 2.0 \mu\text{m}$. This slight difference is not surprising because these connection observations relate to the articulation points which are constrained by the more accurate RASNIK-CCD observations.

The latter have the residuals given in Annex 2h, with a rms error of the order of $\pm 0.8 \mu\text{m}$.

It is the observations of offsets between parallel wires which have the biggest residuals (Annex 2i) for reasons already discussed above.

Wire network: altimetry

(a) Characteristics of the computed network

This computation only determines the heights of the ends of the wires, along the whole length of one of the CLIC linacs. The observations of offsets between points and wires and between parallel wires are the same as for the first network discussed above, except that they are in a vertical plane. The existence of a solution to the problems of using the HLS for the vertical alignment (see 6.4) has been assumed, and that the catenaries of the wires can thus be determined to the required accuracy. This comes back to considering that it is possible to measure height differences over distances of at least a hundred meters. Vertical distance observations have therefore also been

incorporated into the network at a rate of one per pair of consecutive platforms (Fig. 49), thus implying independent observations.

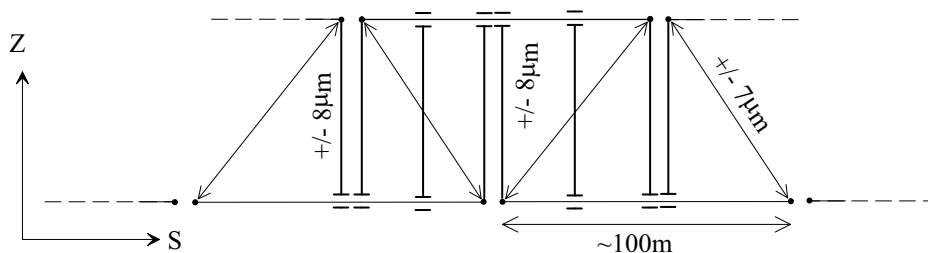


Fig. 49: Wire network: altimetry.

The a priori accuracy of measurements of the offset from a wire is $\pm 8 \mu\text{m}$, while that of height difference observations is $\pm 7 \mu\text{m}$. This network represents 1228 observations to determine 614 unknowns.

(b) Results

The graph in Annex 3a represents the departures of the ends of the wires compared with their ideal positions, in terms of the abscissa S of these points. The rms value of these offsets reaches $\pm 0.12 \mu\text{m}$. This result is substantially better than the $\pm 1.3 \text{ mm}$ of the computation in 6.5.4, thanks to the addition of the HLS observations which do not have any planimetric equivalent.

The graph in Annex 3b shows the alignment errors of the ends of the wires over a length L_d of about 200m in terms of the abscissa S of these points. It can be seen that for the primary metrology network this configuration allows the desired relative alignment of $\pm 10 \mu\text{m}$ over 200 m to be achieved.

The graphs in Annexes 3c, 3d and 3e show the residuals of the two types of offsets observed, together with those of the vertical distance measurements. The rms error of the residuals of the observations between wire ends and overlapping wires is $\pm 5 \mu\text{m}$, while that of the residuals of observations between parallel wires is towards $\pm 7 \mu\text{m}$. The residuals of the HLS observations average $\pm 5 \mu\text{m}$. There is a better balance between the residuals than for the planimetric computation. This confirms that one can expect the HLS observations to improve the determination of the unknowns: the influence of each type of observation on the final solution is more homogeneous which may also be assumed to improve the strength of the solution.

Combined computation of wires and girders: altimetry

(a) Characteristics of the computed network

This computation simultaneously determines the heights of the ends of the wires and the articulation points of one of the lines of girders, over a length of about 2 km.

The first and last points of each line of wires are considered to be known, all other points being variable in Z only. The configuration of the network is analogous to that discussed in 6.5.4 (combined computation of wires and girders: planimetry). The measurements connecting the girders to the wires are made every four or five modules and there is a height difference measurement between each successive platform. The a priori accuracy of the offset measurements to the wire is $\pm 8 \mu\text{m}$, that of the RASNIK-CCD observations is $\pm 2 \mu\text{m}$ and for the vertical distance measurements it is $\pm 7 \mu\text{m}$. This network consists of 1269 observations for the determination of 983 unknowns.

(b) Results

The graph in Annex 4a represents the displacements of the ends of the wires from their ideal positions, in terms of the abscissa S of these ends. The rms value of these displacements can reach $\pm 0.04 \text{ mm}$. This result, which is better than that for the network in 6.5.4 (combined computation of wires and girders : planimetry) was predictable because we already knew the beneficial effect of the HLS on the absolute vertical positions of the platforms.

The graph in Annex 4b represents the alignment errors of the ends of the wires over a length of about 200 m in terms of the abscissa S of these ends. The rms value of these misalignments is slightly under $\pm 10 \mu\text{m}$. As with the planimetry, the combination of RASNIK-CCD, HLS and WPS observations does not improve the relative alignment of the wires.

The graph in Annex 4c represents the displacements of the articulation points of the girders from their ideal positions, in terms of the abscissa S of these articulation points. The general effect is still the same as for the positions of the wires.

The graph in Annex 4d represents the misalignments of girder articulation points over a length of about 200 m. The rms value of these misalignments is around $\pm 13 \mu\text{m}$, exactly as in the analogous planimetric computation, and can be considered to be an acceptable result.

The graph in Annex 4e represents the residuals of the WPS observations between ends of wires and the overlapping wires. Their rms value is about $\pm 6.0 \mu\text{m}$. The residuals of WPS observations for connections between girders and wires, shown in Annex 4f, are smaller: their rms error is about $\pm 4.2 \mu\text{m}$. This difference is again explained by the fact that the connection observations relate to the articulation points which are constrained by the more accurate RASNIK-CCD observations.

The latter have the residuals shown in Annex 4g, whose rms error is around $\pm 0.8 \mu\text{m}$. It is the observations of offsets between parallel wires which have the biggest residuals (Annex 4h), for reasons already discussed above.

6.5.5 Optimum network

The various networks tested are now brought together and the optimum network indicated by the results obtained is described, together with the method of deriving it.

Analysis of the computation

It appears that the computation can be done in two stages, in which the wire network is computed first, followed by the determination of the positions of the articulation points of the girders in a second computation in which the ends of the wires are already known. This assumption does however remain to be confirmed by simulations using the same observed values on the wires in both two-stage and combined computations, and then comparing the positions obtained by the two methods.

Determination of the positions of the wires

(a) Planimetry

In planimetry, the network shown in Fig. 47 satisfies the condition of alignment to $\pm 10 \mu\text{m}$ over 200 m.

The accuracy of $\pm 5 \mu\text{m}$ in the two types of measurement involved represents not only the accuracy of the WPS sensors but also the accuracy with which the dimensions of the mechanical mountings are known. Assuming that the WPSs measure to $\pm 1 \mu\text{m}$, this requires the distance between the mechanical centres of two sensors on one platform to be known to an accuracy of $\pm 4.8 \mu\text{m}$. It is thus likely to be necessary to calibrate the mountings of each platform and to take special care with their stability, especially in terms of variations in temperature.

This strict tolerance for the measured offset could be relaxed somewhat by increasing the length of the wires. However this renders them less stable (their natural frequency is reduced), which presents problems which are no less tricky.

(b) Altimetry

In altimetry, the network shown in Fig. 49 satisfies the condition of $\pm 10 \mu\text{m}$ over 200 m.

The measurements can be a little less accurate than in planimetry, because of the presence of hydrostatic level measurements. As in the planimetric case, the same remarks about knowledge of the mechanical dimensions of course also apply here. It must be remembered that height differences measured by the HLSs as well as the offsets obtained with the pairs of WPSs are in fact pseudo-observations, that is to say direct observations corrected for deformations of the equipotential surface and for the vertical curvature of the wires respectively. Depending on the available knowledge of the equipotential (see 6.4), it is possible that these accuracies, although lower than for planimetry, may be harder to achieve.

Determination of the positions of the girders

For the determination of the positions of the girders, a network of overlapping RASNIK-CCD systems (Fig. 24) combined with connections by WPS every four or five modules enables a satisfactory accuracy to be achieved. This can be slightly improved by, for example, connecting every third module. However this represents a

significant number of extra WPSs, which runs counter to the cost advantages of using RASNIK-CCD for the alignment of the girders.

The only difference to note here between planimetry and altimetry concerns the connection observations which are in fact pseudo-observations to which the remarks made earlier also apply.

6.6 Practical operation of the alignment system

In this section the stages envisaged for the practical operation of the alignment system are introduced. It is assumed that the components are prealigned and only the initial alignment and the operation with beam is covered.

Determination of the geometry of the equipotential surfaces under gravity

As we have seen in 6.4, this stage is crucial to the use of hydrostatic levels and inclinometers. This determination must enable both the height differences obtained from the HLSs to be brought into the local coordinate system and the TMS readings to be corrected for the deviation of the vertical.

HLS observations for the establishment of a local tidal model

This stage is also essential for the effective use of the HLSs (see 6.4.3). Records covering a period of one to three months can begin as soon as the HLS network is installed

Determination of the vertical curve (catenary) of each wire

Relative height measurements of three points of each wire (6.2.1) will allow the determination of the equation of the catenary in the vertical plane. The vertical offsets measured subsequently by the sensors may thus be reduced to offsets relative to the straight line joining the end points of the wires. Knowing the approximate coordinates of each wire thanks to the prealignment, it is also possible, if necessary, to calculate corrections for the effects of nonuniformity of the gravity field (see 6.4.2).

Computation of the positions of the ends of the wires

The next stage is the computation of the positions of the ends of the wires, using the observational network described in 6.5.5.

Computation of the positions of the articulation points of the girders and of the quadrupoles

Once the positions of the wires have been determined, it is then possible :

- to determine the positions of the articulation points of the girders by making use of the network described in 6.5.5;
- to determine the positions of the quadrupoles by direct measurements relative to the wires.

Computation and transmission of instructions to the micro-movers

Knowing the positions of all of the components, the displacements required for the initial alignment can then be computed. The corresponding instructions are then sent to the micro-movers fitted to the girder cradles and the quadrupole platforms. The sensors can then check that the desired positions have been reached.

Injection of the beam

When the initial alignment has been achieved the beam can be injected. The initial positions of the components are saved in memory in order to be able to restore a configuration which allows the beam to circulate once again in case of failure of the circulation of the beam.

Subsequently, while the beam is circulating, alignment is maintained by the beam-based alignment system.

Regular monitoring of the positions of the components

At regular intervals, for example every six hours, all of the sensors can be read and the positions of all the components can be computed. This allows the monitoring and recording of changes in the alignment of the accelerator, as well as enabling preventive measures to be taken if the alignment approaches a critical configuration.

7 Practical demonstration of the active alignment system in CTF2

7.1 CTF2 30GHz module layout

CTF2 was built to demonstrate the feasibility of the Two Beam Acceleration scheme, but also to test the operation of the active alignment system in a working accelerator with typical CLIC components and with an electron beam.

The four 30 GHz modules of CTF2 constitute a representative section of the CLIC linac. Each module consists of two power-generating PETS structures driving four accelerating sections, each module is equipped with BPMs and quadrupoles. A photograph of the CTF2 30 GHz modules is shown in

Fig. 50. A layout of the motors and the sensors for the four modules is given in Fig. 51.



Fig. 50: CTF2 30 GHz modules

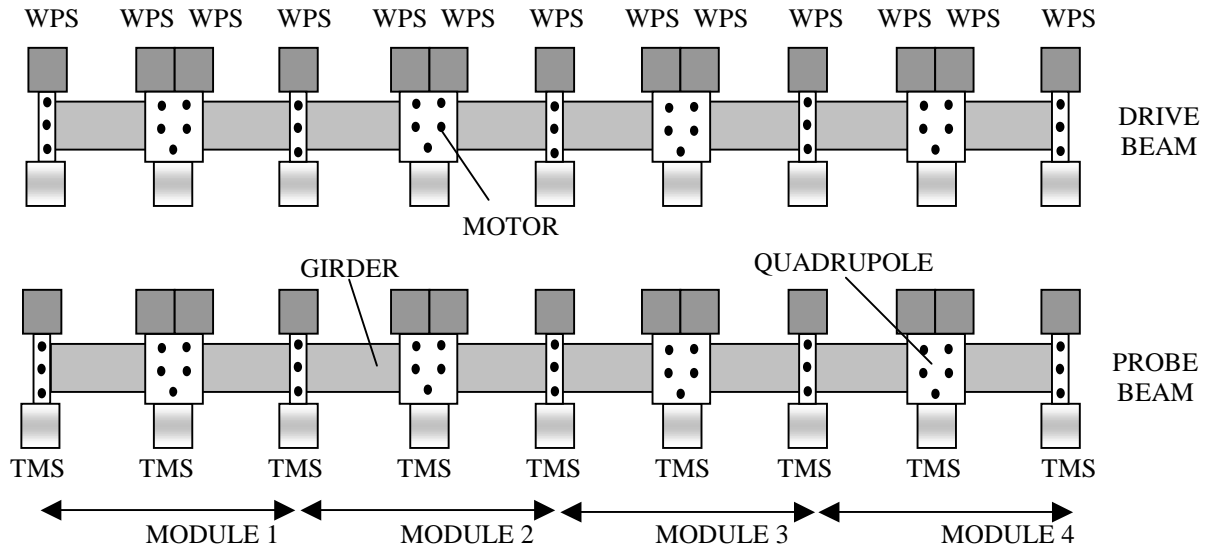


Fig. 51: Micro-movers and sensors in CTF2

7.2 CTF2 Alignment control system

The alignment control system of CTF2 [Delahaye et al., 1994] [19] [Bouché et al., 1997] [20], was specified to regulate the transverse positions of the girders and quadrupoles to within $\pm 10 \mu\text{m}$.

The total number of units to be controlled is : 70 motors, 26 WPS and 18 TMS. Since each WPS delivers two signals (one for x and one for z), and each TMS provides three (one for each dimension), 106 signals (WPS plus TMS) must be acquired. To this must be added the temperature and HLS readings, present in the system, so there are 134 signals to be acquired for a section of four modules.

As regards the dynamic characteristics of the readings of WPS, these show significant damped sinusoids between 30 and 50 Hz. This is due to the mechanical resonance of the reference. For frequencies lower than 30 Hz, there are no significant alterations in comparison with the required resolution. To filter these perturbations, Moving Average (MA) filters are implemented which are applied to each sensor output.

The displacements must respect the mechanical laws in order to avoid "lost step" errors. Due to mechanical inertia, friction and the starting load torque, it is necessary to limit the acceleration. So for displacements requiring a small number of steps (<100), low and constant speeds are preferred, using speed profiles for movements with a higher number of steps. The speed profiles imply a variation of speed that is trapezoidal for the case presented.

From the above, it can be concluded that the electronics of the alignment system must fulfill the following specifications:

- A high quantity of signals to read, filter and process (134);
- A high quantity of motors to drive following speed profiles;
- High accuracy ($10 \mu\text{m}$);
- Processing speed: due to the dynamics of the system, the reading of the 134 signals, their processing, the execution of the corresponding control algorithms and the execution of the algorithms of the movement of the motors (speed profiles) must be accomplished in less than 3 ms. This imposes demands on the processing time;
- Communication capacity with more hierarchic systems: the system must communicate with other systems through a VME bus. The amount of data and parameters to exchange demand a flow of information specified in 512 words of 16 bits;
- Low cost: the perspective to apply the electronics of CTF2 (four times 1.4 m) to CLIC 0.5 Tev (two times 3500 m), that is about 1400 times the length of CTF2, imposes cost and small packaging constraints;
- Reduction of the wiring volume: the number of motors and sensors justifies the search for wiring alternatives that lead to significant reductions;
- Immunity to electrical and radiation noise: the requirement for high accuracy in a strong radioactive environment generates strict conditions on the EMC (Electromagnetic Compatibility);

- Flexibility: the system must be able to accommodate the inevitable changes associated with a development program such as CTF2 without compromising the ability to extend the system in the future to CLIC;
- Modularity: ability to add more modules based on the same technology to create more elaborate systems.

An electronic system has been developed that fulfills the demands of CTF2 and that is also applicable to CLIC [Carrica et al., 1999] [21].

7.3 General Architecture of the system

In order to fulfil the specifications, the electronic system is based on the following principles :

- Generalised use of Field Programmable Gate Arrays (FPGA);
- Use of intelligent systems with high-speed and high-processing capacity;
- Division of the system in modules of similar characteristics;
- Galvanic isolation between boards and modules.

The electronics of the CTF2 alignment system is composed of two almost identical systems that operate independently except that both are slaves to a more hierarchical control. One is dedicated to the control of the Drive Beam and the other to the Probe Beam.

Each of these systems as shown in Fig. 52 includes three subsystems: the Control Subsystem, the Acquisition Subsystem and the Driver Subsystem.

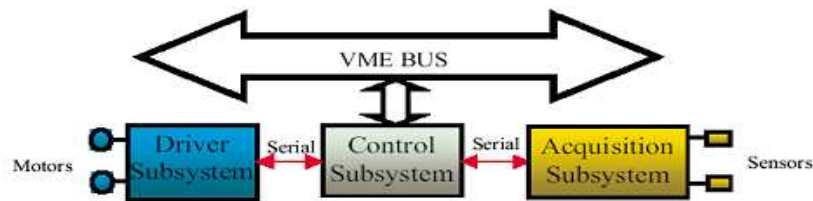


Fig. 52: General architecture of the electronics in CTF2

7.3.1 The Control Subsystem

The Control Subsystem cyclically performs the functions that are shown in the flow diagram of Fig. 53.

The Control Subsystem communicates with a system of higher hierarchy through a standard VME bus [VME, 1995] [22]. The communication is bi-directional, that is the alignment system receives and sends information to the higher hierarchical system. The type of information received and transmitted is detailed below.

- Information received: offsets for the correction of the catenary, individual adjustments of sensors, MA filter parameters, velocity profile parameters, characteristics of each motor (μm /step ratio, currents), the desired displacement of each motor, characteristics of the counters of the μm 's accumulated in each motor;
- Information transmitted: TMS and WPS acquisitions, MA outputs for the TMS and WPS, the state of each motor (failure, position), the state of the counters of the μm 's accumulated in each motor.

The Control Subsystem is implemented through a 5U board (Alignment Main Control Card, AMCC) that is plugged in the VME bus. The communication with the VME bus is of a parallel type.

After communicating with the VME bus, the AMCC initiates a process of acquisition of all the sensors. It sends to the Acquisition Subsystem the start conversion command and it immediately starts to receive the readings corresponding to the previous cycle, which are transmitted by the Acquisition Subsystem.

Once the parameters via the VME bus are obtained, and after fulfilling the acquisitions, the Control Subsystem is in a condition to execute the adjustments that the motors must perform. These are previously processed to fulfill the movements within the framework of speed profiles. Finally, the sequences to be executed by each motor are sent to the Driver Subsystem, where the power stages are found. The architecture of the AMCC is given in Fig. 54.

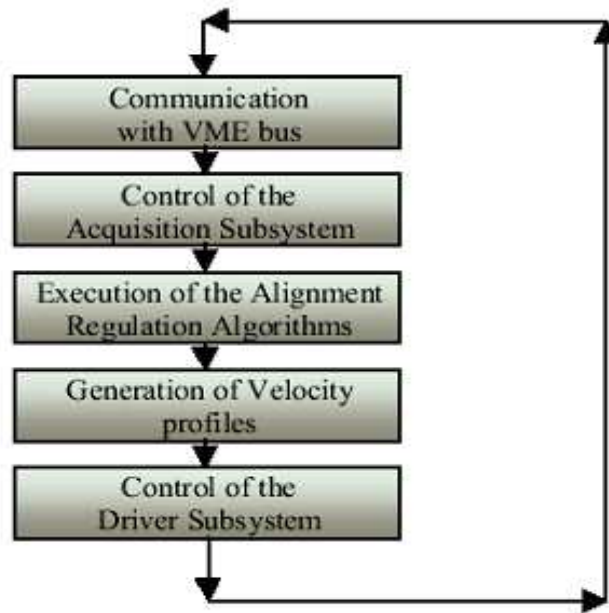


Fig. 53: Flowchart of Control Subsystem

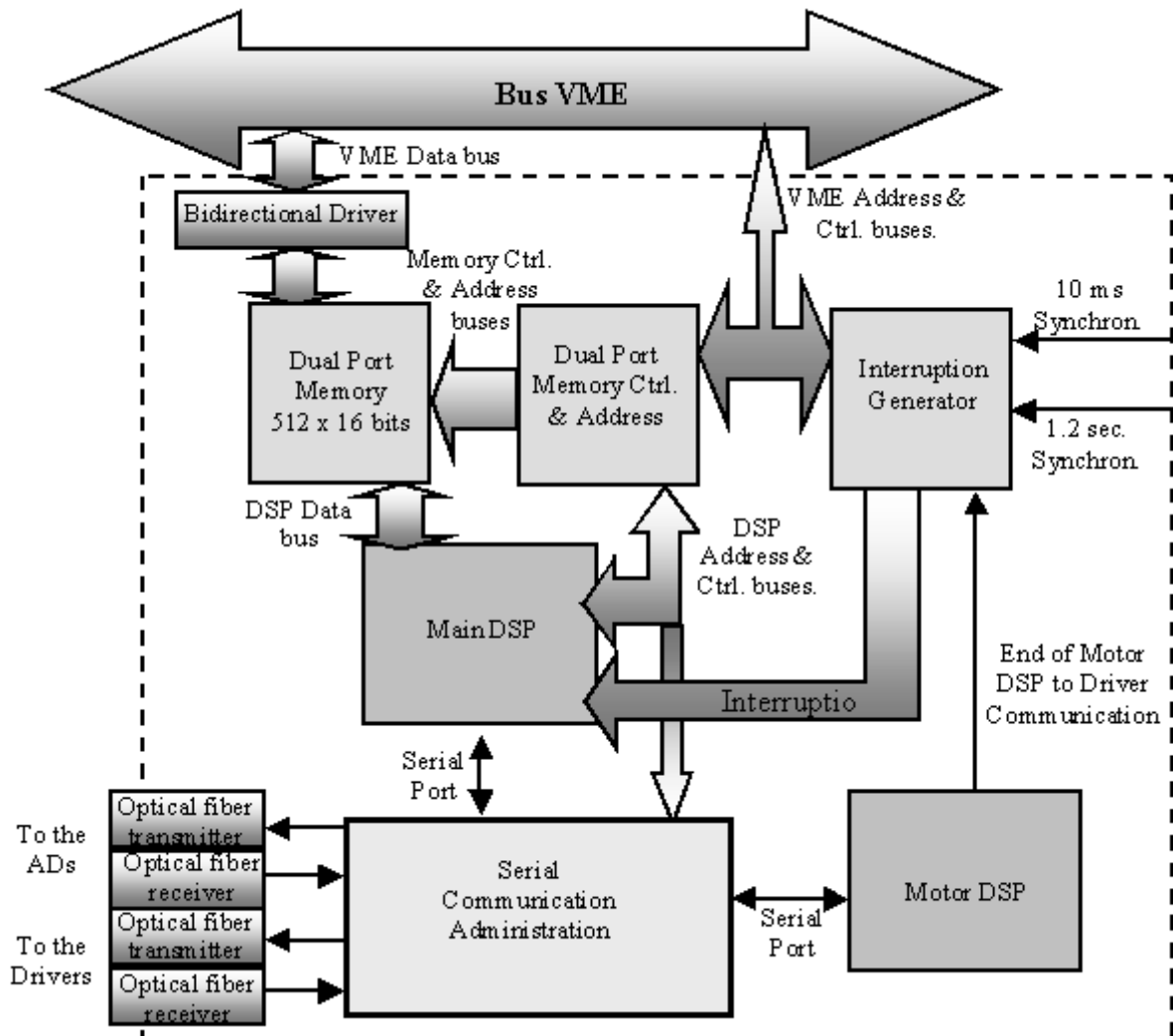


Fig. 54: AMCC Architecture

7.3.2 Acquisition Subsystem

The Acquisition Subsystem performs the following functions :

- Acquisition of sensor signals (67 signals) with a 16 bit resolution;
- Communication with the Control Subsystem.

The architecture of the Acquisition Subsystem consists of a set of chassis that inter-communicate in a daisy-chain way (Fig. 55). Each chassis has an acquisition board, and includes boards where the electronic conditioning of the sensor signals is accomplished.

The acquisition boards are of 14 channels each, with a 16 bit resolution and a maximum sampling rate of 500 Hz. This board possesses a digital electronics that performs the channel selection and the AD series communication. The acquisition board also includes the serial communication logic of the chassis and the corresponding decoding circuit. All the digital devices mentioned are implemented in FPGA, this results in a board of reduced dimensions (3U: 100 x 160 mm), whose layout is shown in Fig. 56.

The serial communication between the Control and the Acquisition Subsystems is asynchronous, with speed of 5 Mbit/s. An optical fiber is used for this for galvanic isolation, and to eliminate electromagnetic perturbations produced in the tunnel.

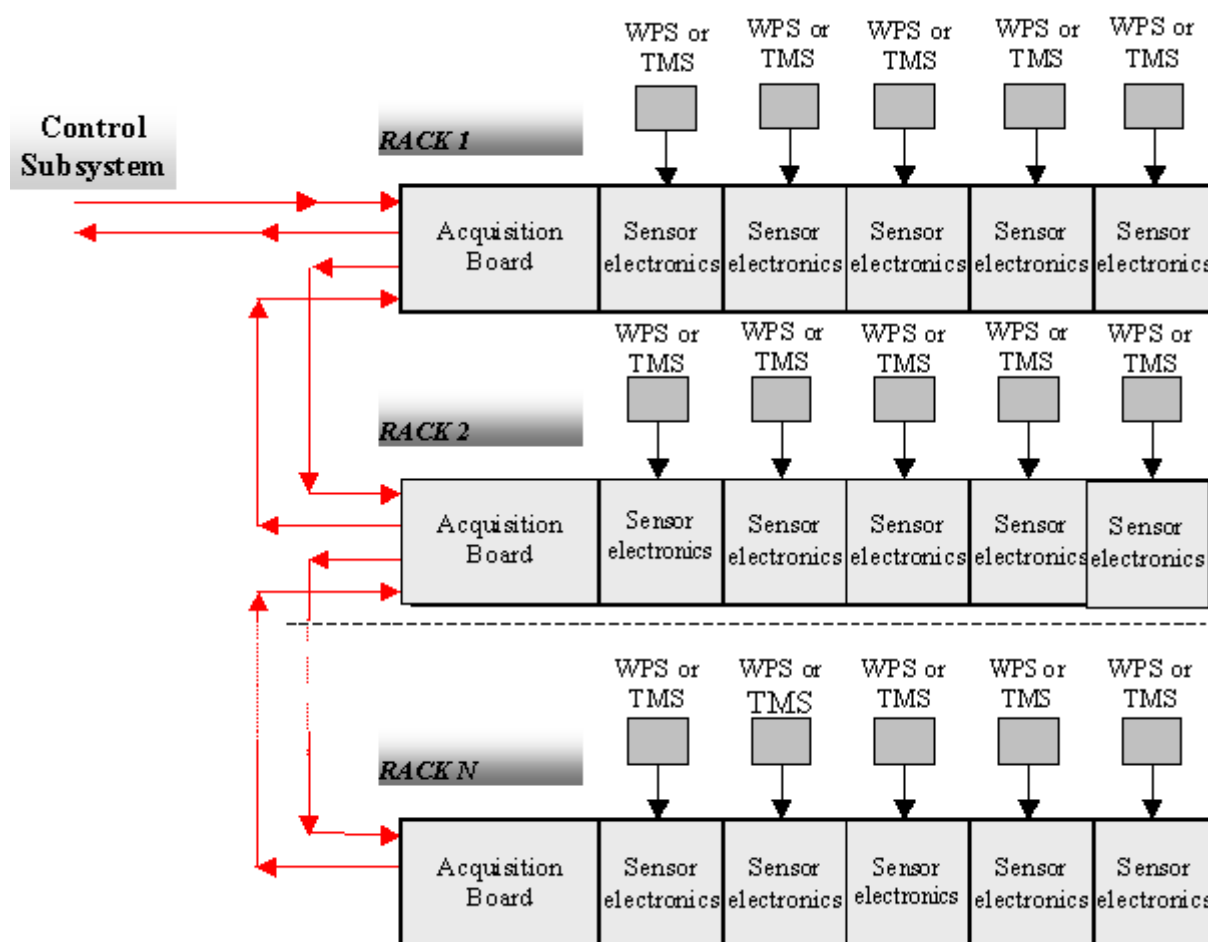


Fig. 55: Acquisition Subsystem

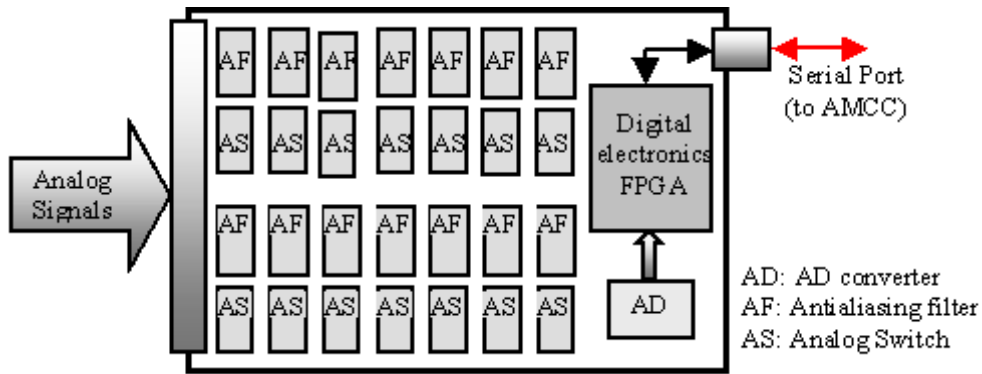


Fig. 56: Acquisition Card

7.3.3 Drive Subsystem

The Drive Subsystem is structured round a set of racks, inter-communicating in a daisy-chain way, see Fig.57.

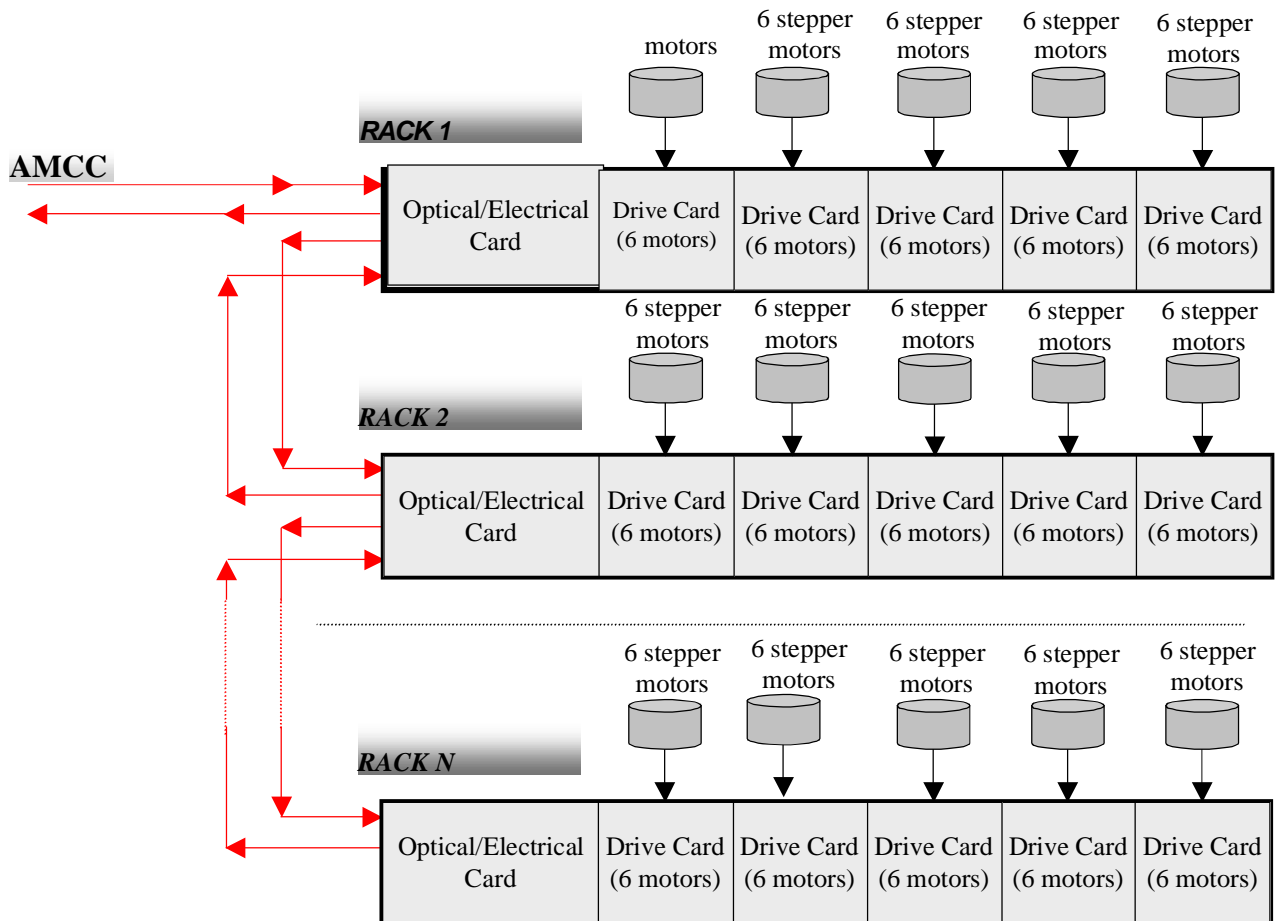


Fig. 57: Drive Subsystem

Each rack includes up to five boards (Driver Cards), each card possess the electronic drive for 6 motors. Thus, each rack can drive up to 30 motors. The internal communication of the rack is performed through a bus plane.

The inter-racks communication and the communication with the respective AMCC is performed through an optical fiber for isolation purposes and to reduce noise problems. In each rack, there is a board that changes optical signals into electrical ones. The communication between the Control Subsystem and each Driver Card (through the rack) is serial asynchronous, with a speed of 5 Mbit/s.

The power electronics needed to drive the six motors, with a maximum current of 2A per phase, is supplied by the Driver Card. Each motor is driven with current pulses (imposed currents), which are generated in a PWM form.

The Driver card includes a failure monitoring system (open circuit failures) and the corresponding protection. In this card, in addition to the control logic associated with the generation of PWM and the protection of faults, there are additional circuits for the programming of the maximum current per motor, the management of the information of the state of each motor (failure and position of each motor), the asynchronous communication and the address decoding.

This is all implemented through a FPGA with a capacity of 6000 logic gates. In this way, a 3U board is obtained (100 x 160 mm) which is addressable, capable of driving six motors with protections included, very flexible, and which allows the programming of the currents of each motor (Fig. 58).

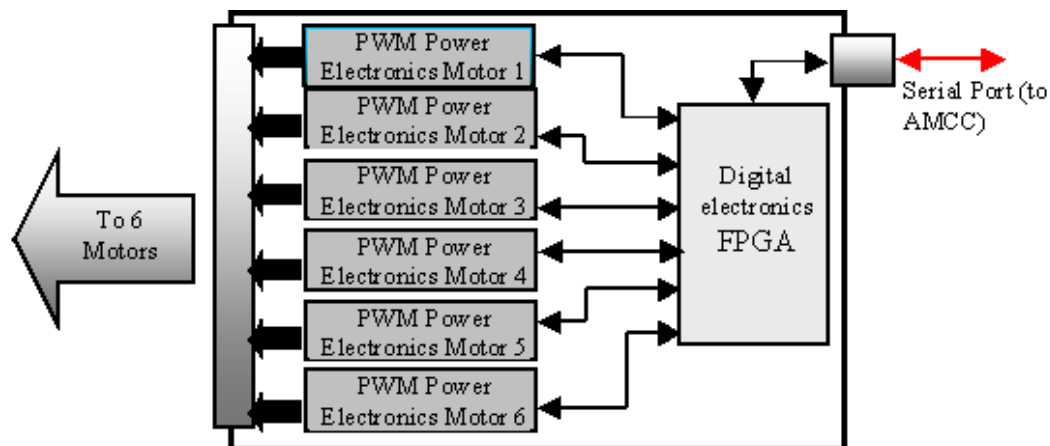


Fig. 58: Driver Card

The address of each driver consists of a 5-bit word, so that the AMCC can control up to 32 Driver Cards, that is up to 192 motors. In the CTF2 application, each AMCC drives only 35 motors.

The number of motors that can be controlled is limited by the processing speed of the AMCC. With the motion algorithms developed for this application, moving the six motors one step takes 30 μ s. In terms of the speed of movement, this means that the maximum speed that a motor can be moved is $1/(N \cdot 30 \mu\text{s})$, N being the number of groups of six motors to be moved simultaneously. Thus, the maximum possible speed are 1040 steps/s and 33333 steps/s respectively if one group or 32 are driven simultaneously.

Since the CTF2 requires a simultaneous movement of 7 groups of motors ($N = 7$), the maximum speed that the system allows is 4760 steps/s, that exceeds the needs of CTF2 when the system is in closed-loop (in closed-loop the movements are small and the speeds are reduced).

When the system is in open-loop, large movements could be necessary but driving one motor at a time. In this case the speeds, that follow profiles, reach 33333 steps/s, this exceeds by far the maximum mechanical speed of the motors that are used in this application.

7.4 Results

All the requirements specified for CTF2 (see following list) were accomplished :

- 134 signals to be read and processed;
- 70 motors to be driven, following the speed;
- 3 ms processing time to acquire 134 signals, to perform the control and adjustment algorithms of the motors (speed profiles);
- Communication with a more hierarchical system via VME bus.

The resulting system consists of :

- 2 AMCC;
- 4 driver Racks that include 12 Driver Cards;
- 13 AD Racks that include 13 AD 16-bit cards.

The whole system is commanded through 8 optical fibers. This was feasible because a serial type communication system was adopted.

The accuracy of the system was tested in open-loop mode. For these tests, the acquisition system inputs were provided by highly-stable dc signals in the place of the sensor inputs. The variations of the readings around the acquired value are shown in Fig. 59. It was observed that in 100 acquisitions the maximum deviation was 2 least significant bits or lsb (1 lsb corresponds to 0.3 μm). The statistical values obtained were : Mean Value = 4000.16 lsb Standard Deviation = 0.746 lsb.

The accuracy of the system was tested in closed-loop mode. The WPS readings showed a maximum deviation of 1 μm as shown in Fig. 59b. The statistical values obtained were : Mean Value = 0.08 μm , Standard Deviation = 0.493 μm .

The following graphic shows the deviation of 13 WPS's on the Y axis, to reach the value (0,5 mm) in closed-loop mode. All the motors were moved at the same time. The initial precision (5 μm) was obtained all along the four modules 12 s after the motors were started.

Acquisition Tests: 5.000 V input, 100 acquisitions / Alignment errors, 100 acquisitions

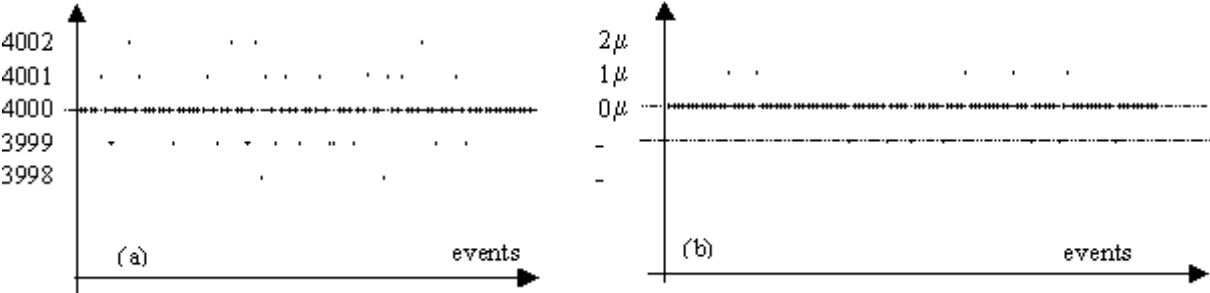


Fig. 59: Acquisition Tests

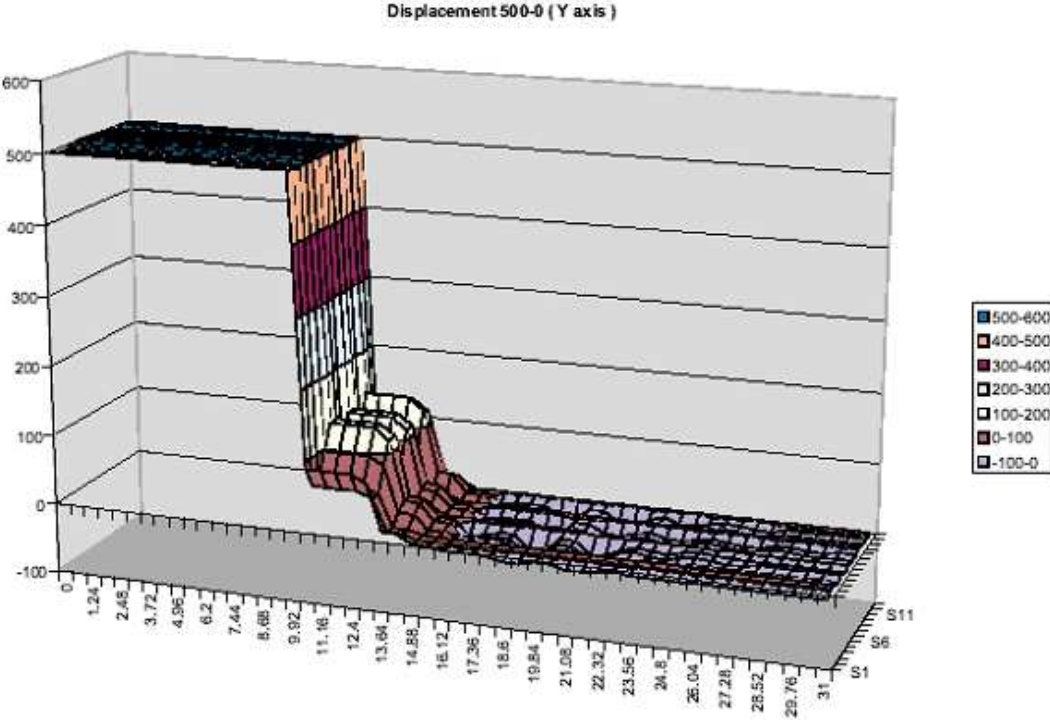


Fig. 60: Deviation of WPS on the Y axis

7.5 Real Time Task

The ALGN RT task provides the mechanism to communicate with the AMCC cards and serves all cards and connected equipment that is installed on the DSC. It does three very important things: initialisation, acquisitions and control.

7.5.1 Initialisation

At the start of the initialisation procedure, the RT task first opens the AMCC loop and sends all initial values from the database to the AMCC cards. These values are :

- Scaling factors for all sensors;
- The values for Cwin and Titer for the TMS and WPS;
- The maximum and minimum speed, the maximum and minimum current and the accelerations for motors;
- Initial values for the calculated offsets;
- Initial values for the manual offsets;
- Reset all motors from fault state;
- Initialise the motors counters using the values from the database (in the first step it is 0).

In case of any problems, the RT task will interrupt the initialisation procedure and will try to re-initialise the AMCC during the main loop. Until the initialisation is done, no control or acquisitions are possible. The initialisation procedure is made each time the RT task starts.

7.5.2 Main Loop

Reading

During the acquisition loop, the RT task acquires the following:

The AMCC flag;

- Mean values for all the sensors;
- Motor states;
- Motor counters - These values are only acquired in closed loop operation;
- The motor's power supply value (MPS).

The reading is only available if the AMCC card has a new data and indicates that by the flag byte. If the AMCC is in closed loop, RT task checks the MPS value and the motor's state. The RT task can open the loop automatically if the MPS value is less than 20V, or some of the motors have a fault state. In open loop, the RT task just collects the acquisitions to store in the database. The frequency of acquisitions is about 0.8 Hz.

Writing

If there is new data in the database, the RT task passes this data to the AMCC card in the following order :

- Manual o_sets;
- Calculated o_sets;
- Cwin and Titer;
- Motor displacements.

7.5.3 30GHz Alignment System Console Application

The new console program has been created and installed. This program helps to communicate with the RT task and control the alignment. The layout of the interface display is the same as the real layout of CTF2 (Probe and Drive beams). Each sensor has its own window to display the acquisitions (see Fig. 61).

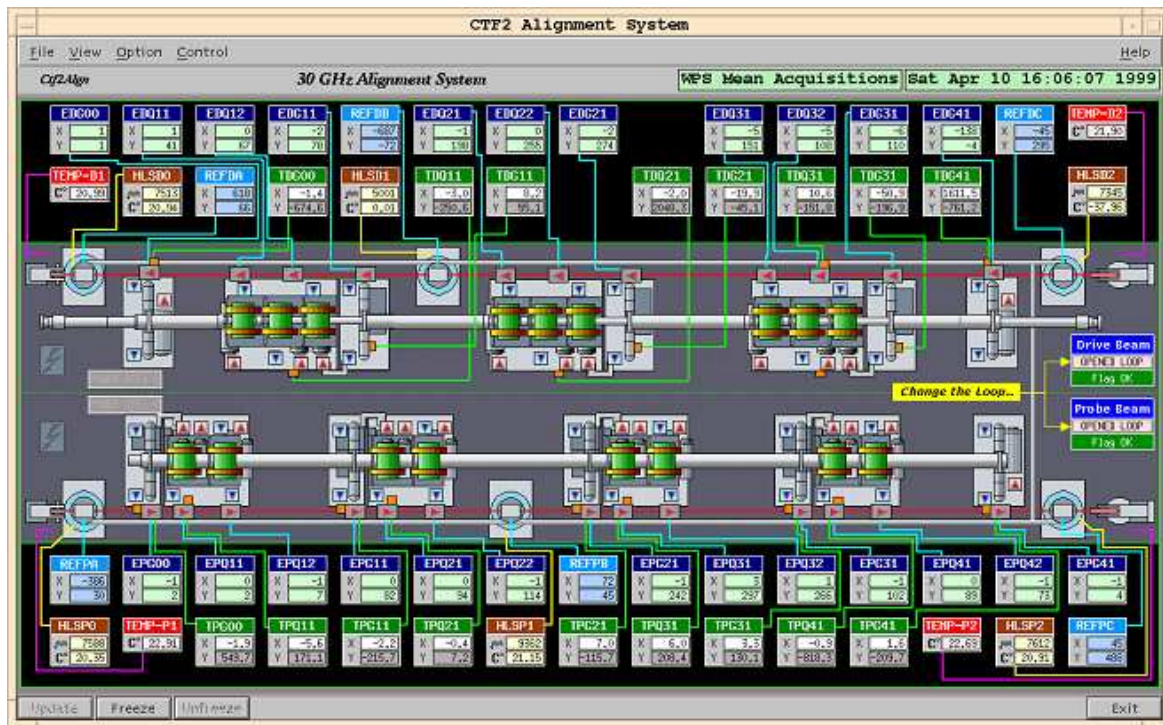


Fig. 61: Alignment system console program

In the scheme, all active parts are marked with arrows (up/down for motors and left/right for sensors).

With this program it is possible to control the following.

- The acquisitions for all sensors;
- The calculated offsets for WPS;
- The "Option" menu is used to change the acquisitions from sensor's position to calculated offsets;
- The motor's states and motor's counters. When the mouse is placed over the motor's button, a small yellow window pops-up and displays the selected motor name, status and counter;
- Move motors to any positions - specified in steps or in microns. This action is only available in open loop;
- Control the Motors Power Supply value;
- Close or Open the alignment loop. The buttons for this are marked with a yellow arrow on the layout picture;
- Control the AMCC flag (Flag : OK, Not Ready, Old Data, Error);
- The manual offsets for WPS. For the manual offsets modifications, the left/right arrow buttons are used. When the mouse is placed on these buttons the small window pops up and shows the current values for the manual offsets. When the sensor's button is clicked, the Manual Offsets window pops-up (one window for each group of sensors);
- Change the Cwin and Titer value for TMS and WPS. The command button is under the "Control" menu;

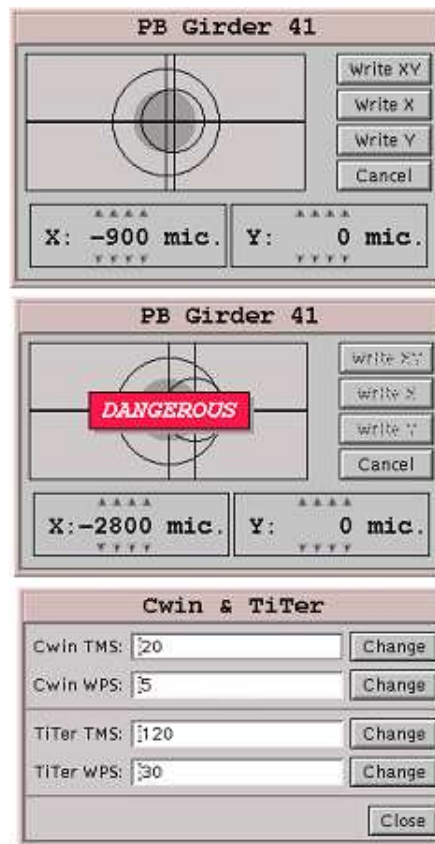


Fig. 62: Offset windows and Cwin-Titer window

Change the Cwin and Titer value for TMS and WPS. The command button is under the "Control" menu.

7.6 Remarks

In spite of the magnitude and the complexity of the system to be controlled, a modular and compact scheme has been conceived and implemented in its different boards with FPGA technology and using high speed processors with a high processing capacity (DSP).

The system mounted in CTF2 possess a high noise immunity because of galvanic isolation (optical fibers) among the different components of the system. In addition, the generalized use of series communication has considerably reduced the number of fibre-optic cables.

The overall performance of the system was very good, in the experiments performed a very small alignment error (1 μm) was obtained, this is to be compared with the specified value of 10 μm .

The system as designed, thanks to its flexibility, simplicity and small number of components, is both suited to the present application (CTF2) and larger applications (the system could control modules that involve up to a maximum of 384 motors and 896 sensors without making substantial changes). It can also be considered as a standard building block for a future CLIC system.

8 Conclusions

A possible active alignment system for CLIC has been proposed based on the overlapping stretched wire technique. Although the reference system proposed is essentially mechanically-based, use is also made of an optical technique developed for the LHC experiments to align some points over short distances.

Although the solution proposed is simple to put in place and makes the connection between the linac components and the reference network more direct, in contrast to purely optical techniques it is directly dependent on knowledge of the geoid and of the phenomena which disturb it.

The active alignment system which has been developed and tested meets the requirements specified for the alignment of the various components of the accelerator.

The experience gained with the CERN accelerators which have been built up to now, provides a reasonably precise idea of the techniques and procedures that will be required for CLIC starting from the drilling of the tunnel right through to the prealignment of the CLIC components.

The metrology sensors which are foreseen to be put in place, and which have been tested, operate at the required level of accuracy and are suitable for use in a radioactive environment.

The positioning of these sensors has been optimized throughout the length of the accelerator so that the combined data provided by these sensors enables the components to be positioned with the specified accuracy.

The network which has been devised meets the specifications for the transverse alignment of the machine. Its ability to meet the specifications for the vertical alignment however requires an exceptionally precise knowledge of the geometry of the gravitational field. Further research is needed to determine whether such a degree of understanding can be achieved. If this proves to be possible, the solution which is proposed should be able to meet the alignment requirements of CLIC.

One of the spin-off benefits of this CLIC development work is that in the process of finding solutions for the initial alignment of the CLIC accelerator, the instrumentation and techniques developed have provided ready solutions for some of the alignment problems of other projects whose accuracy requirements are less stringent.

9 Acknowledgements

The study of the CLIC active-alignment system was initiated in 1988 by I. Wilson, W. Coosemans and W. Schnell. G. Fischer, on leave from SLAC at that time, helped to get the work started and considerably influenced the basic design philosophy of the system. Since that time, many people have been associated with the study, and their contributions to the development of the sophisticated equipment, instrumentation, support structures and control systems of the active-alignment system are gratefully acknowledged. Special thanks are due to the following people who have played key roles in the development programme.

- P. Poirier (student survey engineer 1989-1991)
- H. Mainaud (student survey engineer 1994-1996)
- C. Achard (design studies)
- R. Gave, H. Chavanel, E. Keller and S. Leblanc (mechanical support)
- G. Ramseiere (electrical support)
- V. Maire (technical student 1997-1999)
- J.-P. Potier, D. Carrica, and J.-L. Gomez-Costa (electronics)
- J.-M. Bouché and V. Lakimchouk (control system).

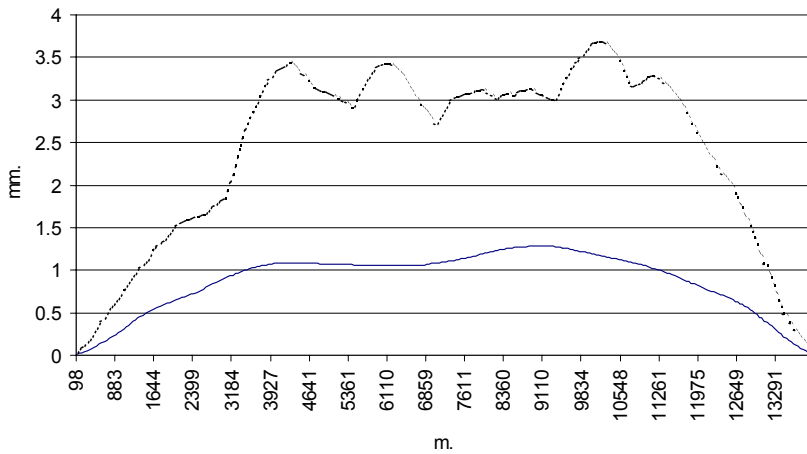
10 References

1. G. Guignard, and All. *A 3 TeV $e^+ e^-$ Linear Collider Based on CLIC Technology*. CERN-2000-008
2. P. Poirier. *L'alignement dynamique submicrométrique de cavités accélératrices*. Mémoire de soutenance du Diplôme de Recherches Spécialisées en Sciences, Strasbourg, 1991
3. W. Coosemans, P. Poirier, I. Wilson. *A micro-movement test facility for CERN linear collider studies*. CLIC note 113, 1990
4. H. van der Graaf, H. Groenstege, F. Linde, P. Rewiersma - *RasNik an Alignment System for the ATLAS MDT Barrel Muon Chambers* NIKHEF, avril 2000
5. W. Coosemans. *Alignement initial du main linac CLIC : métrologie des poutres*, CLIC note 139, 1991
6. W. Coosemans. *Métrologie pour un grand collisionneur linéaire*, XVIIe Colloque de l'Association Française de Topographie, CERN, 1991
7. H. Favre. *Cours de mécanique, Tome I: statique*. Editions Leeman Zurich, 1953
8. F. Merrit. *Standard handbook for civil engineers, 3rd edition*. McGraw-Hill, 1983
9. H. Mainaud. *Une nouvelle approche métrologique : l'écartométrie biaxiale. Application à l'alignement des accélérateurs linéaires*. Ph.D. thesis, Université Louis Pasteur, 1996
10. W. Coosemans and H. Mainaud. *Pre-alignment of CLIC using the double-wire method*. CLIC note 343, 1997
11. B.A. Bell. *A simulation of gravity field around LEP*, 1985
12. P. Melchior. *The Tides of the Planet Barth*. Pergamon Press, 1973
13. P. Melchior. *The Earth tides*. Pergamon Press, 1966
14. G. Jobert and J. Coulomb. *Traité de géophysique interne, Tome I: sismologie et pesanteur*, chapter 18. Editions Masson, 1973
15. P. Vanicek and E. Krakiwsky. *Geodesy : the concepts*. North Rolland Publ. Co., 1982
16. B. Ducarme. « Observatoire Royal de Belgique » Communication personnelle. 2001
17. M. Mayoud. *Computing and analysis methods*. CERN Accelerator School, Applied geodesy for particle accelerators, 1987
18. T. Budd. *Introduction à la programmation par objets*. Addison-Wesley, 1992
19. J.P. Delahaye, I. Wilson, et al. *Performances obtained with the Cern linear collider test facility*. European Particle Accelerator Conference, 1994
20. J.M. Bouché, W. Coosemans, and R. Pittin. *Active Alignment for 30 GHz Modules in CTF2*. CLIC note 350, 1997
21. D. Carrica, R. Pittin, M. Benedetti, G. Uicich, D. Calcoen, S. Scherbakov, and J.M. Bouché. *CTF Notes for Sub Systems of Electronic Active Alignment*. CTF notes 99-09, 99-10, 99-11, 99-12, 99-13, 99-16, 1999
22. American National Standard for VMB64. VMEbus International Trade Association, 1995

11 Annexes

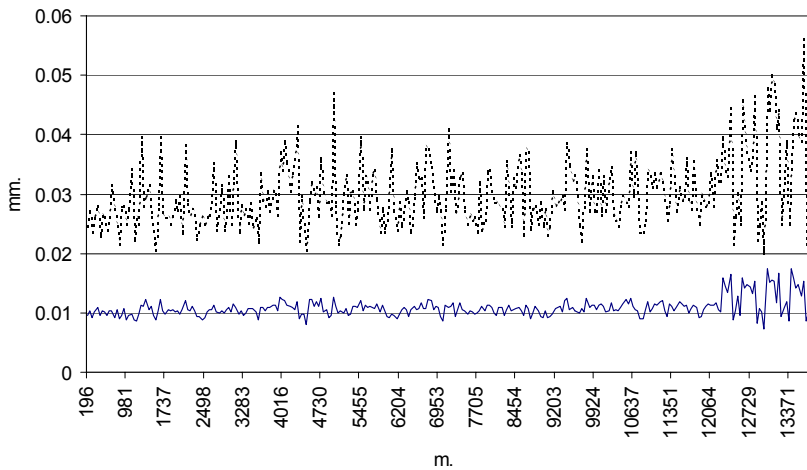
ANNEX 1a

Reference plate offsets with respect to their theoretical position, wire 100m, WPS and WTW sigma 5 microns, 100 simulations.



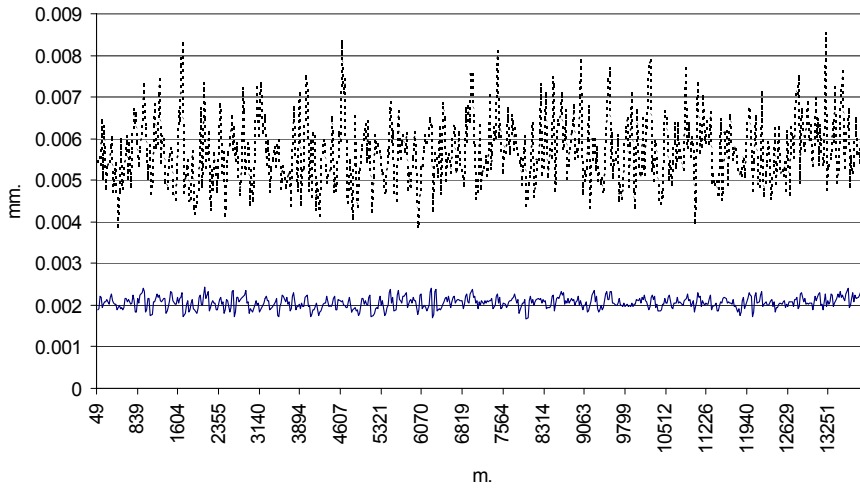
ANNEX 1b

Alignment error of the reference plates over ~200 m, Wire 100m, WPS and WTW sigma 5 microns, 100 simulations.

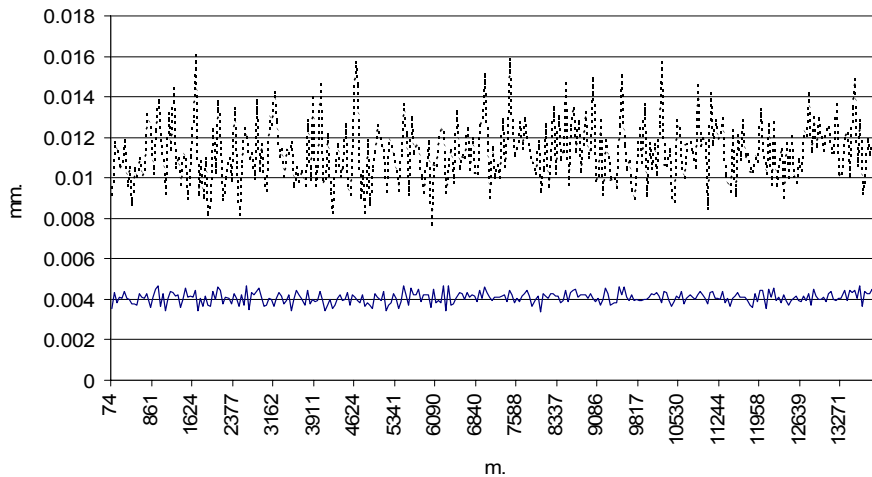


quadratic mean ————— maximum

ANNEX 1c
 Residuals of the WPS observations,
 Wire 100m., WPS and WTW sigma 5 microns, 100 simulations.



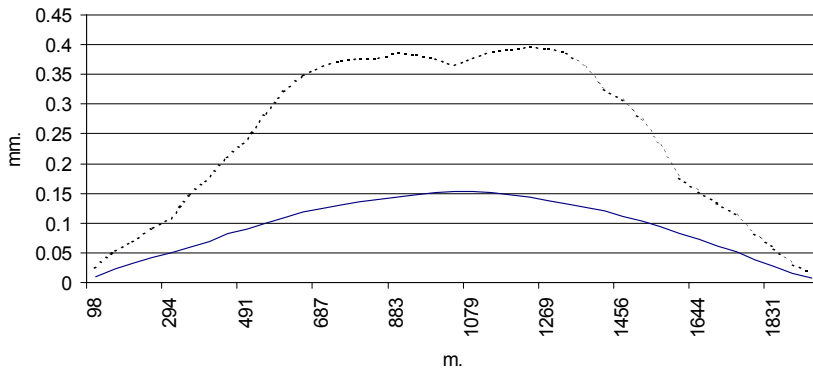
ANNEX 1d
 Residuals of the WTW observations,
 Wire 100m., WPS and WTW sigma 5 microns, 100 simulations.



quadratic mean		maximum	
----------------	--	---------	--

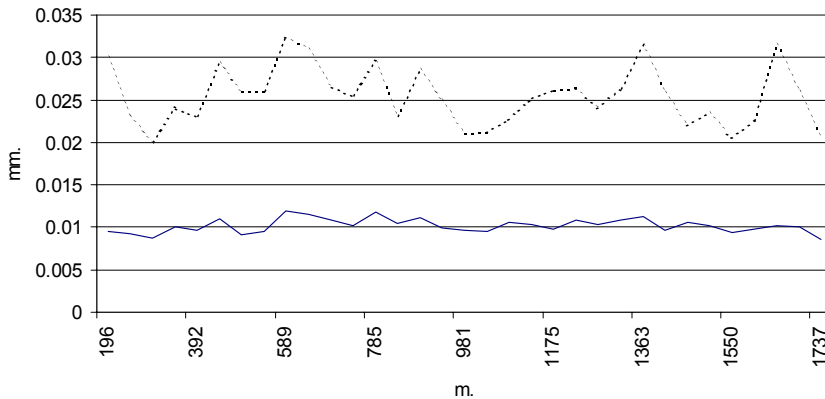
ANNEX 2a

Reference plate offsets with respect to their theoretical position,
 Wire-Girder combined calculation, Wire 100m.,
 WPS and WTW sigma 5 microns,
 RASNIK-CCD sigma 2 microns attached to WPS every 22 modules,
 71 simulations.



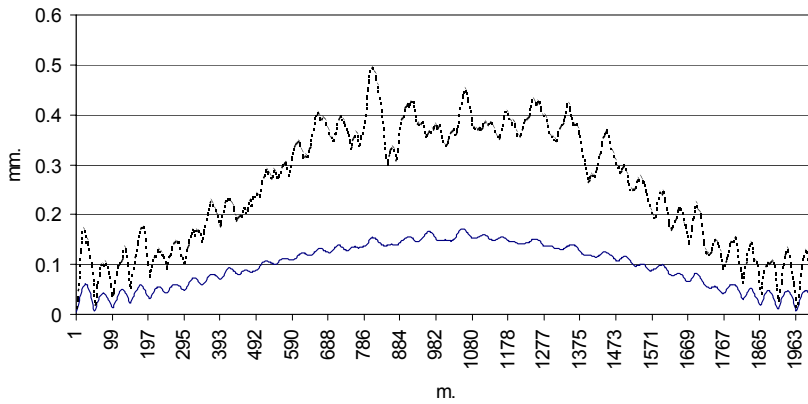
ANNEX 2b

Alignment error of the reference plates over ~200 m,
 Wire-RASNIK combined calculation, Wire 100m.,
 WPS and WTW sigma 5 microns,
 RASNIK-CCD sigma 2 microns attached to WPS every 22 modules,
 71 simulations .



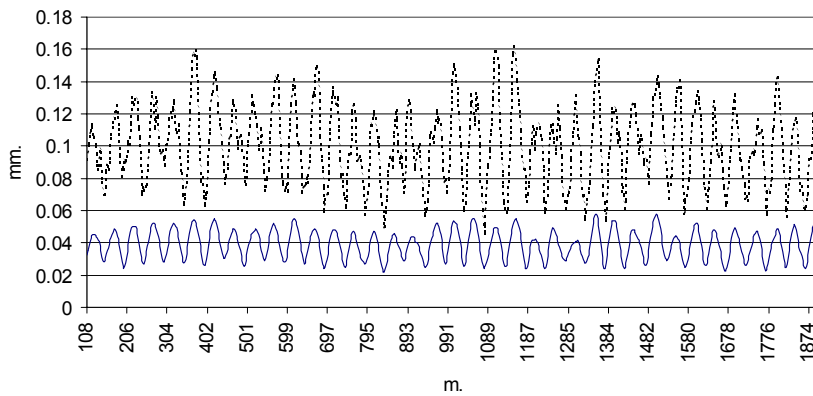
ANNEX 2c

Offsets of the articulations with respect to their theoretical position,
 Wire-RASNIK-CCD combined calculation, Wire 100m.,
 WPS and WTW sigma 5 microns
 RASNIK-CCD sigma 2 microns attached to WPS every 22 modules,
 71 simulations.



ANNEX 2d

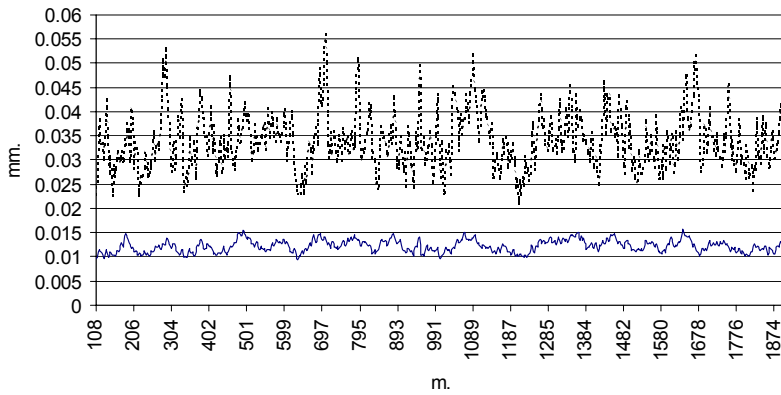
Alignment error of the reference plates over ~200 m.,
 Wire-RASNIK-CCD combined calculation, Wire 100m.,
 WPS and WTW sigma 5 microns,
 RASNIK-CCD sigma 2 microns attached to WPS every 22 modules
 71 simulations.



quadratic mean		maximum	
----------------	--	---------	--

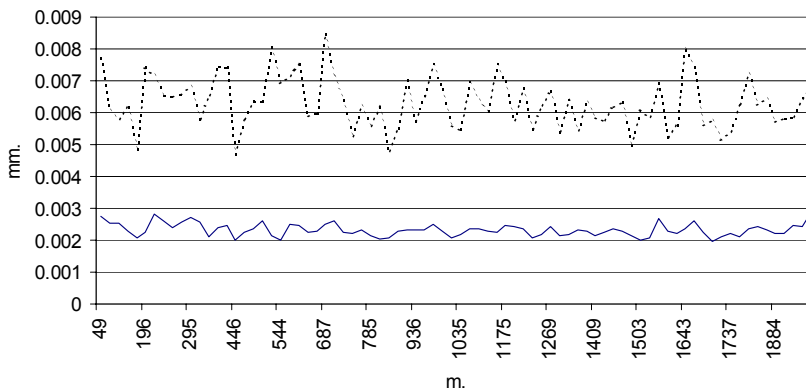
ANNEX 2e

Alignment error of the reference plates over ~200 m.,
Wire-Girder combined calculation, Wire 100m.,
WPS and WTW sigma 5 microns,
RASNIK-CCD sigma 2 microns attached to WPS every 4 or 5 modules,
105 simulations.



Annex 2f

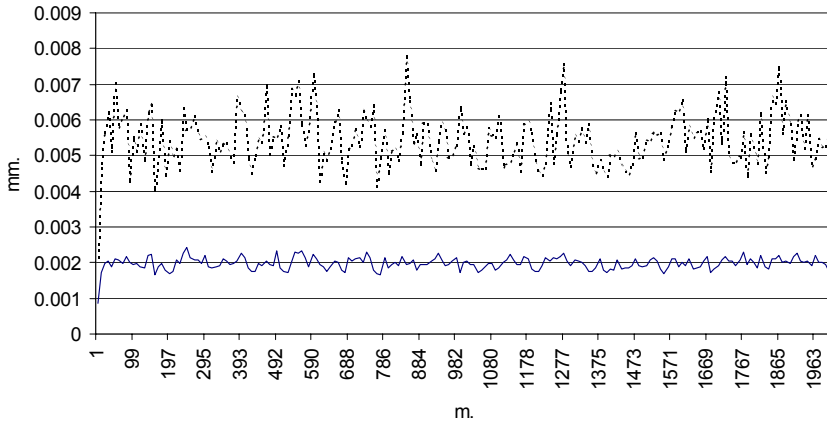
Residuals of the WPS observations between wires,
Wire-Girder combined calculation, Wire 100m.,
WPS and WTW sigma 5 microns,
RASNIK-CCD sigma 2 microns attached to WPS every 4 or 5 modules
105 simulations.



quadratic mean	—————	maximum
----------------	-------	---------	-------

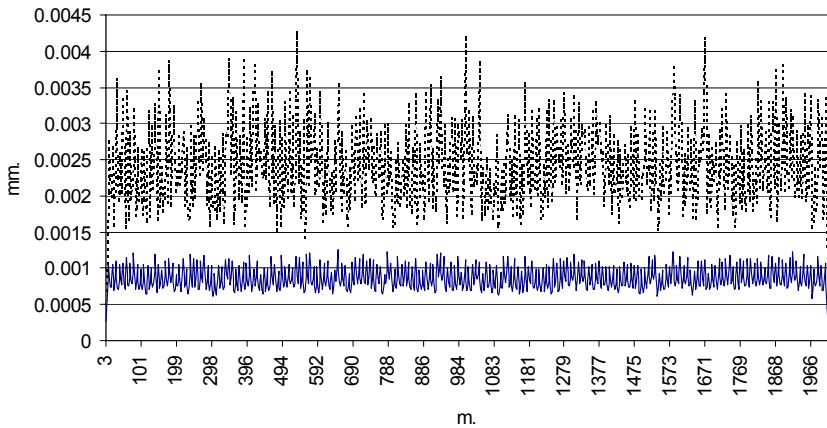
Annex 2g

Residuals of the linking WPS observations, Wire-Girder combined calculation,
Wire 100m., WPS and WTW sigma 5 microns,
RASNIK-CCD sigma 2 microns attached to WPS every 4 or 5 modules
105 simulations.



Annex 2h

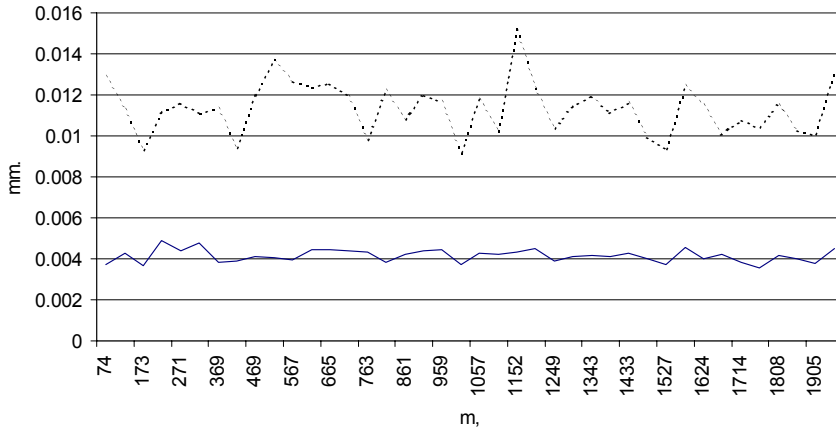
Residuals of the RASNIK observations, Wire-Girder combined calculation,
Wire 100m., WPS and WTW sigma 5 microns,
RASNIK-CCD sigma 2 microns attached to WPS every 4 or 5 modules
105 simulations.



quadratic mean ————— maximum

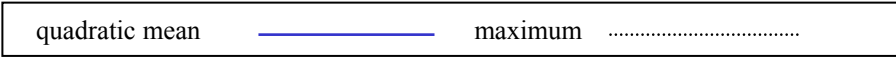
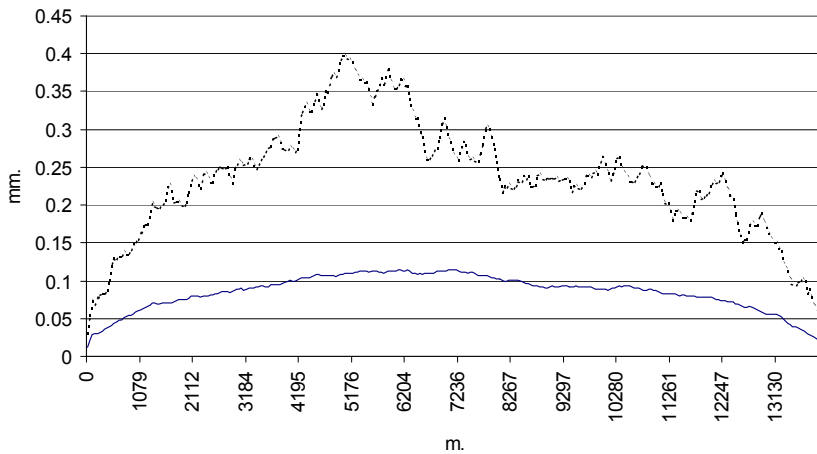
Annex 2i

Residuals of the WTW observations Wire-Girder combined calculation,
 Fils 100m., WPS and WTW sigma 5 microns,
 RASNIK-CCD sigma 2 microns attached to WPS every 4 or 5 modules,
 105 simulations.

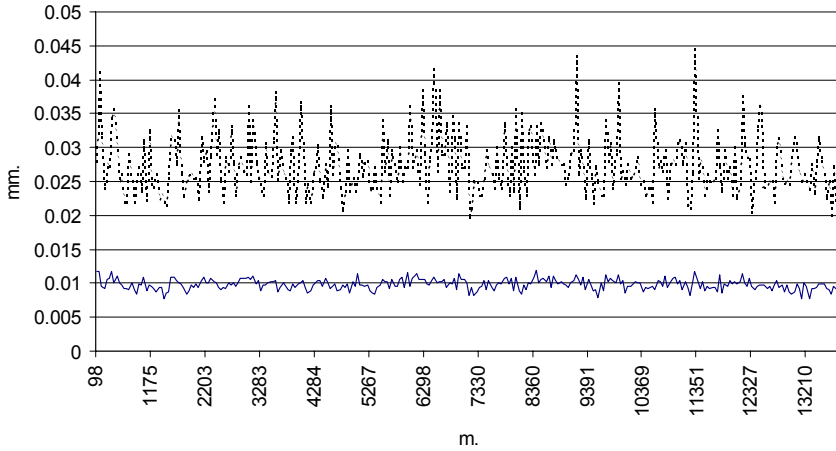


Annex 3a

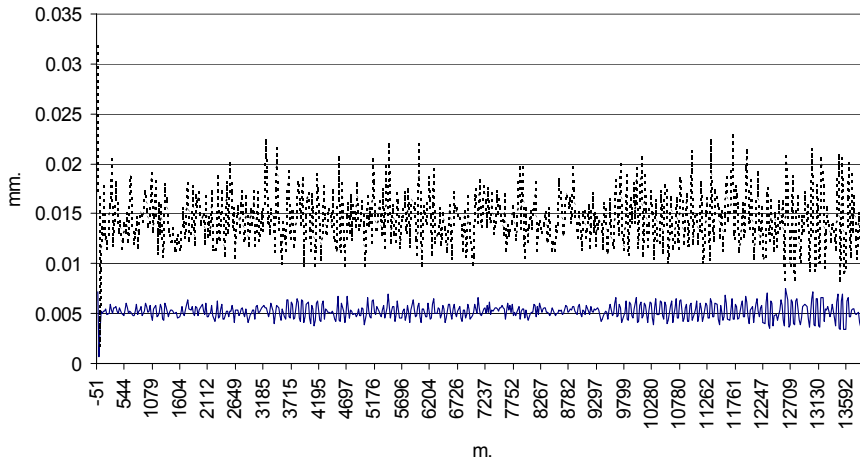
Reference plate offsets in Z with respect to their theoretical position,
 Wire 100m., WPS and WTW sigma 8 microns, DVER sigma 7 microns,
 102 simulations.



Annex 3b
 Alignment error of the reference plates over ~200 m,
 Wire 100m., WPS and WTW sigma 8 microns, DVER sigma 7 microns,
 102 simulations.

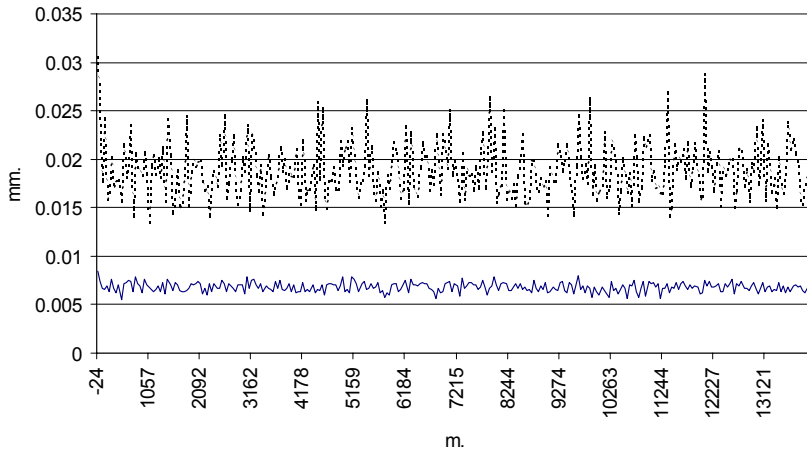


Annex 3c
 Residuals of the vertical WPS observations,
 Wire 100m., WPS and WTW sigma 8 microns, DVER sigma 7 microns,
 102 simulations.

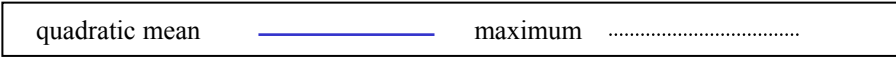
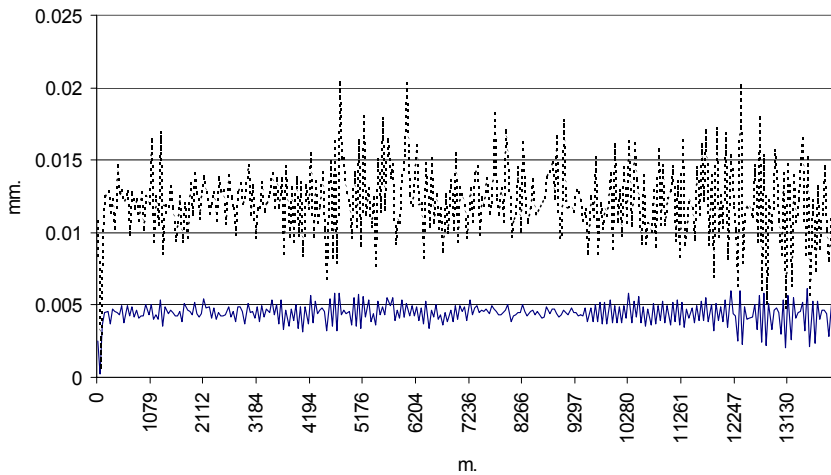


quadratic mean		maximum	
----------------	--	---------	--

Annex 3d
 Residuals of the vertical WTW observations, Wire 100m.,
 WPS and WTW sigma 8 microns, DVER sigma 7 microns,
 102 simulations.

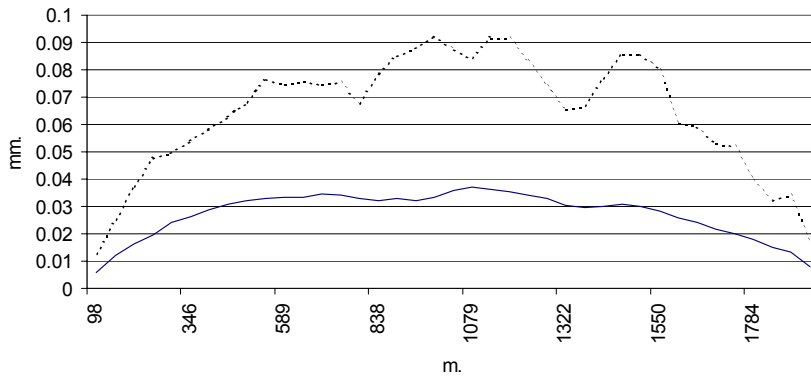


Annex 3e
 Residuals of the DVER observations, Wire 100m., WPS and WTW sigma 8 microns,
 DVER sigma 7 microns, 101 simulations.



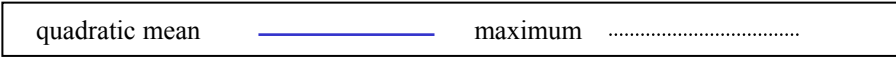
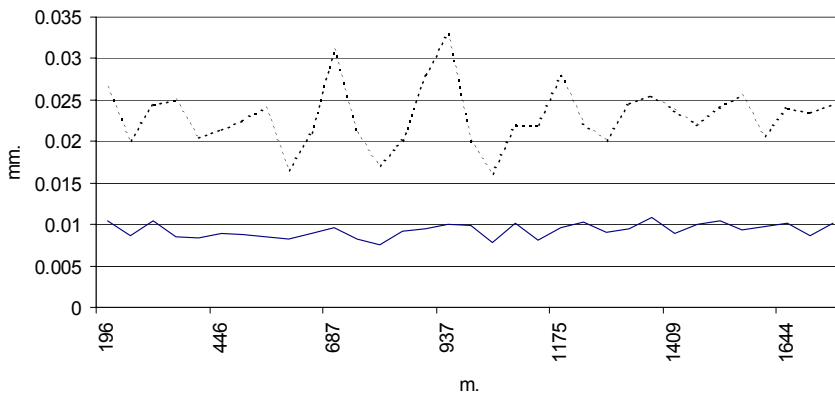
Annex 4a

Offsets of the articulations in Z with respect to theoretical position,
 Wire-RASNIK combined calculation, Wire 100m., DVER sigma 7 microns,
 WPS et WTW sigma 8 microns,
 RASNIK-CCD sigma 2 microns attached to WPS every 4 or 5 modules,
 52 simulations.



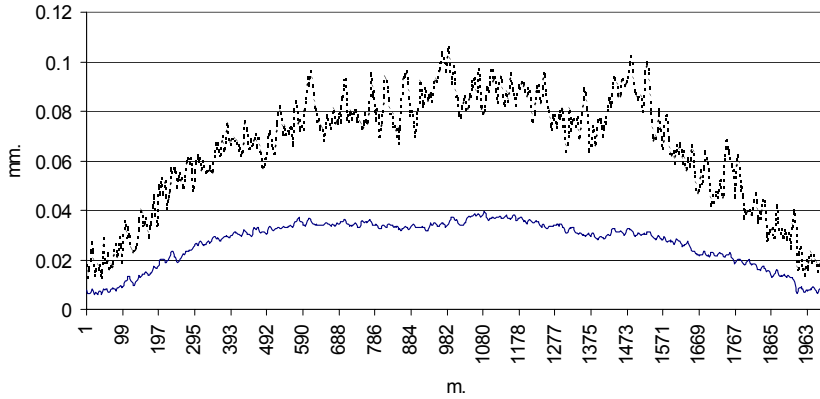
Annex 4b

Alignment error of the reference plates over ~200 m,
 Wire-RASNIK combined calculation, Wire 100m., DVER sigma 7 microns,
 WPS and WTW sigma 8 microns,
 RASNIK-CCD sigma 2 microns attached to WPS every 4 or 5 modules,
 52 simulations.



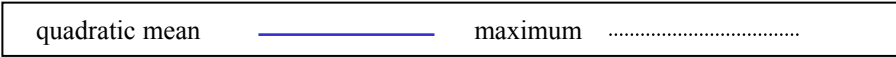
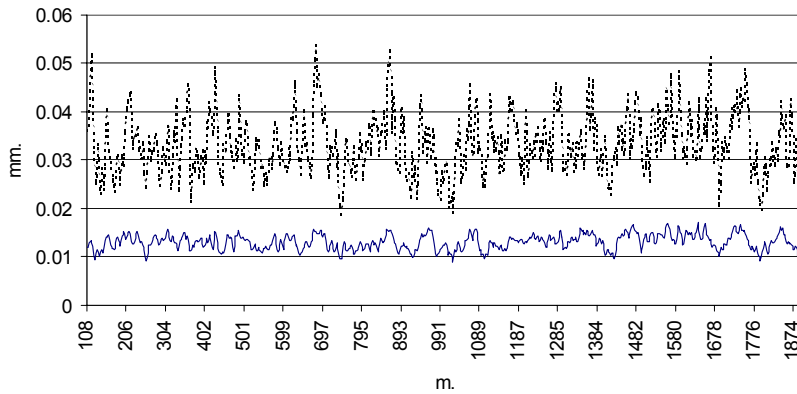
Annex 4c

Offset of the girder in Z with respect to their theoretical position,
 Wire-RASNIK combined calculation, Wire 100m., DVER sigma 7 microns,
 WPS and WTW sigma 8 microns,
 RASNIK-CCD sigma 2 microns attached to WPS every 4 or 5 modules,
 52 simulations.

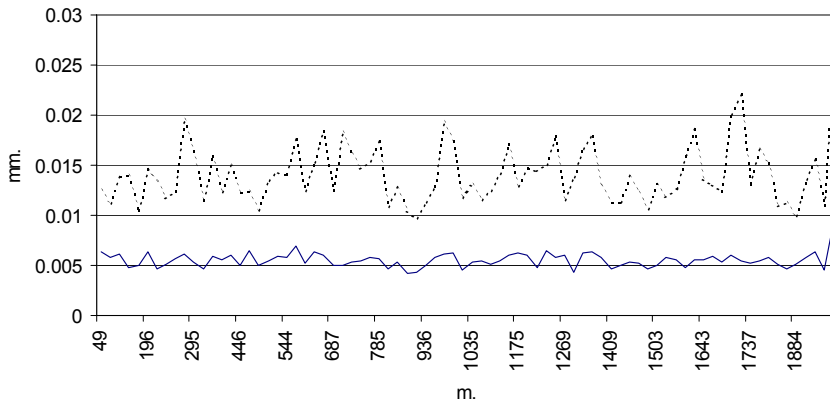


Annex 4d

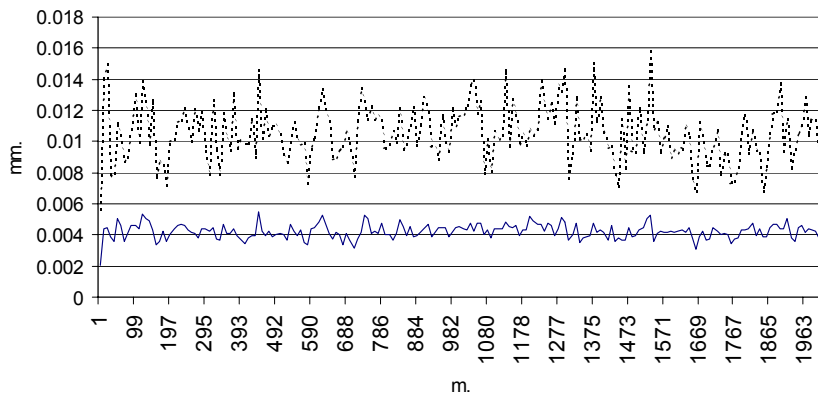
Alignment error in Z of the girder over ~200 m,
 Wire-RASNIK combined calculation, Wire 100m., DVER sigma 7 microns,
 WPS et WTW sigma 8 microns,
 RASNIK-CCD sigma 2 microns attached to WPS every 4 or 5 modules,
 52 simulations.



Annex 4e
 Residuals of the WPSV observations between wires,
 Wire-RASNIK combined calculation, Wire 100m., DVER sigma 7 microns,
 WPS and WTW sigma 8 microns,
 RASNIK-CCD sigma 2 microns attached to WPS every 4 or 5 modules,
 52 simulations.



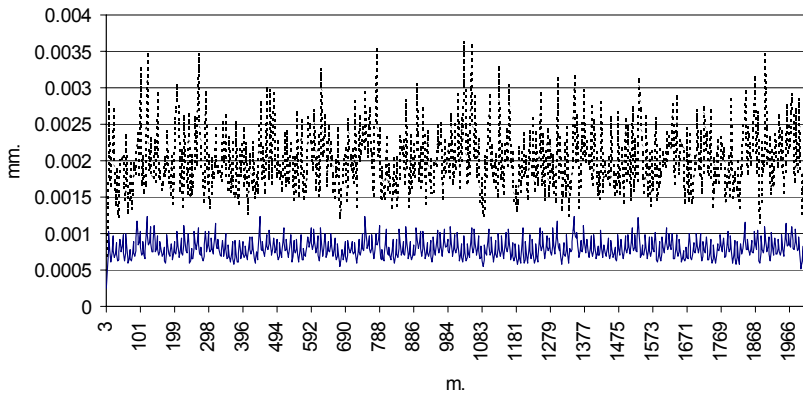
Annex 4f
 Residuals of the linking WPSV observations,
 Wire-RASNIK combined calculation, WIRE 100m., DVER sigma 7 microns,
 WPS and WTW sigma 8 microns,
 RASNIK-CCD sigma 2 microns attached to WPS every 4 or 5 modules,
 52 simulations.



quadratic mean		maximum	
----------------	--	---------	--

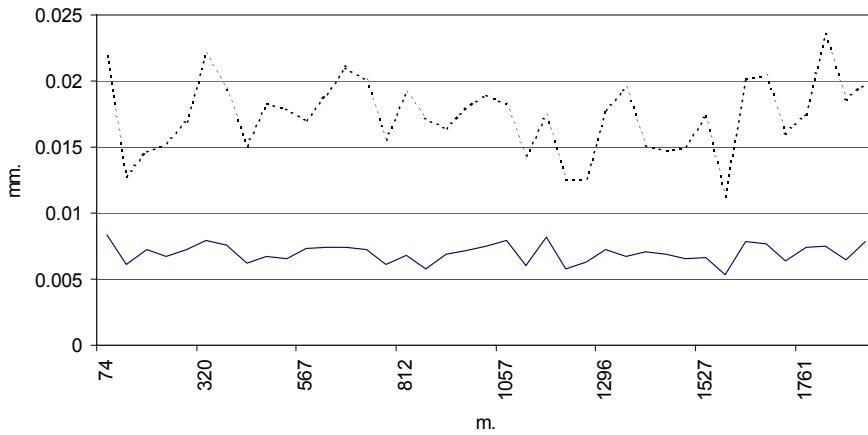
Annex 4g

Residuals of the RASNIK-CCD V observations,
Wire-RASNIK combined calculation, Wire 100m., DVER sigma 7 microns,
WPS and WTW sigma 8 microns,
RASNIK-CCD sigma 2 microns attached to WPS every 4 or 5 modules,
52 simulations.



Annex 4h

Residuals of the WTW observations, Wire-RASNIK combined calculation,
Wire 100m., DVER sigma 7 microns, WPS and WTW sigma 8 microns,
RASNIK-CCD sigma 2 microns attached to WPS every 4 or 5 modules,
52 simulations.



quadratic mean ————— maximum